Institute of Anatomy and Cell Biology

Faculty of Medicine

Saarland University, Homburg (Saar)

The effects of brush cell-derived acetylcholine on the sensory innervation of the airways and lungs

A Dissertation

Submitted in Fulfillment of the Requirements for the Degree of

Doctor of Philosophy (Ph.D.)

of the Medical Faculty of Saarland University

2023

By Alaa' Hisham Salah

Born on 04.10.1988 in Jerusalem

Dekan:	**Prof. Dr. M. D. Menger**
Berichterstatter:	**Prof. G. Krasteva-Christ**
	Prof. R. Bals
Tag der Promotion:	**18.09.2023**

Disclosure

This work was funded by: DFG

All experiments were executed in the **Institute for Anatomy and Cell Biology,** University of Saarland, 66421 Homburg, Germany

Supervisor: Prof. Dr. Gabriela Krasteva-Christ

Acknowledgments

My deepest gratitude is extended to my mentor and idol, Prof. Dr. Gabriela Krasteva-Christ. The support and encouragement you have given me throughout this research process have been greatly cherished. I greatly appreciate your guidance during my stay in your lab and the knowledge you provided me with. I'm very lucky to have had the chance to work with you.

Special thanks to Dr. Maxeiner, Dr. Hollenhorst, Dr. Zhao, Dr. Elhawy, Noran, Saskia, Praveen, Clara, Nora, and Nosaibah - the lab became remarkably more enjoyable with your presence, and the experiments became notably more captivating. Thanks for the help and encouragement and for being more like friends than colleagues. Andrea and Aline, words cannot express my gratitude to both of you.

This endeavor would not have been possible without the support of my soulmate (Osama) and the tolerance of my kids (Zaid and Maha).

Mom and Dad, I did this for you. I hope I made you proud. I'm extremely grateful for your support and unconditional love. I appreciate the constant support and love I have received from my siblings. Thank you for being a constant source of strength throughout my life.

I could not have undertaken this journey without the help and support from all my professors throughout my academic life, starting from primary school, BZU, CIHEAM-MAICh, Al-Quds University, HZI, and finally here at Saarland University.

I would like to thank the defense committee, our funding partners, and everyone else who made this happen.

It is important to make a dream of life and of a dream reality.

Marie Curie

To my family

Table of Contents

List of Figures

List of Tables

List of Abbreviations

$[Ca^{2+}]i$	intracellular Calcium concentration
°C	degrees Celsius
µ	micro
A	adenine
a	arteriole
ACh	acetylcholine
AChRs	Acetylcholine receptors
AChE	Acetylcholine esterase
ATP	adenosine triphosphate
ASL	airway surface liquid
BC	brush cells
β-MG	β2 microglobulin
bp	base pair
BSA	bovine serum albumin
C	cytosine
c	capillary
CA	cinnamaldehyde
cAMP	cyclic adenosine monophosphate
cDNA	coding deoxyribonucleic acid
CGRP	calcitonin gene-related peptide
CNO	clozapine N-oxide
CNS	central nervous system
CO_2	carbon dioxide
COPD	chronic obstructive pulmonary disease
DAG	diacylglycerol
Den	denatonium
DMEM	Dulbecco's modified eagle medium
DMSO	dimethyl sulfoxide
DNA	deoxyribonucleic acid
dNTP	deoxyribonucleotide triphosphate
DPBS	Dulbecco's phosphate-buffered saline

DRG	dorsal root ganglia
DREADD	designer receptors exclusively activated by designer drug
DT	diphtheria toxin
DTR	diphtheria toxin receptor
EB	Evans' blue
EDTA	ethylenediaminetetraacetic acid
Em	emission
FCS	fetal calf serum
G	guanine
g	gram
GAPDH	glyceraldehyde 3-phosphate dehydrogenase
GFP	green fluorescent protein
GPCR	G protein-coupled receptor
h	Hour
HEPES	4-(2-Hydroxyethyl)-1-piperazineethanesulfonic acid
HIS	immunohistochemistry
i.p.	intraperitoneal
IT	intratracheal
JNC	jugular-nodose complex
K+	potassium
KCl	potassium chloride
kDa	kilodalton
$KHCO_3$	potassium bicarbonate
KO	knockout
L	liter
LB	medium lysogeny broth-medium
m	meter
m	milli
M	mol/l
mAChRs	muscarinic acetylcholine receptors
MEC	mecamylamine
Mg^{2+}	magnesium ion
min	minute(s)

MW	molecular weight
n-	nano
n	number of experiments
$NaCHO_3$	sodium bicarbonate
NaCl	sodium chloride
nAChRs	nicotinic acetylcholine receptors
NGI	neurogenic inflammation
NH_3	ammonia
P	probability value
PBS	phosphate buffer saline
PCR	polymerase chain reaction
PFA	paraformaldehyde
pH	potential hydrogen
PIP_2	phosphatidylinositol bisphosphate
PKA	protein kinase A
PLC β2	phospholipase C β2
PLL	poly-L-lysine
qPCR	quantitative polymerase chain reaction
QSM	quorum sensing molecules
RNA	ribonucleic acid
ROI	region of interest
rpm	round per minute
RT	room temperature
RT	real-time
s	second(s)
SDS	sodium dodecyl sulfate
SP	substance P
T	thymine
Tas2R	bitter taste receptor (mouse)
TAE	tris-acetate-EDTA
Taq	Thermus aquaticus
TBST	Tris-buffered saline (Tween)
Tris	Tris(hydroxymethyl)aminomethane

TRP channels:	transient receptor potential channels:
TRPA	transient receptor potential ankyrin
TRPC	transient receptor potential canonical
TRPM	transient receptor potential melastatin
TRPML	transient receptor potential mucolipin
TRPN	transient receptor potential nompC
TRPP	transient receptor potential polycystic
TRPV	transient receptor potential vanilloid
U	units
UV	ultraviolet
V	volts
v	veniole
WT	wild-type
α	alpha
β	beta
βME	β-mercaptoethanol
γ	gamma
λ	lambda

Zusammenfassung

In der Luftröhre exprimieren epitheliale Chemorezeptorzellen, sogenannte Bürstenzellen (BC), viele Subtypen von Bittergeschmacksrezeptoren, begleitet vom transienten Rezeptor-Potential-Kationenkanal der Unterfamilie M5 (*Trpm5*). Frühere Arbeiten zeigten, dass der Bitterstoff Denatonium und bitter schmeckende bakterielle Stoffwechselprodukte wie Quorum-Sensing-Moleküle, die von gramnegativen Bakterien wie Pseudomonas aeruginosa produziert werden, die Aktivierung der gustatorischen Geschmackssignale auslösen. Die Signalübertragung umfasst die Freisetzung von PLCβ2 und Inositoltriphosphat (IP3), gefolgt von einer Calcium-abhängigen TRPM5-vermittelten Signalübertragung, die Freisetzung Acetylcholin (ACh) umfasst. Dies wurde als signifikant für die Auslösung einer neurogenen Entzündung identifiziert, die durch die Freisetzung der neurogenen Peptide *Calcitonin Gene-Related Peptide* (CGRP) und Substanz P (SP) gekennzeichnet ist und zu einer Rekrutierung von neutrophilen Granulozyten führt. Außerdem führt die Freisetzung dieser Neuropeptide zur Plasmaextravasation und Diapedese. In dieser Studie untersuchten wir daher die Beteiligung cholinerger Rezeptoren auf den sensorischen Nervenfasern an der Induktion neurogener Entzündung in den Atemwegen. Darüber hinaus untersuchten wir das Vorhandensein des TRPM5-Kanals in den Neuronen der Spinalganglien (DRG) und des Jugulare-Nodosum-Komplexes (JNC) und testeten die Auswirkungen der TRPM5-Kanalfunktion auf die Sensitivität der TRPV1- und TRPA1-Kanäle in sensorischen Neuronen. Wir untersuchten auch die Rolle von ACh, das von BC stammt, auf die *Trpa1*+ und *Trpv1*+-Neuronen, die Atemwege innervieren. In dieser Studie wurden folgende Mausmodelle verwendet: Wildtyp (WT), *Trpm5*-defiziente, *Trpm5*-DTR (Mäuse, die den Diphtherie-Toxin-Rezeptor (DTR) in den *Trpm5*+ Zellen exprimieren, und in denen die *Trpm5*-exprimierenden Zellen nach Verabreichung von Diphtherie-Toxin (DT) deplitiert wurden), *Trpm5*-DREADD (Mäuse, die einen Designer-Rezeptor aktivierbar ausschließlich durch Designer-Medikamente (DREADD) in den *Trpm5*+ Zellen exprimieren, und in denen die *Trpm5*-exprimierenden Zellen nach Verabreichung von Clozapin-N-oxid (CNO) aktiviert wurden) und *Trpa1*-DTR (Mäuse, die das DTR in den *Trpa1*+ Neuronen exprimieren, und in denen die Trpa1-exprimierenden Neuronen spezifisch durch DT-Gabe deplitiert wurden). Zur Quantifizierung der Plasmaextravasation und die Einwanderung von neutrophilen Granulozyten erhielten Mäuse Evans Blau und inhalierten Denatonium. Nach 30 min wurden die Luftröhren explantiert. Zusätzlich erhielten manche WT-Mäuse eine Lösung mit den cholinergen Rezeptorinhibitoren Mecamylamin (MEC) und Atropin injiziert. Für die Deplitionsversuche wurden die Mäuse an drei aufeinanderfolgenden Tagen mit DT (20 ng/kg Körpergewicht, *i.p.*) injiziert. Der Verlust der *Trpa1*+ Nervenfasern wurde durch Immunhistochemie, $[Ca^{2+}]i$ -Imaging und real-time RT-PCR charakterisiert. Zusätzlich wurden Western Blot-Analyse, RT-PCR und Immunhistochemie angewendet, um das Vorhandensein des TRPM5-Kanals in den sensorischen Neuronen zu untersuchen. Darüber hinaus wurden Neuronen des sensorischen Ganglions (DRG und JNC) von WT-Mäusen und *Trpm5*-defizienten

Mäusen isoliert, und die EC50-Antwort auf die Gabe vom Zimtaldehyd (CA, ein TRPA1-Agonist) und Capsaicin (ein TRPV1-Agonist) untersucht und vergleichen. Darüber hinaus erhielten Mäuse, die den DTR in den *Trpm5*+ BC im Trachealepithel exprimieren, eine Einzeldosis von 40 µl 200 ng DT intratracheal (IT). DRG und JNC wurden 48 Stunden später explantiert und vorsichtig für [Ca^{2+}]i-Imaging dissoziiert. Ebenso wurden Mäuse, die den DREADD-Rezeptor in *Trpm5*+-Zellen exprimieren, dreißig Minuten nach der Inhalation von 100 µM CNO getötet, und anschließend wurden DRG und JNC für [Ca^{2+}]i-Imaging explantiert und dissoziiert. [Ca^{2+}]i-Imaging wurde eingesetzt , um die Sensitivität der sensorischen Neuronen in akuten und chronischen Infektionsmodellen zu untersuchen. Zusätzlich wurde der Effekt von Acetylcholin (ACh) auf die Aktivierung von *Trpa1*+ und *Trpv1*+ sensorischen Neuronen vom JNC untersucht, indem frisch isolierte Neuronen mit ACh behandelt wurden und die Veränderungen in der Sensitivität gegenüber TRPA1- und TRPV1-Agonisten gemessen wurden. Die Hemmung der cholinergen Rezeptoren führte im Vergleich zu der Gruppe, die mit dem mit Vehikel behandelt wurde, zu einer signifikanten Abnahme der Plasmaextravasation und der Neutrophilenrekrutierung. Immunohistochemie von DRG-Neuronen von DT-behandelten *Trpa1*tauGFP-DTR-Mäusen zeigte einen Verlust von *Trpa1*tauGFP+ Neuronen. Die Anzahl der *Trpv1*-exprimierenden Neuronen wurde um 80% reduziert. CGRP/SP-doppelimmunoreaktive Neuronen wurden nur vereinzelt gefunden. Unterstützend wurde das Volumen der CGRP+/SP+-Nervenfasern in trachealen Whole-mount-Präparaten von Mäusen, die in den die *Trpa1*+ Neuronen deplitiert wurden, reduziert. Eine geringe Anzahl von Primärneuronen, die aus DRG und JNC isoliert wurden, reagierte auf den TRPA1-Agonisten CA und den TRPV1-Agonisten Capsaicin. qRT-PCR zeigte, dass die *Trpa1*- und *Trpv1*-Expression in Neuronen in beiden sensorischen Ganglien signifikant herunterreguliert war. DT-behandelte *Trpa1*tauGFP-DTR wiesen nach BC-Stimulation keine EB-Extravasation und Neutrophilenrekrutierung auf. Zusätzlich haben wir festgestellt, dass der TRPM5-Kanal in den sensorischen Neuronen, die die Lunge innervieren, vollständig abwesend ist. In Immunohistochemie mit DRG und JNC sowie im Western Blot mit Proteinlysaten von DRG und JNC aus Wildtyp-Mäusen fehlten ein TRPM5-Labeling. qRT-PCR mit cDNA, die aus DRG und JNC von Wildtyp- und *Trpm5*-defizienten Mäusen isoliert wurden, ergab keinen signifikanten Unterschied in der *Trpa1*- und *Trpv1*-Genexpression zwischen beiden Genotypen. Interessanterweise fanden wir bei einer *Trpm5*-Defizienz einer höheren Sensitivität von TRPV1 und TRPA1 gegenüber CA und Zimtaldehyd im Vergleich zur Antwort bei Wildtyp-Mäusen. Mehr noch führte die spezifische Depletion von BC unter Verwendung von DT im *Trpm5*-DTR-Mausmodell zu einer signifikanten Abnahme der EC50 für sowohl Capsaicin als auch CA im Vergleich zum Wildtyp. Dissoziierte Neuronen zeigten einen signifikanten Unterschied in ihrer Sensitivität, wenn BC selektiv im *Trpm5*-DREADD-Mausmodell aktiviert wurden. Die TRPA1-Reaktion auf 200 µM CA wurde gehemmt, während die TRPV1 eine signifikant höhere Empfindlichkeit gegenüber 50 nM Capsaicin zeigte. Dieses Ergebnis war ähnlich wie die beobachteten Reaktionen nach BC-Aktivierung durch Denatonium oder akute bakterielle Infektionen. Interessanterweise zeigten Mäuse mit chronischer Infektion

nur eine Abnahme der Empfindlichkeit von *Trpa1* und nicht von *Trpv1*+ Neuronen. Bemerkenswerterweise führte die Exposition der sensorischen Neuronen gegenüber ACh zu einer Hemmung von TRPA1 und einer Aktivierung von TRPV1. Diese Effekte wurden mit den nikotinischen ACh-Rezeptorantaganisten MEC und Hexamethonium sowie mit dem generellen muskarinischen ACh-Rezeptorantaganisten Atropin gehemmt. Basierend auf all diesen Beobachtungen schlagen wir vor, dass die durch BC-induzierte protektive neurogene Entzündung von der cholinergen Übertragung von BC zu sensorischen Nervenfasern abhängt. Darüber hinaus mussen Die TRPA1- und TRPV1-Kanäle sowie ihre Interaktionen mit AChRs müssen als therapeutisches Ziel gegen neurogene Entzündungen und akute Lungeninfektionen wie beispielsweise Lungenentzündung weiter erforscht werden.

Summary

In the trachea, epithelial chemoreceptor cells named brush cells (BC) express many bitter taste receptor subtypes accompanied by the transient receptor potential channel M5 (*Trpm5*). Previous work demonstrated that the bitter substance denatonium and bitter-tasting bacterial metabolites such as quorum-sensing molecules (QSM) produced by Gram-negative bacteria *Pseudomonas aeruginosa,* for example, triggered the activation of the gustatory taste signaling. The signaling involves phospholipase C β2 (PLCβ2) and the generation of inositol triphosphate (IP_3) and subsequent TRPM5-dependent calcium-mediated signaling and the release of acetylcholine (ACh). This was found significant for provoking the generation of a neurogenic inflammation characterized by the release of the neurogenic peptides: calcitonin gene-related peptide (CGRP) and substance P (SP), and the subsequent neutrophils recruitment, plasma extravasation, and diapedesis. Therefore, in this study, we explored the involvement of cholinergic receptors (AChRs) on the sensory nerve fibers for the induction of neurogenic inflammation in the airways. Further, we investigated the occurrence of the TRPM5 channel in the dorsal root ganglia (DRG) and the jugular nodose complex (JNC) neurons, and tested the impact of TRPM5 on the *Trpv1*+ and *Trpa1*+ function in sensory neurons. We also looked at the role of ACh derived from BC on the *Trpa1*+ and *Trpv1*+ vagal nerve afferents innervating the airways. Here, wild-type (WT), *Trpm5*-deficient, *Trpm5*-DTR (mice that express diphtheria toxin receptor (DTR) in the *Trpm5*+ cells in which *Trpm5*-expressing cells were specifically ablated upon diphtheria toxin (DT) administration), *Trpm5*-DREADD (mice that express the DREADD receptor (Designer Receptors Exclusively Activated by Designer Drug) in the *Trpm5*+ cells in which *Trpm5*-expressing cells were specifically activated upon clozapine N-oxide (CNO) administration), and *Trpa1*-DTR (mice that express the DTR in the *Trpa1*+ neurons in which *Trpa1*-expressing neurons were specifically ablated upon DT administration) mice models were used. WT mice were injected with inhibitors of AChRs mecamylamine (MEC) (nicotinic, 1mg/kg body weight, *i.p.)* and atropine (muscarinic, 1mg/kg body weight, *i.p.*). Next, these mice received Evans's blue (EB, 20 mg/kg, *i.v.*). After inhalation of 1, 10, or 20 mM denatonium, tracheas were explanted, and EB and neutrophil extravasation were estimated. Additionally, *Trpa1*-DTR were injected with (DT) on three consecutive days. *Trpa1*+ nerve-fiber depletion was confirmed by immunohistochemistry and real-time RT-PCR. Next, mice with depleted *Trpa1* sensory innervation received similar treatment to the mice with inhibited cholinergic signaling. In addition, Western blotting, RT-PCR, and immunohistochemistry were applied to investigate the occurrence of the TRPM5 channel in the sensory neurons. Moreover, neurons were isolated from WT mice and *Trpm5*-deficient mice to compare the EC_{50} response to the application of cinnamaldehyde (CA) and capsaicin, TRPA1 and TRPV1 agonists, respectively. Furthermore, *Trpm5*-DTR mice received a single dose of DT intratracheally (IT). DRG and JNC were explanted and dissociated for $[Ca^{2+}]$i imaging. Likewise, *Trpm5*-DREADD mice were sacrificed after inhalation of CNO. Then, the DRG and JNC were explanted and dissociated for $[Ca^{2+}]$i –

imaging. The sensitivity of sensory neurons in an acute infection model: mice from WT and *Trpm5*-KO were infected via the negative gram bacterium *Pseudomonas aeruginosa* was investigated using $[Ca^{2+}]i$ – imaging. On the other hand, WT and *Trpm5*-KO mice chronically infected with the bacteria *Rodentobacter heylii* were assessed in the same manner. Additionally, the effect of ACh on the response of JNC *Trpa1+* and *Trpv1+* sensory neurons was studied by applying ACh to freshly isolated neurons, and measuring the changes in the sensitivity to TRPA1 and TRPV1 agonists. AChRs inhibition led to a significant decrease in plasma extravasation and neutrophil recruitment compared to the group treated with a vehicle. In DT-treated *Trpa1*-DTR mice, RT-PCR demonstrated that the *Trpa1* and *Trpv1* expression was significantly down-regulated in neurons in both sensory ganglia. On the other hand, immunohistochemistry on DRG sections from these mice had a significant increase in the numbers of *Trpa1+* and *Trpv1+* sensory neurons. Additionally, the same neuronal sections demonstrated a significant loss in the positive labeling of CGRP and SP compared to the vehicle. Furthermore, tracheal wholemount preparations showed a significant difference between the DT-treated *Trpa1*-DTR and vehicle in the volume of CGRP and SP. As a result, DT-treated *Trpa1*tauGFP-DTR mice lacked EB extravasation and neutrophil recruitment after BC-stimulation. Additionally, we have found that the TRPM5 channel is completely absent in the sensory neurons innervating the lung. Western blotting using protein lysates of DRG and JNC and Immunohistochemistry from WT mice lacked TRPM5-labeling. RT-PCR using cDNA isolated from DRG and the JNC of WT and *Trpm5*-deficient mice resulted in a non-significant difference between *Trpa1* and *Trpv1* gene expression among both genotypes. Moreover, *Trpm5*-deficiency correlated with a higher sensitivity of both TRPV1 and TRPA1 to capsaicin and CA compared to the response in WT mice. Interestingly, specific depletion of the BC using the DT on the *Trpm5*-DTR mouse model led to a significant decrease in the EC_{50} for both capsaicin and CA compared to the WT. Dissociated neurons showed a significant difference in their sensitivity when BC were activated using CNO in the *Trpm5*-DREADD mouse model. The TRPA1 response to 200 µM CA was inhibited, while the TRPV1 showed significantly higher sensitivity to 50 nM capsaicin. This result was similar to the observed responses after BC activation via denatonium or in acute bacterial infection. Interestingly, mice with chronic infection exhibited a decrease only in the sensitivity of *Trpa1+* and not in the *Trpv1+* neurons. Remarkably, exposing the sensory neurons to ACh resulted in an inhibition of TRPA1 and activation of TRPV1. These effects were inhibited with the ACh receptors-inhibitors MEC and atropine as well as the nicotinic antagonist hexamethonium. Based on all these observations, we propose that the BC-induced protective neurogenic inflammation is needed to eliminate inhaled substances via neutrophil recruitment and it depends on the cholinergic transmission from BC to the sensory nerve fibers. Moreover, the TRPA1 and TRPV1 channels and their communications with AChRs must be further explored as a novel and attractive therapeutic target against neurogenic inflammation and acute pulmonary infections such as pneumonia.

CHAPTER 1: LITERATURE REVIEW

1.1 The respiratory system

The respiratory system's primary role is breathing: once the air is inhaled into the lungs, the oxygen is absorbed into the bloodstream and transported to the cells. On the other hand, exhaling the air expels carbon dioxide from the body. Gas exchange is facilitated by the respiratory system between the lungs and the bloodstream. pH is another parameter regulated via the respiratory system by controlling the amount of acidic carbon dioxide in the bloodstream. Furthermore, it acts as a barrier from harmful objects and microorganisms in which is an important protective function of the respiratory system.

The respiratory system is comprised of various components: the nasal cavity, the pharynx, the larynx, the trachea, and the lungs (Figure 1.1). The space inside the nose is called the nasal cavity. The air inside this space is warmed-up and humidified. Another important feature of the nasal cavity is that it is coved by ciliated epithelium that removes small particles before they reach the lung. The pharynx is a muscular tube that is divided into three parts (the nasopharynx, the oropharynx, and the laryngopharynx) connecting the nasal cavity cavities to the larynx. The larynx plays together with the pharynx an important role in swallowing and breathing. The trachea connects the larynx to the lungs and is lined with an epithelial layer containing mainly ciliated and mucus producing cells. The main organs in the respiratory system are the lungs, located in the chest. In humans, the right lung is divided into three lobes while the left lung has two. Moreover, gas exchange is the responsibility of the lung. Air enters the lung through the bronchi, leading to bronchioles that end in surfactant-lined air sacs containing the alveoli.

Furthermore, the lung is innervated by postganglionic sympathetic and parasympathetic nerve fibers which regulate the breathing (Coburn and Tomita, 1973; Wood, 1984; Dey, Mitchell and Coburn, 1990). The sympathetic nervous system promotes bronchodilation while the parasympathetic nervous system promotes bronchoconstriction (widening and narrowing the airways, leading to an increased or decreased respiratory rate, respectively). The postganglionic sympathetic neurons that provide innervation to the lungs originate from the stellate and thoracic sympathetic chain ganglia T2-T4. On the other hand, the ones that supply the trachea are derived from the stellate and superior cervical ganglia. (Kummer *et al*., 1992). The parasympathetic fibers originate from the vagus nerve which they synapse with postganglionic neurons located within the lungs. The neurotransmitters released from the postganglionic sympathetic and parasympathetic neurons are norepinephrine and ACh, respectively (Figure 1.2). On the other hand, in humans, the cell bodies of the sensory nerve fibers are located in the dorsal root ganglia (DRG), and in the nodose and jugular ganglion (Silva, Czeisler and Otero, 2021).

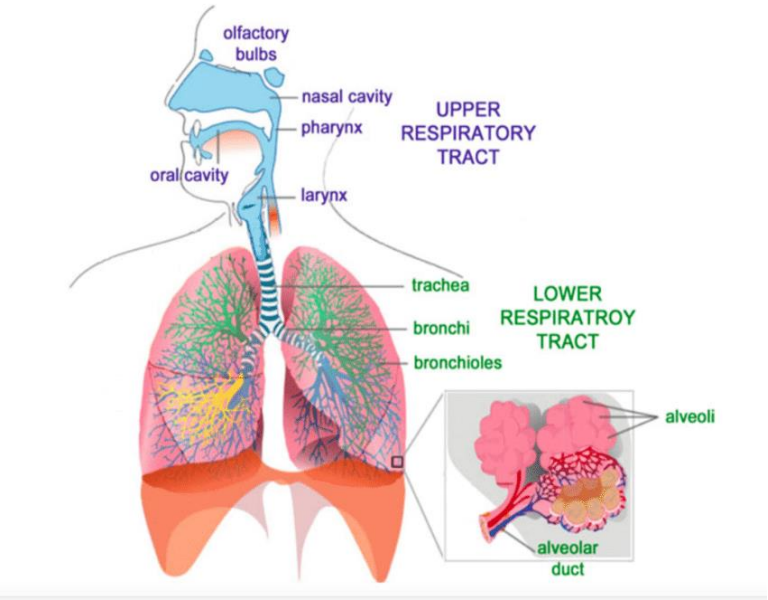

Figure 1.1: The respiratory system (Image reprinted with permission from Staerz, Weimar and Barsan, 2016)

1.2 The nervous system

The nervous system in humans consists of a complex network of specialized cells. The main role of these cells is to transmit signals between the different body parts to control and coordinate the body's functions. Mostly, it consists of two main components: the central nervous system (CNS) and the peripheral nervous system (PNS). The CNS is the body's central processing unit, composed of the brain and the spinal cord. The PNS is made out of the nerves extending from the CNS to other parts and organs of the body. Two subdivisions of the PNS are the autonomic nervous system (ANS) and the somatic nervous system (SNS). The latter receives sensory information from the environment external to the body and controls voluntary movements. The ANS, on the other hand, controls spontaneous functions such as digestion, heartbeat, and breathing. Additionally, the sensory and motor fibers include large numbers of neuronal cell bodies outside the CNS and are arranged into collections called ganglia. The axons of the cell bodies project to other body organs such as the muscles and the airways.

The airway tone is believed to be a function of the relative activities of cholinergic and adrenergic intervention (Wood 1984; Coburn and Tomita 1973; Dey, Mitchell, and Coburn 1990). Furthermore, the airways and lungs are innervated densely by nerves. For example, in a human's trachea, there is one axon per hundred muscle cells (Daniel et al. 1986). The airway mucosa from the nares to the bronchioles as well as the alveolar epithelium contain sensory nerve endings responding to pollutants and inhaled irritants (L. Y. Lee and Yu 2014). Vagal nerve fibers can be distinguished by their sensitivity to either mechanical

(mechanosensors) or chemical (chemosensors) stimuli. Chemosensors are often referred to as nociceptors and they are silent in normal airways. However, when they are repeatedly or prolonged activated by noxious stimuli, they can be sensitized (Leroux et al. 2020; Nassenstein, Krasteva-Christ, and Renz 2018). Nociceptors can be either C-fibers or Aa and Ad-fibers, depending on their myelination, size, and conductivity (Eftekhari et al. 2013) (Figure 12).

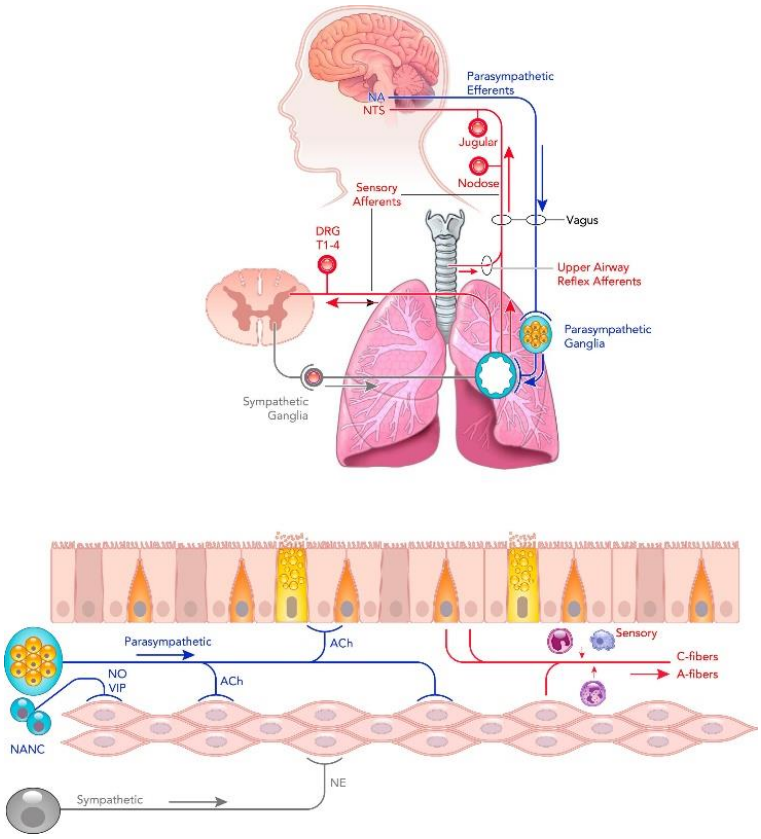

Figure 1.2: The sensory innervation of the respiratory system (Image reprinted with permission from Kistemaker and Prakash, 2019)

1.3 The immune system

The immune system is an enormous network consisting of lymphoid organs and tissues, and immune cells that defend the body against harm (infection and disease). The immune system is composed of two major components: adaptive and innate immunity (Soderberg *et al.*, 2005) (Figure 1.3). The main function of the adaptive immune system is the recognition of antigens, followed by the production of antibodies. Furthermore, the adaptive immune system can remember past infections which enables the body to respond faster and more efficiently to previously encountered pathogens. The functions of the innate immune system will be discussed below.

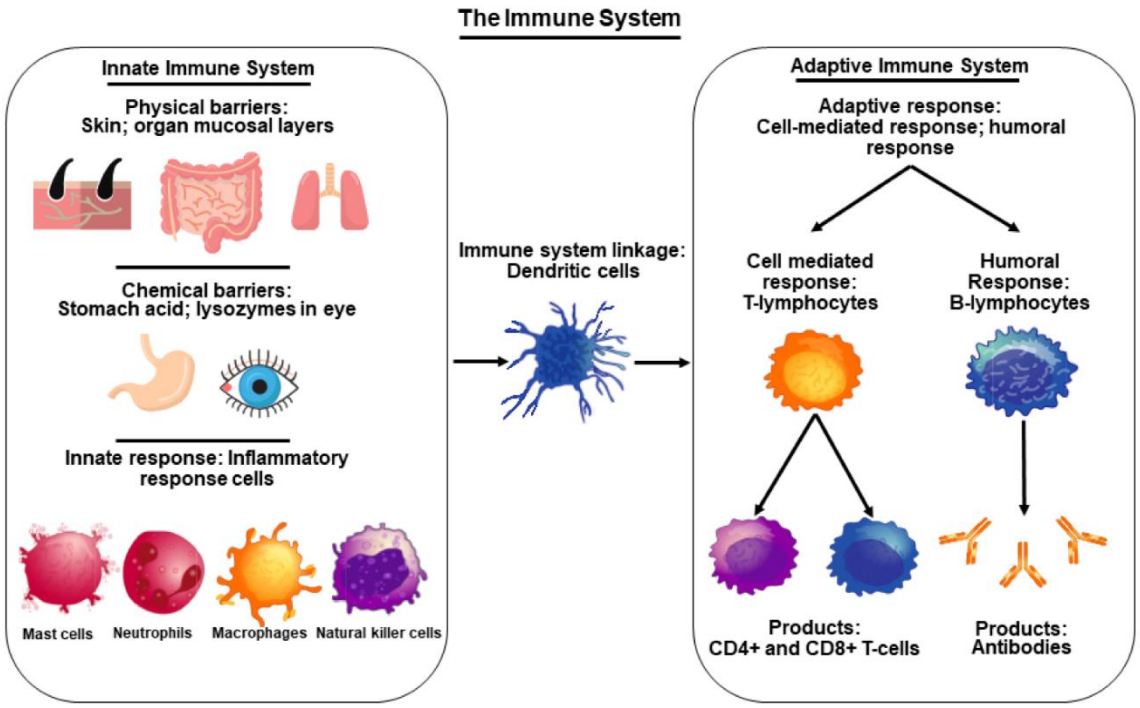

Figure 1.3: An illustration of the immune system showing innate and adaptive immune system components
(Image reprinted with permission from Manna, Gray and Hemachandra Reddy, 2022)

1.3.1 Innate immunity

Innate immunity is the first line of defense against infections and harmful substances (Ezekowitz and Hoffmann, 2002). This type of immunity exists from birth and doesn't require previous exposure to recognize a harmful substance. Innate immunity consists of chemical and physical barriers such as the skin, the mucus lining epithelial tissues, secreted enzymes, tears, and cytokines (Figure 1.3). Each fragment of innate immunity carries an important role in defending the body against invaders. For example, the initiation of coughing and sneezing is an important part of innate immunity (Rogers, 1997). This process helps to clear large particles that settled in the upper nasopharynx and laryngeal regions. The epithelial layer beneath the mucus layer is also important for acting as a chemical shield against pathogens. Adding to that, due to the mucociliary clearance, small particles and bacteria in the lower respiratory tract are captured and expelled (Knowles and Boucher, 2002). This mechanical clearance of mucus includes the ciliary beat regulation and the mucus transport (Knowles and Boucher, 2002). Additionally, antimicrobial components in the epithelial lining fluid such as surfactant proteins facilitates the recognition of harmful agents by the innate immune cells (Bals, Weiner and Wilson, 1999; Driscoll, Brody and Kollef, 2007). Epithelial cells

also contribute to innate immune defense and some cells can sense and regulate the volume of liquid on their surfaces, while others can regulate mucus transport rates (Knowles and Boucher, 2002).

1.4 Inflammation, pain, and neurogenic inflammation

Inflammation and pain are closely interconnected processes. Inflammation occurs when the immune system reacts to different insults such as infections, irritants, cancer, and tissue injury. It is defined as the interaction between immune cells and non-immune cells, followed by a collection of responses including chemical mediators such as cytokines, nitric oxide, growth factors, and eicosanoids (Baluk *et al.*, 1999; Liu *et al.*, 2004; Grando *et al.*, 2015; Talbot, Foster and Woolf, 2016). The normal inflammatory response is divided into three different phases: acute, sub-acute, and resolution (Ballaz and Mulshine, 2003). These phases contribute to recovery using different mechanisms, especially in the case of chronic inflammation. The acute phase is characterized by increased capillary permeability and local vasodilation accompanied by neutrophil recruitment (Quie, 1986; Vane *et al.*, 1994). The sub-acute phase is when phagocytotic and leukocytic infiltration happens. The result of this process fluctuates between erythema, edema, and pain (Ballaz and Mulshine, 2003).

Scientists think of pain as an unpleasant protective sensation resulting from actual tissue damage. Pain could help avoid invaders and harmful objects. Additionally, pain can be considered a facilitator of healing inflammation accompanied by damaged tissues (Matsuda, Huh and Ji, 2019a). However, chronic pain is not useful and is a great health concern (Matsuda, Huh and Ji, 2019). During the inflammation inflammatory mediators such as cytokines, chemokines, and prostaglandin activate sensory afferents inducing pain. Nociceptors involve immune cells in a neuro-immune interaction. As a result, the response and regulation of immune cells occur.

In neurogenic inflammation, the detection of irritants results in the activation of sensory nerves, notably C-fibers, which transmit the sensation of potentially noxious stimuli to the brain, and leads to the release of neurogenic peptides such as the calcitonin gene-related peptide (CGRP), and tachykinins such as substance p (SP) (Rogers, 1997). The proximate location of sensory fibers to epithelial cells such as in the trachea and lung suggests a potential communication between them and a potential contribution to the development of neurogenic inflammation and its pathophysiology (Bertrand and Geppetti, 1996; Rogers, 1997). Once the sensory peptides are released, swift plasma extravasation and vasodilation happen, followed by the recruitment and infiltration of the tissue with immune cells (Mathison and Davison, 1993). Moreover, pain is a well-known companion to neurogenic inflammation after stroke, tissue trauma, and surgery (Balestrini *et al.*, 2021a).

1.5 CGRP and SP

Small protein molecules such as SP and CGRP which are released from primary neurons are called neuropeptides; such peptides are important on behalf of neurogenic pain and the generation of hyperalgesia. The role of CGRP and SP in pain development is not yet fully understood. Different studies illustrated that when the innervating sensory neurons are stimulated mechanically or chemically, CGRP is steadily released to maintain central sensitization including cross-signaling between neurons and glial cells (Greco *et al.*, 2008; Seybold, 2009). Scientists have found that CGRP is mostly involved in arterial vasodilatation that leads to an increase in blood flow. A link to the intracellular increase in cyclic adenosine monophosphate (cAMP) has been established for the vasodilation effect. Yet, CGRP does not activate the sensory afferents directly. Instead, it might up-regulate the production of pro-nociceptive molecules and receptor proteins (Levy, Burstein and Strassman, 2005; Li, Vause and Durham, 2008; Russell *et al.*, 2014; Messlinger, 2018). On the other hand, stimulation of plasma extravasation was found to be the main function of SP along with other neurotransmitters such as bradykinin (Figini *et al.*, 1995, 1997; Seybold, 2009). Additionally, SP plays a role in the very early response to pain (Greco *et al.*, 2008; Seybold, 2009). Mood regulation, nausea, and the body's inflammatory response are other physiological processes where SP is involved. The use of SP receptor antagonists has been found as a healing potential in inflammatory illnesses such as asthma (Rogers, 1997; O'Connor *et al.*, 2004).

1.6 Transient Receptor Potential (TRP) Channels

Transient Receptor Potential (TRP) channels are a group of evolutionary conserved essential membrane proteins. They are of vital significance for human health and are involved in many physiological processes. Each TRP channel has a role as a physiological sensor (Kaske *et al.*, 2007; Venkatachalam and Montell, 2007b; Greka and Mundel, 2012; Tsai *et al.*, 2021) e.g in taste, touch, and pain perception, or in thermo-sensation. The superfamily of the TRP channels consists of five family groups: TRPV, TRPA, TRPM, TRPN, and TRPC (Figure 1.4). Additionally, scientists have discovered two more subfamilies: TRPP and TRPML (Venkatachalam and Montell, 2007a; Moran, 2018). TRP channels are a class of cationic channels that act by altering membrane potential or intracellular calcium concentration (Saimi and Kung, 2002). They are notable in their diversity with regard to the activation mechanisms and their ion selectivity.

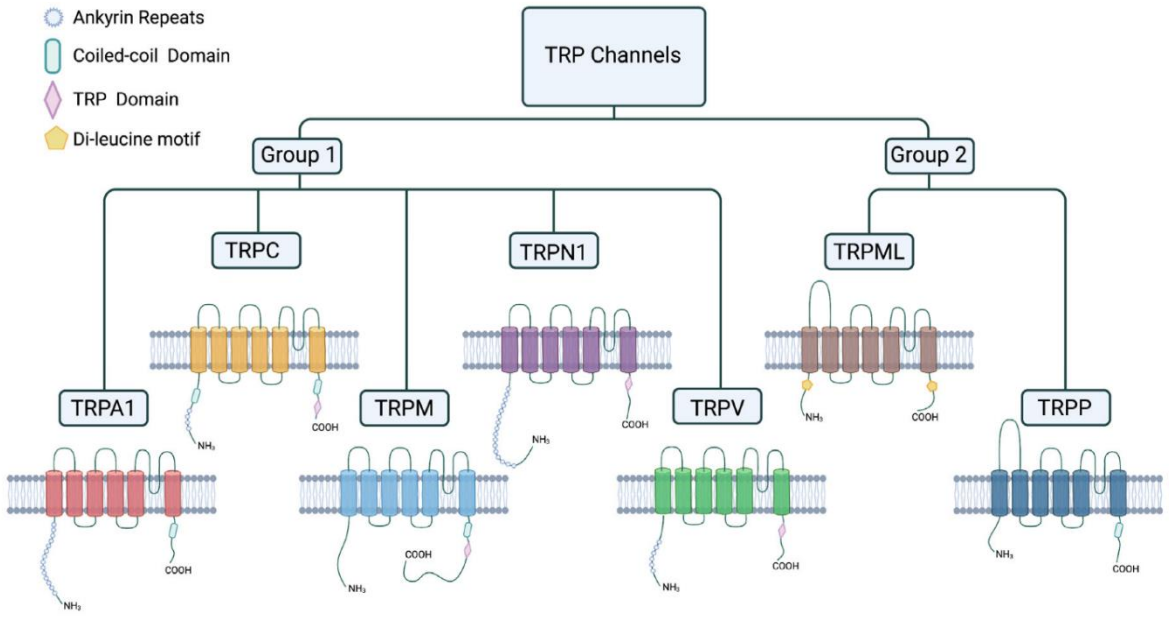

Figure 1.4*:* Schematic illustration of the subfamilies of TRP channels showing their structural domains (Image reprinted with permission from Hellenthal *et al*., 2021)

Dysfunction of TRP channels has implications in many diseases such as chronic pain, cancer, and neurogenic disorders, making them a very important research and therapeutic target. However, concerning their abundance in either the airways or in the sensory nerves, this study focused on three different subtypes from three different TRP families: TRPA1, TRPV1, and TRPM5.

1.6.1 The transient receptor potential vanilloid 1 channel (TRPV1)

TRPV1 (transient receptor potential vanilloid 1) is a member of a big TRP subfamily composed of six different subtypes, and all are named accordingly. This subfamily has a significant role in thermosensation, osmosensation, mechanosensation, and calcium uptake. Members of the TRPV subfamily function as tetrameric complexes with each subunit containing six N-terminal ankyrin repeats (Dhaka, Viswanath and Patapoutian, 2006; Ramsey, Delling and Clapham, 2006). Additionally, all TRPV subfamily members are highly permeable to calcium ions (Liu *et al.*, 2007; Hsu and Lee, 2015). TRPV1 is considered the most studied member of this group. It can be activated via high temperatures, noxious stimuli, pH changes, spicy compounds, and some cytokines such as TNF-a. Upon activation, Ca^{2+} and Na^{+} flow into the cell causing the activation of different pathways.

TRPV1 protein is distributed all over the human body. It has been found in many organs such as the heart, the lung, the intestine, as well as in sensory neurons. On the other hand, TRPV1 is implicated in various

diseases and pathological conditions, such as autoimmune syndromes, neuropathic pain, chronic pain, and inflammation (Tränkner *et al.*, 2014; Juárez-Contreras *et al.*, 2020). The exact signaling pathway of TRPV1 is not fully understood, and thus, research is needed to explore this issue in health and disease. Additionally, there is evidence that TRPV1 may become a therapeutic target for different diseases. For example, recent studies in mice resulted in longer lives and better metabolism when the *Trpv1* gene was knocked out (Lee *et al.*, 2015; Ferdowsi *et al.*, 2021).

1.6.2 The transient receptor potential ankyrin 1 channel (TRPA1*)*

The ankyrin subfamily consists of seven subfamilies. Among them, TRPA1 is the most abundant across animals and is considered the only member of the mammalian TRP ankyrin subfamily. TRPA1 is a unique Ca^{2+}-permeable and non-selective cation channel. Similar to other TRP channels, TRPA1 has a cytosolic N-terminal domain and a trans-membrane domain containing six trans-membrane helices with a trans-membrane loop and a cytosolic C-terminal domain. A robust influx of cations such as Ca^{2+} and Na^{+} happen as a result of TRPA1 activation. Substances such as acrolein, ozone and chlorine, and spicy substances such as mustard oil, bacterial lipopolysaccharides and CA are all activators of the channel. Similar to the TRPV1 channel, TRPA1 is abundant in the nociceptor sensory neurons. TRPA1 has been reported to be involved in pathological and physiological conditions including pain, cold, and damage sensation (Meseguer *et al.*, 2014; Kamei *et al.*, 2018; Wang *et al.*, 2019). The activation of the TRPA1 channel leads to pain, sneezing, coughing, and respiratory depression (Shapiro *et al.*, 2013; Grace *et al.*, 2014; Achanta and Jordt, 2020). *Trpa1*-knocked-out mice appeared normal in most physical functions. Nevertheless, a study that used these knockouts showed physical hypersensitivity compared to the WT (Bodkin *et al*., 2014).

1.6.3 The transient receptor potential melastatin 5 channel (TRPM5*)*

As the name suggests, the TRP melastatin (TRPM) subfamily is another subfamily belonging to the TRP group of cation channels. With eight subtypes (M1-M8), the first-ever cloned TRPM channel was the TRPM1 of drosophila in 1989 (Montell and Rubin, 1989). Each subtype consists of six trans-membrane domains, which together form a pore to allow the passage of ions from side to side for the cell membranes, such as the cell wall. In mammals, TRPM channels are essential for various physiological processes, including hearing (Venkatachalam and Montell, 2007b), thermo-sensation, lung function, and cytokine production, among others.

The transient receptor potential M5 channel (TRPM5) is expressed in secreting tissues such as the intestine, the trachea and the taste buds, with high expression. Furthermore, the TRPM5 channel role involves the transduction of bitter, umami, and sweet taste signals (Lin *et al.*, 2008; Turner and Liman, 2022). In mice,

the *Trpm5* gene encodes a protein of 1.158 amino acids. Additionally, scientists suggested that the TRPM5 protein has 6 trans-membrane domains that function as a tetramer (Owsianik *et al.*, 2006). However, since the signaling pathway of the TRPM5 channel involves taste, the activation of GPCRs stimulates phospholipase C (PLC) β2, which leads to the breakdown of PIP2 (phosphatidylinositol bisphosphate) into DAG (diacylglycerol) and IP3 (inositol triphosphate), leading to the discharge of calcium ions from their stores inside the cell (Kaske *et al*., 2007). The intracellular Ca^{2+} change directly activates TRPM5. The activation of the TRPM5 channel can also be regulated by voltage and temperature (Ramsey, Delling and Clapham, 2006). It is worthy to mention that the TRPM5 channel is found in the airway epithelia in BC and is very important in immunity and neurogenic inflammation (Kaske *et al.*, 2007; Hollenhorst *et al.*, 2019; Perniss *et al.*, 2020). However, the exact signaling pathway is still not completely clear.

1.7 Taste perception and bitter taste receptors

Taste perception is the ability to detect different flavors through taste buds. The understanding of chemosensory sensation is highly essential in terms of obesity and immunology. Compounds that mammals could taste can be distinguished into five basic groups: sweet, bitter, sour, salt, and umami. Each taste is perceived by a specific receptor located on the taste buds.

Bitter taste receptors in humans (T2Rs) are referred to as twenty-five members of the G- protein-coupled receptor (GPCR) superfamily. GPCR family is a group of important transmembrane receptors found in all organisms. They play a role in communication between the cell and its environment. G- proteins are divided into three different subunits, known as alpha, beta, and gamma each receptor is sensitive to a different range of bitter compounds (Avau *et al.*, 2015). G-proteins, such as Gαi, Gαs, and Gαq. For example, Gαi is important for sensing bitter and sweet tastes by slowing down a process called adenylate cyclase and lowering levels of a molecule called cAMP. On the other hand, Gαs helps us detect sweet and umami tastes by speeding up adenylate cyclase and increasing cAMP levels. Lastly, Gαq helps us sense sour and salty tastes by triggering another process called phospholipase C, which releases calcium ions (Ahmad & Dalziel, 2020; Ferry et al., 2002; Kamato et al., 2015; Shukla, 2016).

Researchers have rounded the age of the mammalian taste cells to as short as ten days, suggesting that for proper signal transduction, nerve terminals have to detach from an aging cell to a new developing taste cell (Beidler and Smallman, 1965; Farbman, 1980). On the other hand, taste receptor in mice (TasR) cells are not only present in the tongue. Many of them are localized in different epithelial organs as well, such as in the gut and the trachea. Scientists have found many chemically distinct classes of bitter-tasting compounds. However, given the wide variety of these compounds, the use of different TasR and different transduction pathways can be expected. Interestingly, about 40 bitter taste receptors have been cloned, some of which

are expressed in the same cell. The abundance of these receptors is very important as they function as a sensory warning against the ingestion of toxic and poisonous substances. For example, the activation of T2R and its downstream transduction components including the TRPM5 channel is very important for initiating neurogenic inflammation and the recruitment of immune cells in the trachea (Hollenhorst *et al*., 2019, 2022). When a bitter compound binds to a bitter taste receptor in mice (Tas2R) on a taste bud, the downstream signaling pathway of the gustatory G-protein gustducin is triggered (Caicedo *et al*., 2003). Furthermore, Tas2Rs were discovered in epithelial cells such as ciliated cells (Sha *et al*., 2009), in BC (Krasteva *et al*., 2011) and in nasal solitary chemosensory cells (SCC, Tizzano *et al*., 2010). This suggested instantly that these receptors play a role in sensing foreign particles and bitter substances secreted from pathogens such as QSM and endotoxins (Hollenhorst *et al*., 2019)

1.8 Brush cells (BC)

Brush cells (BC) are considered a specialized tuft cell population (Figure, 1.5). BC were first demonstrated sixty years ago in the rat mucosal epithelium (Rhodin and Dalhamn, 1956). They are broadly spread in the epithelial organs, such as the trachea's epithelium and the upper airway's nasal cavity (Bezençon *et al*., 2008; Deckmann *et al*., 2015; Kummer & Deckmann, 2017; Ualiyeva *et al*., 2020). Phenotypically, these cells have a distinctive pear shape distinguished by their brush or tuft-like apical exterior, which is formed by densely thick microvilli (Reid *et al*., 1970).

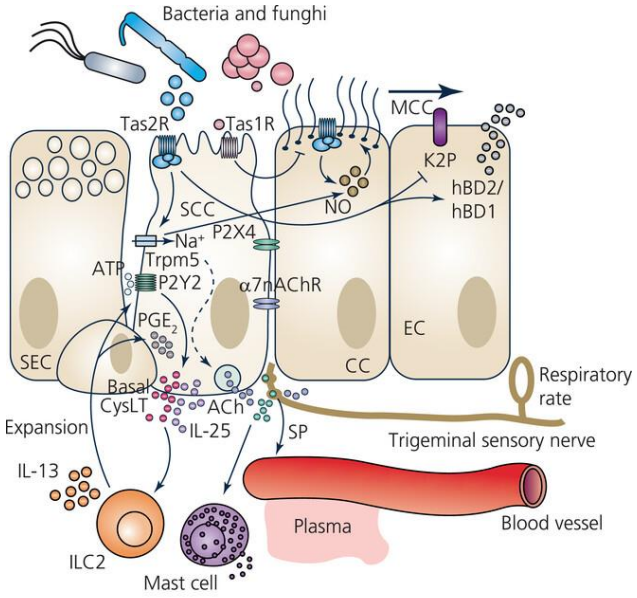

Figure 1.5: Graphic illustration of a tuft cell (BC), showing its downstream activation and ACh release (Image reprinted with permission from (Hollenhorst *et al*., 2023*)*

Initially, the function of BC wasn't clear. Nevertheless, a chemosensory function for BC was guessed because of their proximity to the non-myelinated sensory nerve fibers. Finally, in our recent studies we could show that BC have a role in detecting pathogens and harmful objects, as well as initiating immune responses (Hollenhorst *et al.*, 2019, 2022). On the other hand, tuft-2 cells express high levels of Th2 related cytokines, (Haber *et al.*, 2017). Tracheal BC have an implication in the development of respiratory diseases such as asthma and COPD.

1.9 Acetylcholine and cholinergic receptors

Acetylcholine (ACh) is a neurotransmitter that plays a very important role in the nervous system. In the cholinergic nerves, ACh is manufactured in the terminals of nerves from choline and acetyl CoA. This reaction is catalyzed by choline acetyl-transferase. Once a new ACh is formed, it is put in vesicles in the cytosol. The vesicles then need an action potential to reach the axon terminus, and then to be freed into the synaptic cleft. ACh then binds to the AChRs (Colquhoun and Patrick, 1997; Stauderman *et al.*, 1998; Krasteva *et al.*, 2012), either muscarinic (mAChR) or nicotinic (nAChR). The enzyme acetylcholinesterase (AChE) rapidly decreases its concentration from the presynaptic terminal (Wonnacott, 2014; Bader and Diener, 2015; Lottig *et al.*, 2019). Additionally, evidence of ACh synthesis and compounds involved in the cholinergic system in non-neuronal cells was confirmed in many cell types such as B cells, macrophages and dendritic cells (Reardon *et al.*, 2013), T cells (Rinner and Schauenstein, 1993; Rosas-Ballina *et al.*, 2011) and epithelial cells (Moffatt and Franks, 2004; Kummer, Lips and Pfeil, 2008b; Bader *et al.*, 2014; Kummer and Krasteva-Christ, 2014; Bankova *et al.*, 2018).

1.9.1 Muscarinic receptors

Muscarinic AChRs are a family of receptors consisting of five different subtypes (M1- M5). Each bind to ACh, and they are considered G-protein-coupled receptors. They are composed of a single polypeptide with seven regions arranged in a hydrophobic α-helix spanning the cell membrane seven times (Hulme, Birdsall and Buckley, 1990a). Muscarinic AChR are found in the CNS and PNS. On the other hand, when ACh bounds to the mAChR, the G protein, which is composed of α, β, and γ subunits, changes its conformation. This causes the α subunit to release the molecule guanosine diphosphate that is natively bound to the receptor, allowing diverse possibilities for the function of mAChR in a mammal's physiology (Hulme, Birdsall and Buckley, 1990b; Kabbani *et al.*, 2013). In addition to ACh, muscarine and other choline esters, for instance, bethanechol and pilocarpine, are considered mAChR agonists. Conversely, atropine, which is used as an inhibitor of the heart's excessive vagal activation, is considered a mAChR antagonist.

In the airways, mAChRs play an important role in regulating bronchoconstriction, mucus secretion, and airway inflammation (Heike Schlenz *et al.*, 2010). The activation of mAChRs lead to contraction of airway

smooth muscle, causing a difficulty in breathing and narrowing of the airways. Furthermore, mAChRs on submucosal glands increase mucus secretion leading to airway obstruction. On the contrary, in in the presence of inflammation, mAChRs have broncho dilatory effects (Konishi *et al*., 2019; Meurs *et al.*, 2013).

1.9.2 Nicotinic receptors

According to their name, nicotinic receptors (nAChRs) bind to nicotine as their main agonist; this differentiates them from the mAChRs. nAChRs are considered pentametric-neurotransmitter-gated ion channels, in charge of the fast excitatory neurotransmission in the peripheral and central nervous systems. Furthermore, nAChRs are activated by ACh, nicotine, and structurally-related agonists (Zhang, and Berg, 1994; Puskar *et al.*, 2011). The activation of nAChRs had an impact on multiple neurological disorders, making them a sought-after target for therapeutic research. nAChRs can be found in the central and peripheral nervous systems, the skeletal muscles and the adrenal glands, where they mediate the release of adrenaline. Moreover, nAChRs open to allow the flux of sodium, calcium, and potassium ions into the cells after activation (Kabbani *et al*., 2013). However, three main classes of nAChRs were established in mammals (Papke *et al.*, 2008): muscle-type receptors, homomeric neuronal receptors, and heteromeric neuronal receptors. Each nAChRs is made out of five subunits arranged around a pseudo-axis of symmetry: α1- α10, β1- β4, γ, δ, and ε (Millar, 2003; Moroni *et al.*, 2006). Additionally, mecamylamine (MEC) is considered a general antagonist for nAChRs. It is partially selective to β4-containing nAChRs (Papke *et al.*, 2008; David *et al*., 2010). Though MEC was found to be a TRPA1 inhibitor, scientists found concentrations of 5 mM MEC to inhibit TRPA1 currents pre-activated with nicotine in a human TRPA1 stable transfected cell line (Talavera *et al.*, 2009).

The presence of nAChRs in the respiratory system has been described and established in many studies, including (Krasteva *et al*.,2011). This study identified the presence of nAChRs in the epithelial cells, smooth muscle cells and nerve endings in trachea. These receptors are involved in the regulation of respiration and their activation can affect ion transport in the tracheal epithelium. For instance, denatonium inhibits sodium channels via the bitter signaling cascade and Gα signaling, resulting in decreased ion transport and contributing to fluid homeostasis regulation via BC activation (Hollenhorst et al., 2022). Similarly, in murine airways, nAChRs activate ion transport and mediate nicotine-induced current changes (Kumar et al., 2020).

The aims of the thesis:

In this thesis, we explored the involvement of sensory nerve fibers and cholinergic receptors in the initiation of neurogenic inflammation in the airways. Additionally, we examined the occurrence of the TRPM5 channel in the dorsal root ganglia (DRG) and the jugular nodose complex (JNC). Furthermore, we studied the impact of the TRPM5 channel activation and ACh derived from BC on the sensitivity of TRPV1+ and TRPA1+ sensory neurons innervating the airways.

CHAPTER 2: MATERIALS AND METHODS

2.1 Materials

This section of the thesis enumerates the materials utilized in the research such as chemicals, solutions, antibodies, bacteria, and specialized equipment.

2.1.1 Chemicals

The chemicals used in this study were obtained from the companies listed in Table 1 below.

Chemical	**Company**
A 967079	Tocris Bioscience Abingdon, UK
Acetylcholine chloride	Sigma Aldrich, Taufkirchen, Germany
Adenosine 5'-triphosphate	Sigma Aldrich, Taufkirchen, Germany
Alpha-beta methylene adenosine	Sigma Aldrich, Taufkirchen, Germany
Atropine	Sigma Aldrich, Taufkirchen, Germany
Capsaicin	Sigma Aldrich, Taufkirchen, Germany
Cinnamaldehyde	Sigma Aldrich, Taufkirchen, Germany
Collagenase	Sigma Aldrich, Taufkirchen, Germany
Complete Mini, EDTA–free	Roche, Edenkoben, Germany
Denatonium benzoate	Sigma Aldrich, Taufkirchen, Germany
D-glucose	Sigma Aldrich, Taufkirchen, Germany
Dispase	Roche, Edenkoben, Germany
DMEM	Gibco, Dreieich, Germany
DMEM F12	Gibco, Dreieich, Germany
DMPP	Sigma Aldrich, Taufkirchen, Germany
EDTA	Sigma Aldrich, Taufkirchen, Germany
Evans’s blue	Sigma Aldrich, Taufkirchen, Germany
Fura-2, AM	Invitrogen, now: Thermo Fisher Scientific, Waltham, MA, USA
G-418 disulphate salt	Sigma Aldrich, Taufkirchen, Germany
Gallein	Tocris Bioscience, Abingdon, UK
Glycerol	Merck, Darmstadt, Germany
HBSS	Gibco, Dreieich, Germany
Heparin - natrium	Braun, Hessen, Germany
HEPES	Roth, Hessen, Germany
Hexamethonium chloride	Sigma Aldrich, Taufkirchen, Germany
Isoflurane	Piramal, Hallbergmoos, Germany
KCL	Merck, Darmstadt, Germany
Ursotamin	Serumwerk, Bernburg, Germany

KH_2PO_4	Merck, Darmstadt, Germany
Laminin	Gibco, Dreieich, Germany
LE agarose	Biozym, Hessisch Oldendorf, Germany
L-glutamine	Gibco, Dreieich, Germany
Lipofectamine 2000	Invitrogen, now: Thermo Fisher Scientific, Waltham, MA, USA
Solution A	Merck, Darmstadt, Germany
Solution B	Merck, Darmstadt, Germany
Mecamylamine-hydrochloride	Sigma Aldrich, Taufkirchen, Germany
Methanol	VWR, Hamburg, Germany
$MgCl_2$	Merck, Darmstadt, Germany
MIDORI Green	NIPPON Genetics EUROPE, Düren, Germany
MOWIOL	Sigma Aldrich, Taufkirchen, Germany
NaCl	Gruessing GmbH, Filsum, Germany
NaCl 0.9%	Braun, Hessen, Germany
NaCl 0.9% sterile	Fresenius Kabe Deutch Land GmbH, Homburg, Germany
Nuclease-free water	Thermo Fisher Scientific, Waltham, MA, USA
Optimum	Gibco, Dreieich, Germany
Paraformaldehyde	Merck, Darmstadt, Germany
PBS	Gibco, Dreieich, Germany
PLL	Sigma Aldrich, Taufkirchen, Germany
Pluronic	Sigma Aldrich, Taufkirchen, Germany
Ponceau S	Roth, Hessen, Germany
Potassium chloride	Sigma Aldrich, Taufkirchen, Germany
Silicone solution	Serva, Heidelberg, Germany
Sterile H_2O	Fresenius Kabe Deutch Land GmbH, Homburg, Germany
Super signal	Thermo Fisher Scientific, Waltham, MA, USA
ECL Western blot substrates	Thermo Fisher Scientific, Waltham, MA, USA
TEMED	Bio-Rad, Hertfordshire, UK
TRIS	Roth, Hessen, Germany
Tris-base	Sigma Aldrich, Taufkirchen, Germany
Tris-HCL	Roth, Hessen, Germany
Triton X 100	Roth, Hessen, Germany
Trypsin 0.05% - EDTA -1X	Gibco, Dreieich, Germany
Tween	Sigma Aldrich, Taufkirchen, Germany
Xylazine 20mg/ml	WDT, Garbsen, Germany

Table 1: List of chemicals that was used during the study, along with their manufacturing companies.

2.1.2 Solutions

The solutions employed in this research, including those for western blotting, calcium imaging, and cell culture, are listed in this section of the thesis.

2.1.2.1 Western blotting

The solutions used for Western blotting are listed in Table 2 below.

RIPA buffer (pH ~7.4)	HEPES	2.38 g
	EDTA	0.93 g
	NaCl	4.38 g
	SDS	0.5 g
	Sodium deoxycholate	2.5 g
	TritonX-100	1%
Coomassie 0.1%	Acetic acid 100%	92 ml
	Brilliant blue G250	2.5 g
	dd H2O	454 ml
	Isopropanol	454 ml
Ponceau S	dd H2O	100 ml
	Ponceau S	0.5 g
	Trichloroacetic acid	3 g
10% Gel	10% APS	80µl
	20% SDS	75 µl
	2M TRIS/ HCl, pH ~ 8.8	2,8 ml
	30% Acrylamide	5,0 ml
	dd H2O	7,2 ml
	TEMED	7,5 µl
Stacking gel	30% Acrylamide	0,5 ml
	10% APS	40 µl
	20% SDS	25 µl
	2M TRIS/HCl, pH ~6.8	0,625 ml
	dd H2O	3,85 ml
	TEMED	5,0 µl
10x Running buffer	0,25M TRIS	30 g
	1,92M Glycine	144 g
	dd H2O	1000 ml
	SDS	10 g
1x Running buffer (pH ~8.3)	10x Running buffer	100 ml
	dd H2O	900 ml
TBST (pH ~7.4)	dd H2O	2000 ml
	NaCl	5.8 g
	Tris- base	0.4 g

	Tris- HCL	2.68 g
	tween	2 ml
10x Transfer buffer	dd H2O	1000 ml
	Glycine	144 g
	Tris-base	30.3 g
1x Transfer buffer (pH ~8.3)	10x Transfer buffer	100 ml
	dd H2O	700 ml
	methanol	200 ml

***Table 2*:** List of solutions used for Western blotting.

2.1.2.2 Immunohistochemistry and Tissue Reservation

The solutions used in this study for immunohistochemistry and tissue reservation are listed in Table 3 below.

Solution A (0.2 M)	dd H2O	1000 ml
	NaH2Po4 x 2H2O	31.2 g
Solution B (0.2 M)	dd H2O	1000 ml
	NaHPo4 x 2H2O	35.6 g
4% PFA (pH ~7.4)	Paraformaldehyde	4 g
	Phosphate buffer	100 ml
0.2 M Phosphate buffer PB (pH ~7.4)	dd H2O	500 ml
	Solution A 0.2 M	115 ml
	Solution B 0.2 M	385 ml
PVP	PVP	25 g
	dd H2O	1000 ml
	NaCl	9 g
	Procaine hydrochloride	5 g
Histo-block solution 1 (pH ~7.4)	0.1% BSA	0.1 g
	0.5% Tween	0.5 ml
	10% Horse serum	10 ml
	PBS	89.4 ml
Histo-block solution 2 (pH ~7.4)	0.03% Triton X	30 µl
	10% Bovine serum	10 ml
	PBS	90 ml
10x PBS (pH ~7.4)	dd H2O	923.3 ml
	NaCl	44.8 g
	Solution A 0.2 M	57.5 ml
	Solution B 0.2 M	19.2 ml

PBS-S (pH ~7.4)	10x PBS	100 ml
	NaCl	44.8 g
Zamboni	0.2 M phosphate buffer	500 ml
	37% formaldehyde	50 ml
	dd H2O	300 ml
	Picric acid	150 ml

Table 3: List of solutions used for immunohistochemistry and tissue reservation.

2.1.2.3 Calcium Imaging

The solutions used in this study for calcium imaging are listed in Table 4 below.

Tyrode 1 (pH ~7.4)	Glucose	198.17 g
	HEPES	238.3 g
	KCl	1 g
	$MgCl_2$	1 g
	NaCl	58.44 g
	Sodium pyruvate	0.1 g
Tyrode 3 (pH ~7.4)	1M $CaCl_2$	0.8 ml
	1M KCl	0.5 ml
	1M $MgCl_2$	0.1 ml
	Glucose	0.19817 g
	HEPES	0.2383 g
	NaCl	0.75972 g
	$NaHCO_3$	0.5 ml
	Sodium pyruvate	10 ml
Locke buffer (pH ~7.4)	$CaCl_2$	0.1615 g
	dd H2O	1000 ml
	Glucose	1.81 g
	KCl	0.418 g
	$MgCl_2$	0.1015 g
	NaCl	7.79 g
	NaH_2PO4	0.1875 g
	$NaHCO_3$	1.2 g

Table 4: List of buffer solutions used for calcium imaging.

2.1.2.4 Gel Electrophoresis

The solutions used in this study for Gel electrophoresis are listed in Table 5 below.

50x TAE buffer	dd H_2O	500 ml

	EDTA	0.37 g
	Acetic acid	57.1 ml
	Tris base	242 g

Table 5*:* List of solutions used for gel electrophoresis.

2.1.2.5 Cell Culture

The solutions used in this study for cell culture are listed in Table 6 below.

DH10 Solution (neurons)	DMEM F12	100 ml
	Antibiotic-Antimycotic	1 mL
	FBS	10 ml
DH10 solution (cells)	DMEM	100 ml
	Antibiotic-Antimycotic	1 mL
	FBS	10 ml

Table 6: List of solutions used in cell culture.

2.1.3 Antibodies

The antibodies utilized in the research, such as those for western blotting and immunohistochemistry, are listed in this section.

2.1.3.1 Primary Antibodies for Immunohistochemistry

The primary antibodies used in this study for immunohistochemistry are listed in Table 7 below.

Name	Species	Dilution	Company	Ref. number
CD31	Rat	1:400	Dianova, Hamburg, Germany	DIA-310
CGRP	Goat	1:1600	Acris, now: Origene, MD, USA	BP022
GFP	Chicken	1:2000	Novus Biological, Centennial, CO, USA	NB100-1614
Ly6g	Rat	1:3000	Invitrogen, now: Thermo Fisher Scientific, Waltham, MA, USA	14-5931-82
Ly6g-Fitc	Rat	1:200	Invitrogen, now: Thermo Fisher Scientific, Waltham, MA, USA	RB6-8C5
PGP.9.5	Rabbit	1:800	ABCAM, MA, USA	Ab15503
Substance P	Rat	1:400	Santa Cruz Biotechnology, Dallas, USA	Sc-21715

TRPM5	Rabbit	1:500	Gift from Prof. V. Flockerzi (Kusumakshi *et al*., 2015)	794
TRPV1	Rabbit	1:2000	Alomone labs, Jerusalem	ACC-030

Table 7: List of primary antibodies used in immunohistochemistry, along with their dilutions, and manufacturing companies.

2.1.3.2 Secondary Antibodies for Immunohistochemistry

The secondary antibodies used in this study for immunohistochemistry are listed in Table 8 below.

Dye	Species	Dilution	Company	Ref. number
CY3	donkey- α - rat	1:1000	Jackson Laboratories, Bar Harbor, ME, USA	712-165-150
CY3	donkey- α -rabbit	1:1000	Merck Millipore, Darmstadt, Germany	AP 182C
CY3	donkey- α -chicken	1:500	Jackson laboratories, Bar Harbor, ME, USA	703-165-155
CY5	donkey- α -rat	1:400	Jackson Laboratories, Bar Harbor, ME, USA	712-171-153
CY5	donkey- α -rabbit	1:500	Jackson laboratories, Bar Harbor, ME, USA	711-175-152
Fitc	donkey- α -chicken	1:200	Jackson Laboratories, Bar Harbor, ME, USA	703-096-155
Tx-Rd	donkey- α -goat	1:400	Life Technologies, Darmstadt, Germany	A11058

Table 8: List of secondary antibodies used for immunohistochemistry, along with their dilutions, and manufacturing companies.

2.1.3.3 Primary Antibodies Used for Western Blotting

The primary antibodies used in this study for Western blotting are listed in Table 9 below.

Name	Species	Dilution	Company	Ref. number
TRPM5	Rabbit	1:1000	Gift from Prof. V. Flockerzi (Kusumakshi *et al.*, 2015)	1050
Anti-alpha tubulin	Goat	1:10000	Cell signal technologies, MA, USA	ab18251

Table 9: List of Antibodies, their dilutions, and manufacturing companies used for Western blotting.

2.1.3.4 Secondary Antibodies used for Western Blotting

The secondary antibodies used in this study for Western blotting are listed in Table 10 below.

Species reactivity	Dilution	Company	Ref. number
Mouse	1:10000	Sigma Aldrich, Taufkirchen, Germany	A3673
Rabbit	1:10000	Sigma Aldrich Taufkirchen, Germany	A6154

***Table 10*:** List of secondary antibodies used for Western blotting, along with their dilutions, and manufacturing companies.

2.1.4 Instruments and disposables

The instruments and disposables used in this study are listed in Table 11 below.

Instruments and disposables	Information (model, company, city)
Agarose gel electrophoresis system	Bio-Rad, Hertfordshire, UK
Blades	Leica D880 HS, Wetzlar, Germany
Blotting paper	Bio-Rad, Hertfordshire, UK
Microscope for Ca^{2+} imaging	E Clips FN1 Nikon, Tokyo, Japan
Camera 1 (Zeiss fluorescence microscope)	Axiocam 512 Color, Oberkochen, Germany
Camera 2 (Zeiss fluorescence microscope)	Axiocam 506 Mono, Oberkochen, Germany
Camera (Ca^{2+} imaging setup)	Hamamatsu C13440 Orca- Flash 4.0, Hamamatsu, Japan
Cannulas	Braun, Kronberg im Taunus, Germany
Cell culture microscope	Olympus Ck 40, Hamburg, Germany
Centrifuge	VWR, Galaxy Mini Star, Pa, USA
Centrifuge large	Sigma Aldrich, Taufkirchen, Germany
Centrifuge small	Fisher Scientific, Waltham, MA, USA
Chemi-doc XRS system	Bio-Rad, Hertfordshire, UK
Cloves	B- Braun, Kronberg im Taunus, Germany
Cotton	Hartmann, Heidenheim, Germany.
Coverslips	R. Langenbrinck, Emmendingen, Germany
Coverslips 20 Mm	Thermo Fisher Scientific, Waltham, MA, USA
Cryostat	Leica, Wetzlar, Germany
DG4 Plus/ 30	Sutter Instrument Co, Novato, CA, USA
Fluorescence microscope	Zeiss, Oberkochen, Germany
Freezer - 80	Thermo Fisher Scientific, Waltham, MA, USA

Heat pad	Beurer Hk Limited Edition, Germany
Hood	Biowizard Golden – Line, Philadelphia, PE, USA
Incubator 1x	SANYO MCO- 20 AIC, Osaka, Japan
Incubators 2x	SANYO MCO-SAC, Osaka, Japan
Liquid blocker pen	Science Services, Munich, Germany
Microwave	Ok, Germany
Molecular imager	Camera 2, A14:B33Flourescence Microscope
Oven	Memmert SN 260, Nurnberg, Germany
Pasteur pipettes	Roth, Hessen, Germany
Polyacrylamide gel system	Bio-Rad, Hertfordshire, UK
Pump	Chromaphor Analysen Technik, Oberhausen, Germany
Real-time thermo cycle	Bio-Rad CFX Connect Real-Time System, Hertfordshire, UK
Scale 1	Balingen, Germany
Shaker	Phoenix-Instrument, Garbsen, Germany
Slides	Thermo Scientific, Superfrost Plus, Darmstadt, Germany
Surgery microscope 1	Leica Mz 95, Wetzlar, Germany
Surgery microscope 2	Am Scope, Irvine, UK
Thermo cycler	Bio-Rad T100 Thermal Cycler, Hertfordshire, UK
Tissue-Tek	Science Services, Munich, Germany
Vortex	Phoenix Instrument RS- VAIO, Garbsen, Germany
Water bath	Berlin, Germany

***Table 11*:** List of instruments and disposables used in this study.

2.1.5 Bacteria

For the experimental pulmonary infections in mice, we utilized the clinical isolate NH57388A of P. aeruginosa, which was derived from a cystic fibrosis patient. The isolate was kindly provided by Niels Hoiby from the Department of Clinical Microbiology at Rigshospitalet, University of Copenhagen (Lawrenz *et al*., 2014).

2.1.6 Mice models

The mice models used in this study are listed in Table 12 below.

Mouse Name	Company/ Breeding Parents	References
C57Bl/6N	Jackson Laboratories, Bar Harbor, ME, USA	000664
Trpm5-KO	Kindly provided by V. Chubanov, Ludwig-Maximilian University, Munich, Germany	(Damak *et al.*, 2006)
Trpm5-tauGFP	Generated by Prof. U. Boehm and kindly provided by him	Saarland University, Saarland, Germany (Wyatt *et al.*, 2017)
Trpm5-DTR	*Trpm5* X Rosa26iDTR, kindly provided by Prof. U. Boehm	Not published
Trpm5-tauGFP-DTR	*Trpm5*-tauGFP X Rosa26iDTR, kindly provided by Prof. U. Boehm	Not published
Trpm5-Dreadd	Kindly provided by Prof. U. Boehm and Prof. P. Lipp	Saarland University, Saarland, Germany not published
ChAT-eGFP	Generated by Prof. MI. Kotlikoff and kindly provided by him	Cornell University, NY, USA (Tallini *et al.*, 2006)
Trpa1-tauGFP	TRPA1-Cre X Rosa-tauGFP, generated by Prof. U. Boehm and kindly provided by him	(Bernal *et al.*, 2021)
Trpa1-tauGFP-DTR	TRPA1-tauGFP X Rosa26iDTR, kindly provided by Prof. U. Boehm	(Hollenhorst *et al*., 2022)
Trpa1-DTR	TRPA1 X Rosa26iDTR, kindly provided by Prof. U. Boehm	(Hollenhorst *et al*., 2022)
Trpa1- GCaMP	TRPA1 X Rosa26-GCaMP3, kindly provided by Prof. U. Boehm	(Hollenhorst *et al*., 2022)

***Table 12*:** List of mice models.

2.1.7 Primers

The primers used in this study for RT-PCR are listed in Table 13 below.

Primer name	Primer sequence	Product length (bp)
β-2-Microglobulin	fwd: attcacccccactgagactg rev: gctatttctttctgcgtgcat	192
Tas2r105	fwd: gactggcttccttctcatcg rev: gcaaacaccccaagagaaaa	284

Tas2r108	fwd: tggatgcaaacagtctctggrev rev: ggtgagggctgaaatcagaa	158
Trpa1	fwd: gtccagggcgttgtctatcg rev: cgtgatgcagaggacagagat	163
Trpv1	fwd: tcaccgtcagctctgttgtc rev: gggtctttgaactcgctgtc	285
GADPH	fwd: aggtcggtgtgaacggatttg rev: tgtagaccatgtagttgaggtca	500

***Table 13*:** List of used primers and their sequences.

2.1.8 Animal protocols

Animal Experiments in this study were permitted using the animal protocols used listed in Table 14 below.

Experiment	Animal protocol
Infection	04/2018
IT CNO application	09/2021
IT DT application	40/2018
Trpa1-DTR mice	25/2021
Cholinergic inhibition with MEC and atropine	69/2015

Table 14: List of animal protocols used in this study.

2.2 Methods

2.2.1 Surgery and instillation of drugs into the airways

Adult mice at ages between nine to twenty weeks were used throughout this study. Before starting the surgery, the mice were anesthetized with an intraperitoneal (*i.p.*) injection of an adequate anesthetic solution consisting of xylazine (15 mg/kg weight) and ketamine (85 mg/ kg weight). Mice were then positioned on a heating pad for approximately ten minutes until they were in a deep sleep as indicated by the loss of righting reflex (LORR). The mice's chest was cleanly shaved to prevent the wound from contamination with hairs. Then, 100 µl of Evans blue dye (10 mg/kg) was injected into the mouse's retro-orbital venous eye sinus. Five minutes later a small surgical incision was made in the middle of the cervical region. This cut ensured access to the larynx. At that point, the salivary glands and muscles were carefully moved to the side. A second small surgical incision was then made in the cricothyroid ligament of the larynx, and a small

bent cannula was inserted into the tracheal lumen for breathing. The mice inhaled a 4 µl vehicle (NaCl). To activate the BC in the trachea of WT mice, mice inhaled different doses of denatonium (1, 10, 20 mM) through the breathing cannula. To address the role of ACRs in neurogenic inflammation, each animal was injected 10 minutes before anesthesia intra-peritoneally with atropine (1 mg/kg) dissolved in NaCl. Shortly after anesthesia, MEC (1 mg/kg) was administered intra-peritoneally. Ten minutes later, 100 µl of Evans blue dye was injected retro-orbitally. Five min later, a single dose of denatonium (see above) was inhaled into the trachea. In another protocol, atropine and MEC (1 mg/kg) were dissolved in NaCl and administered simultaneously through the breathing cannula. Five minutes later, denatonium (1, 10, 20 mM) was introduced into the trachea via the breathing tube. In sham mice, after the administration of atropine and MEC, a vehicle was introduced into the trachea. The mice were sacrificed 30 minutes after the substance inhalation. All surgery tools were autoclaved.

2.2.2 IT CNO application

For a selective activation of the BC in the *Trpm5*-DREADD mice, surgery to access the trachea was performed and a 4 µl dose of CNO (100 µM; hallo bio) was introduced into the trachea of the mice through the breathing cannula. The mice were sacrificed 30 minutes after the substance inhalation.

2.2.3 IT diphtheria toxin (DT) application

For specific BC depletion in the trachea of the *Trpm5*-DTR mice, surgery was performed to expose and get access to the trachea. Thereafter, 200 ng of diphtheria toxin (DT) was introduced into the trachea through the breathing cannula. The depletion of BC in the trachea was confirmed using immunohistochemistry with specific antibodies against TRPM5.

2.2.4 Handling of the mice after surgery

Each mouse was handled with care during and after surgery. To keep the animals in optimal conditions, a warm pad maintained their normal body temperature and heart rate for thirty minutes after substance inhalation. Upon completion of the experiment, the mice were perfused with 4% paraformaldehyde (PFA). Following this, organs such as lungs, tracheas, and thoracic ganglia were harvested and prepared for staining. For $[Ca^{2+}]i$ imaging experiments with isolated neurons, no Evans blue dye was injected, and, instead of perfusion, the tissues were collected for dissociation. To assess the influence of BC activation on neurogenic inflammation after surgery and substance application, a series of steps was undertaken: mice were firstly injected with Evans blue and perfused and fixed with 4% PFA. Then, the middle part of the trachea was extracted carefully from each operated mouse. Tracheas were post-fixed in 1.5 ml Eppendorf tubes filled with new 4% PFA for half an hour. These tubes were then washed five times with PBS, each

wash lasting 30 minutes, with all tubes kept on a shaker at room temperature for 2 ½ h. Tracheal tissues were subsequently incubated in 18% sucrose solution in PBS at 4°C overnight. The next day, tissues were frozen in Tissue-Tek and stored at -80°C. Cryo-sections (10 µm) cut 100 µm apart from one another were mounted on glass slides, air-dried for 1h, rehydrated for one minute in distilled water, and mounted with MOWIOL medium. From each tracheal section, 6 to 9 images were taken using a fluorescence microscope (Carl Zeiss) and an Orca Flash 4.0 camera with a 20x objective plus a Texas Red filter (excitation peak at 586 nm/emission peak at 603 nm) to form a tracheal ring. The images were composed in a single image and saved as TIF pictures. The fluorescence intensity was then analyzed as a mean of the intensity of the fluorescence at 585 nm using the ImageJ software.

2.2.5 Perfusion, tissue handling, and preservation

To preserve the tissue from protein degradation, an aldehyde-based fixative fluid such as 4% paraformaldehyde and Zamboni must be perfused through the blood circulatory system. Initially, a surgical incision was carefully made in the mid-axial abdominal-thoracic region to expose access to the heart, followed by an injection of 5 I.U. heparin into the heart to prevent blood clotting and to preserve the patency of the vascular system A few seconds later, the right ventricle is incised to allow drainage. A cannula is inserted into the left ventricle. The blood in the vessels and capillaries in all tissues is then washed with an ice-cold PB followed by the infusion of the fixative. Another perfusion protocol was used for the mice with the Evans blue experiments. A PVP solution washing step followed by a 4% PFA fixation step was administrated. Neurons, tracheas, and parts of the colon were post-fixed in Zamboni for 30 minutes additionally, washed overnight in 0.1 M PB, and then incubated in a sugar solution containing 30% or 18% sucrose in 0.1 M PB. Tissues were then mounted using a clear water-soluble compound consisting of resins and glycols, such as Tissue-Tek. Then, each tissue was immersed in 2-methyl butane cooled in liquid nitrogen for a few seconds. 10µM cryosections were sliced using the Leica CM950 cryostat, mounted on glass slides, and kept at -20°C. After use, the tissue was stored at -80°C.

2.2.6 Immunohistochemistry

Primary antibodies such as TRPV1, CGRP, TRPM5, SP, GFP, Ly6G, and CD31 were used in this study. Before proceeding with the staining protocol, the sections were dried for one hour in the air to prevent the loss of the tissue, and then an incubation step in a blocking solution for two hours. Later, the slides were incubated with one or more appropriate primary antibodies overnight at room temperature. The following day, the slides were first washed three times with PBS. Then they were incubated again with one or more suitable secondary antibodies (Table 2.8) at room temperature for one hour in the dark. An optional staining step with DAPI (0.2 µg/ml) for ten minutes is recommended. The sections were washed three times with

PBS and cover-slipped using a mowiol medium (containing: MOWIOL 4-88, glycerol, Tris-Cl (0.2 M, pH 8.5), and DABCO (1, 4-diazabicyclo-[2, 2, 2]-octane) in water). To determine the numbers of the fluorescent CGRP, SP, TRPA1, and TRPV1 neurons, each stained section from the WT and *Trpa1*-DTR mice was photographed and analyzed using a Zeiss Axio Observer D1 microscope. An Axio-Cam HRc camera was used to photograph each staining. Images were analyzed using ZEN 3.2 software. The number of fluorescent neurons was counted and calculated using ImageJ. Antisera to Ly6G was used to stain neutrophils in the trachea. Every neutrophil in tracheal sections was counted using the Carl Zeiss microscope. Three or more mice from each group were analyzed, with five sections for each mouse.

2.2.7 Whole-mount staining

Tracheas from WT, *Trpm5*-deficient, and *Trpa1*-DTR mice were carefully extracted, cleaned, and then cut into three pieces. Each piece was embedded in Zamboni in a cold environment overnight and washed three times with PBS subsequently. The following day, tracheal pieces were incubated with a permeabilization solution (containing 0.3% Triton X in PBS) Two hours later, the tracheal pieces were blocked in a blocking solution (containing 1% PSA and 4% horse serum in PBS) for another two hours. After permeabilization and blocking, the pieces were incubated with a mix containing an appropriate concentration of one primary antibody or more dissolved in PBSs overnight at room temperature. On the succeeding day, the tracheas were washed with PBS five times, each washing step taking thirty minutes at room temperature. Then the tracheal tissues were blocked again in the blocking solution and incubated with a mix containing an appropriate concentration of an appropriate secondary antibody dissolved in PBSs overnight at room temperature in the dark. The following day's protocol started with another five washing steps. Then, the tracheas were mounted on glass with a MOWIOL medium. The final whole mounts were imaged using a confocal microscope. SP and CGRP whole-mount tracheal perpetration images were analyzed with IMARIS 9.8.0 software, and CD31-stained whole-mount tracheal perpetrations were analyzed using ImageJ. Three or more mice from each group were analyzed.

2.2.8 Cell Culture

2.2.8.1 Bacterial transformation and cloning

Mouse *Tas2r105* and *Tas2r108* coding sequences were cloned using commercial DNA assembly strategies according to the manufacturer's recommendations (NEBuilder HiFi, New England Biolabs GmbH Frankfurt, Germany). This was kindly performed by fellow scientist Dr. Stephan Maxainer. *Trpm5* plasmids were transformed in *E. Coli* XL10-Gold bacteria by using heat and shock treatment. The plasmids were acquired from the laboratory of Dr. Vladimir Chubanov, in Munich, Germany.

2.2.8.2 Transfection of HEK293 cells

The process of introducing foreign nucleic acids into cells is called transfection. The plasmids *Tas2r105, Tas2r108* and *Trpm5* were used in this study. The human embryonic kidney 293 cell line (HEK293 cells) was selected to be used for transfection. A proper number of cells were seeded into a plate one day in advance. Once they have gotten 50-60% confluent, the procedure was achieved according to the manufacturer's protocol: two mixtures were prepared, one from the DNA sample and Opti-MEM, and another from Lipofectamine 2000 and Opti-MEM. The mixtures were kept separately for 5 minutes at RT. Then, both mixtures were combined and kept again at room temperature for 20 minutes. Later, the transfection mixture was added drop-wise to the cells. The cells were put back in the incubator for 6-8 hours and the old medium was washed and substituted with a new medium. The cells were ready for experiments the next day.

2.2.8.3 Primary culture of neurons

To dissociate ganglia into single neurons, freshly dissected DRG and JNC were collected in a DH10 medium containing (90% DMEM/F-12, 10% fetal bovine serum, and 1% Antibiotic-Antimycotic) on ice. Then the sensory neuronal tissues were moved and were digested for 30 min at 37°C in an enzymatic solution containing 5 mg/ml dispase type II and 1 mg/ml collagenase type I in HBSS without Ca^{2+} and Mg^{2+}. Tissues were then mechanically digested using silicone-coated glass pipettes of decreasing diameter. To stop the enzymatic activity, the mixture was washed three times with DH10 and centrifuged at 210 g for two minutes after every washing step while keeping the pellet. Dissociated neurons were pelleted one final time and suspended in an appropriate amount of DH10 medium and mounted on coated coverslips with a laminin (10 mg/ml) and poly-L-lysine (0.1 mg/ml) mix, in water. Neurons were then kept in an incubator (5% CO_2 and 0% O_2) at 37°C for 2 hours before proceeding to $[Ca^{2+}]i$ imaging.

2.2.8.4 Culturing of primary tracheal epithelial cells

ChAT-eGFP mice were used for these experiments. Once the mice were deeply anesthetized, their tracheae were collected in TYRODE I solution on ice. Then each trachea was cut into rings and transferred into a protease solution containing: Papain (10u/mg), L-Cysteine (0.2 M), DNAse grade 1 (100 U), and (1 mM EDTA) for 30 minutes in a hot plate at 37°C, while mixing every 10 minutes with a pipette. Next, the enzymatic activity of the solution was stopped using an appropriate amount of DMEM. The mixture was then centrifuged at 320g for 5 minutes at 4°C, the supernatant was discarded and the pellet was suspended in 100 µl DMEM. Dissociated tracheal cells were then relocated drop-wise on tissue-Tek coated glass

coverslips and left to attach for twenty minutes in an incubator with 5% CO_2 at 37°C before proceeding with calcium imaging.

2.2.9 Western blotting

2.2.9.1 Lysate preparation

To detect the TRPM5 protein levels in the JNC and DRG, both ganglia from an adult WT mouse were collected in Reba buffer (containing 10 mM HEPES, 150 mM NaCl, 1% Triton X-100, 0.5% sodium deoxycholate, 0.1%, SDS, and 1 mM EDTA ddH2O; PH = 7.4). Samples were then disturbed with a homogenizer and kept at 4°C for one hour. Cell homogenates were then spun at 12000 rounds per minute for ten minutes at 4°C. The supernatant was gathered and sheared by sonication. For denaturation of lysates, protein aliquots were mixed with water and sample buffer (1x SDS and 10% β-mercaptoethanol (βME)) to a maximum capacity of 20 µl. Protein samples were then denatured for five minutes at 95°C. As a positive control, HEK293 cells were transfected with *Trpm5* plasmid. Cells were collected from culture 24 hours after transfection in a 50 µl mixture of SDS sample buffer (1x) and 10% βME.

2.2.9.2 Blotting

Electrophoresis was executed by running a mixture of the previously prepared protein lysates, mixed with sample buffer, and βME). Samples were loaded into a 10% gel at 80 V for one hour. The samples were then transferred to a nitrocellulose membrane for 2 hours at 200 mA. The membrane was then incubated with 5% dry milk in 1X TBS-T buffer for 1h at room temperature. Next, the membrane was incubated with rabbit anti-TRPM5 primary antibodies (1:1000) dissolved in 5% dry milk in TBS-T overnight at 4°C. The next day, the membrane was washed three times with TBS–T on a shaker, each washing step taking 30 minutes. One and a half hours later, the membrane was again incubated with the pox anti-rabbit secondary antibody (1:4000) for 1h at RT. The membrane was then washed again three times in 1X TBS-T (0.1%) at RT. Proteins were detected using SuperSignal™ West Pico PLUS chemiluminescent substrates as signal enhancers and images were acquired using Bio-Rad Chemi-Doc (molecular imager). Next, for a protein loading control, the same membrane was washed three times with 1X TBS-T, then blocked again with 5% dry milk in TBS-T buffer for one hour at RT, followed by incubation with mouse anti-alpha tubulin primary antibody for one hour at RT. It was then washed three times with 1X TBS-T buffer (0.1%), and incubated with pox anti-mouse secondary antibody (1:4000) for one hour at RT. After washing three times with TBS –T buffer, the membrane was treated again for chemiluminescence detection using the same procedure as described earlier.

2.2.10 Polymerase Chain Reaction (PCR)

2.2.10.1 RNA extraction

Freshly isolated epithelial tracheal cells, DRG and JNC, HEK293 cells transfected with *Tas2r108*, and HEK293 cells transfected with *Tas2r105* were collected for RNA extraction using an RNAeasy Isolation Kit (QIAGEN) according to the manufacturer's protocol. RNA concentrations were measured using a Nanodrop and stored in the -80°C freezer for further processing.

2.2.10.2 Coding DNA synthesis

Initially, a DNase I Amplification Grade Kit (Thermo Fisher Scientific) was used to remove DNA during RNA purification procedures according to the manufacturer's protocol. A mixture of DNase I, Amplification Grade, and 10x reaction DNA buffer was added to 2 µl of RNA from each sample and incubated for 10 min at 37°C. To stop the enzymatic reaction, 1 µl of EDTA was added to each sample and the samples were then left to incubate again for 10 min at 65°C in a thermocycler. Reverse Transcription SuperScript™ II (Reverse Transcriptase Kit) was used to synthesize cDNA. A maximum of 1 µg of RNA from each sample was mixed with 1 µl of random primers (1 µM), 1 µl of dNTP mix (10 mM), 4 µl of 5x first-strand buffer, 2 µl of DTT, and 1 µl of SuperScript™ II reverse transcriptase, and complemented with RNase-free water to a volume of 20 µl. The mixture was heated in the thermo-cycler at 42°C for 50 min followed by 25 min at 72°C.

2.2.10.3 PCR

For the detection of *Tas2r105* and *Tas2r108* mRNA expression, AmpliTaq Gold Master Mix (Thermo Fisher Scientific) was used to amplify a total of 2 µl of cDNA per sample according to the manufacturer's protocol. Primers for *Tas2r105* were: fwd - tggatgcaaacagtctctgg, rev – ggtgagggctgaaatcagaa, and primers for *Tas2r108* were: fwd - gactggcttccttctcatcg, rev - gcaaacaccccaagagaaaa. Reaction cycles were 95°C for 720 s, then 95°C, 60°C, and 72°C for 20 s, each for a total of 40 cycles, followed by 72°C for 420 s.

2.2.10.4 Quantitative RT-PCR

To determine the difference between *Trpa1* and *Trpv1* gene expression in the *Trpa1*-DTR mice and the WT, a Bio-Rad 96 RT-PCR machine was used to quantify the gene expression using the SYBR Green Master Mix from Thermo Fisher Scientific. Primers for *Trpv1* were: fwd - tcaccgtcagctctgttgtc, rev - gggtctttgaactcgctgtc, primers for *Trpa1* were: fwd - gtccagggcgttgtctatcg, rev - cgtgatgcaggacagagat, and primers for β-2-microglobulin were: fwd - attcacccccactgagactg and rev - gctatttctttctgcgtgcat. Reaction cycles were: 95°C for 600 s, then 95°C and 59°C for 20 s, each for a whole 45 cycles, trailed by 65°C for

5s and lastly 95℃ for 5s. Quantification of the fluorescence was made during every amplification. Each sample's (Cq) values were defined using Bio-Rad CFX software. To determine copy values, Microsoft Excel was used for Cq to divide by β-2-microglobulin copy values for ratio analysis. Three or more mice from each treatment were used. qPCR was also used to investigate whether there was a difference in the *Trpa1* and *Trpv1* gene expression between WT mice and *Trpm5*-knockouts, again using the same procedure as described above.

2.2.11 Neuronal primary cultures and Ca^{2+} imaging

2.2.11.1 Neurons

Neurons isolated from *Trpa1*-GCamp3 mice were used without loading, while all other neurons were loaded with Fura-2-AM and 0.04% Pluronic acid for 30 minutes at 37°C in the dark. The loading mixture was prepared in Locke buffer, pH =7.4.

2.2.11.2 HEK293 Cells

HEK293 cells transfected with the ATP sensor were measured directly without loading as they have a calcium sensor (Lobas *et al.*, 2019). *Trpa1*-stable transfected cells, HEK293 cells and HEK293 cells transfected with Tas2r108 or Tas2r105 were loaded with Fura-2-AM and 0.04% Pluronic acid for 30 minutes at 37°C in a dim incubator. The loading mixture was prepared in TYRODE III.

2.2.11.3 $[Ca^{2+}]$i imaging:

Neuronal coverslips were first washed two times with Locke buffer and then incubated with a loading solution containing a mix of the calcium indicator Fura -2- AM and Pluronic acid solution in Locke buffer. Then the coverslips were put back in an incubator with 0% oxygen and 5% carbon dioxide at 37°C. Thirty to thirty-five minutes later, the coverslips were washed again and the $[Ca^{2+}]$i was measured at 340 and 380 nm excitation ratio to determine differences in the intracellular calcium due to substance application. The coverslips were extensively washed between every substance application. A reaction is considered responsive when the fluorescence ratio of the cells was greater than 20% of the baseline. A light ratio of 340/380 nm from a wavelength-switching xenon arc lamp DG4 was used, and an Orca Flash 4.0 camera was used for fluorescence detection. The software NIS-Elements was used to analyze the results. $[Ca^{2+}]$i changes in GCamp3 and GFP fluorescence were measured at 525 nm emission before and after substance application. An Orca Flash 4.0 camera was used. Analyses were performed using NIS-Elements software.

2.2.12 Data analysis and statistics

For each result, at least three independent experiments were conducted, in which all data were found to be normally distributed and expressed as means ± SD or ± SEM. All experimental results were finally analyzed to examine statistical differences. The one-way ANOVA test and the unpaired Student's t-test were applied. $P < 0.05$ was considered statistically significant. Prism 8.0.1 was used for generating the figures. Unless otherwise stated, it can be assumed that the statistical analysis did not yield significant results.

CHAPTER 3: RESULTS

3.1 Bitter taste receptor subtypes such as Tas2r105 and Tas2r108 are expressed in tracheal epithelial cells

Tas2R signaling is very important for regulating immune responses in the airways and is involved in neurogenic inflammation once stimulated with a bitter substance such as denatonium (Hollenhorst *et al.*, 2020b). This stimulation was shown previously to be responsible for the downstream activation of the TRPM5 channel. BC express a collection of Tas2R and the bitter-taste signaling cascade along with the TRPM5 channel (Hollenhorst *et al*., 2020).

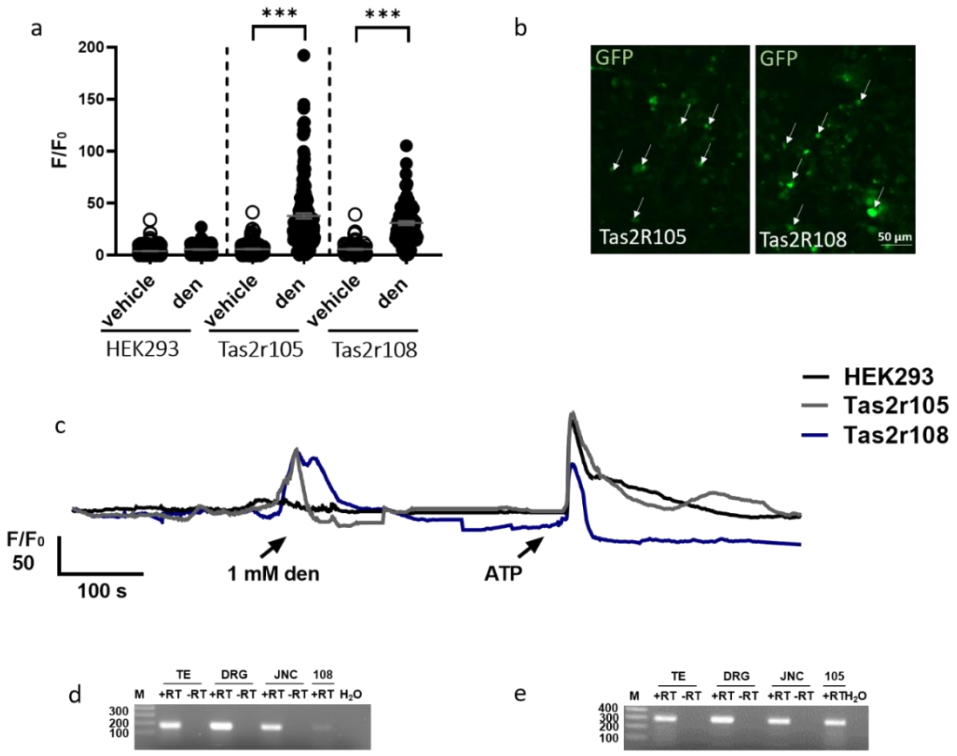

Figure 3.1: The bitter taste receptor signaling cascade is activated via denatonium stimulation. a: Measurements of $[Ca^{2+}]i$ in HEK293 cells and transfected HEK293 cells with the *Tas2R105* and *-108*, showing no significant change after 1mM denatonium application on non-transfected cells (n=99). However, HEK293 cells transfected with *T2R105* and *T2R108* showed a significant change in $[Ca^{2+}]i$ after 1mM denatonium (den) application (n=160 and n=227, respectively). Five coverslips were each expressed as the mean ± SEM. P-values were determined by the unpaired two-tailed Student's T-test, (*** $p<0.001$). b: Immunohistochemistry of HEK293 cells transfected with *Tas2r105* and *Tas2r108* after enhancement with chicken-a-GFP primary antibody (green). Transfection efficacy was 30-35%. c: Representation traces from a WT HEK293 cell (black line) and HEK293 cells transfected with the *Tas2R105* (grey) and *-108* (blue) in the $[Ca^{2+}]i$ imaging experiment using 1 mM den stimulation to T2R105 and T2R108. The den led to an increase in the $[Ca^{2+}]i$ level in Tas2R transfected cells compared to the non-transfected cell. d and e: Representative gel images confirming the successful transfection of HEK293 cells with *Tas2r105* and *Tas2r108* and their expression in the trachea, the JNC, and DRG in mice.

In this experiment, we are interested in the TAS2R105 and TAS2R108 which are the most abundant Tas2R in BC can be stimulated via bitter substances such as denatonium and bacterial bitter QSM (Figure 3.1). HEK293 cells were transfected with the *TAS2R105* and *TAS2R108* genes. Commercial DNA assembly strategies, according to the manufacturer's recommendations (NEBuilder HiFi, New England Biolabs GmbH, Frankfurt, Germany), were used for cloning the two genes. PCR products were generated using PrimeStar HS DNA Polymerase (TaKaRa Inc., Otsu, Japan). Oligonucleotides were designed based on taste receptor sequences annotated in the NCBI database. Gene IDs for *Tas2r105* and *Tas2r108* are *57252* and 57253, respectively (accessed from www.ncbi.nlm.nih.gov/gene on 4 June 2021). To amplify *Tas2r105* and *Tas2r108* sequences, the oligo combinations MX18750/51 and MX18752/53 were used (Hollenhorst *et al.*, 2022a). To prove if cells transfected with Tas2r105 and Tas2r108 are responding with changes in $[Ca^{2+}]i$ upon stimulation with denatonium, a $[Ca^{2+}]i$ imaging experiment with transfected and non-transfected HEK293 cells was designed. The cells were exposed to 1 mM denatonium and the viability of each cell was tested with 100 μM ATP (Figure 3.1, a and c). A 30-35% efficacy rate was achieved with transfection. A calculation was made by dividing the number of green mVenus (transfected) cells by the number of HEK293 WT cells (not transfected). Notably, only mVenus expressing (green) cells showed an increase in $[Ca^{2+}]i$ after denatonium stimulation while the non-transfected HEK293 cells didn't (Figure 3.1, b). Additionally, *Tas2R105* and *Tas2R108* expression was detected in DRG and JNC, as well as in the epithelial cells of the trachea (Figure 3.1, d and e).

3.2 G-protein a-gustducin is significant for bitter taste signaling

Previously, we could establish that BC can recognize bitter substances such as denatonium and this is due to the Tas2R expression in BC (Hollenhorst *et al.*, 2020b). Here, we used $[Ca^{2+}]i$ imaging experiments with the inhibitor gallein to demonstrate that the effect of denatonium is mediated by G-proteins. This result presses on the role of G-proteins in conducting the taste signal (Figure 3.2).

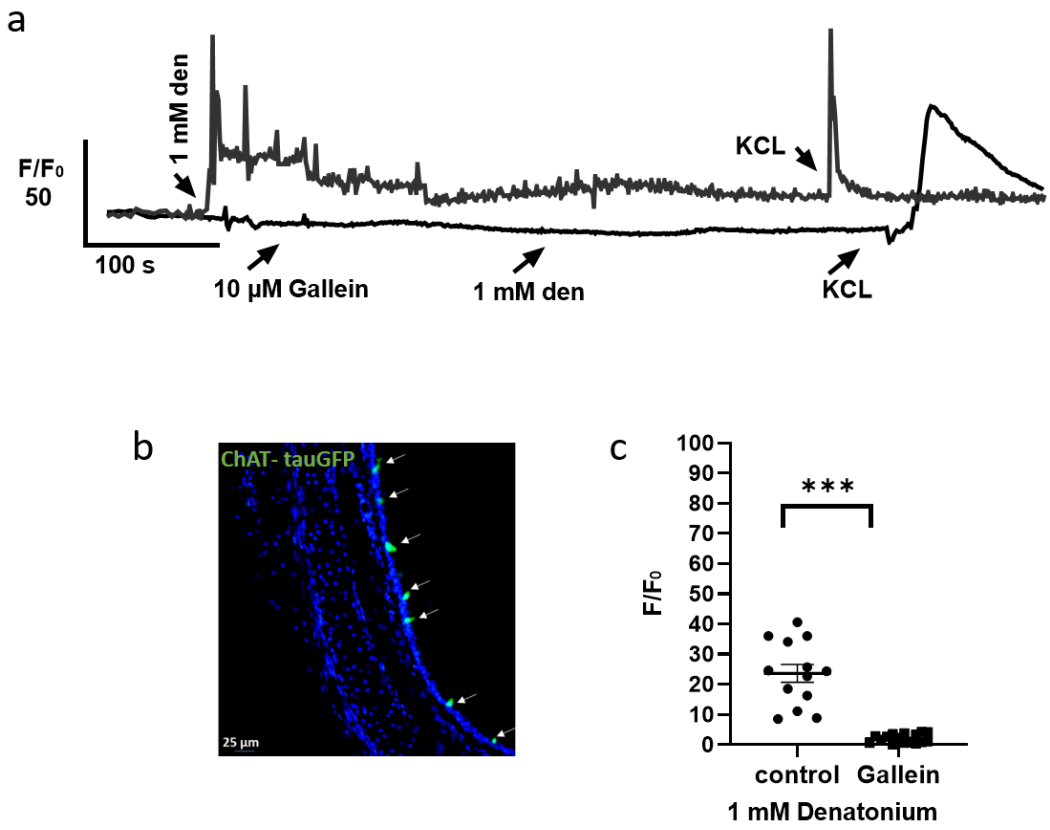

Figure 3.2: Tracheal ChAT-tauGFP cells express the TRPM5 channel and G-proteins. a: Representation traces of two ChAT-tauGFP positive cells. 1 mM den led to the activation of BC, while 10 µM Gallein inhibited the effect. b: Tracheal cross-section showing BC (green) in a ChAT-tauGFP mouse. c: Measurements of $[Ca^{2+}]i$ in primary BC. Gallein (10 µM) significantly reduced the response to 1 mM denatonium shown as the mean ± SEM (denatonium n=13 cells/from 6 mice. denatonium + gallein n=16 cells/from 6 mice). P-values were determined by the unpaired two-tailed Student's T-test (*** $p<0.001$).

ChAT-positive tracheal epithelial cells (BC) from ChAT-eGFP mice were isolated for $[Ca^{2+}]i$ imaging. 1 mM denatonium was applied to each coverslip, which led to a significant increase in $[Ca^{2+}]i$ levels in BC. About 70% of the ChAT-positive cells (BC) had a 10% or higher change in their $[Ca^{2+}]i$. When 10 µM gallein was applied, BC showed no changes in $[Ca^{2+}]i$ levels. The viability of the cells was tested using 40 mM KCl. The result of this experiment demonstrates that the G-protein α-gustducin is involved in BC activation upon stimulation with Tas2R agonists.

3.3 Tas2R stimulation with denatonium induces plasma extravasation in the murine trachea

Plasma and neutrophil extravasation are well-known signatures of neurogenic inflammation (McDonald *et al*., 1996; Rogers, 1997; Andrè *et al*., 2008; Matsuda, Huh and Ji, 2019). Next, we performed an experiment to investigate the effects of tracheal BC activation through the bitter taste signalling pathway in which vehicle mice were injected with Evans's blue, and inhaled denatonium through a breathing tube inserted into their trachea. The tracheae were then removed and examined further.

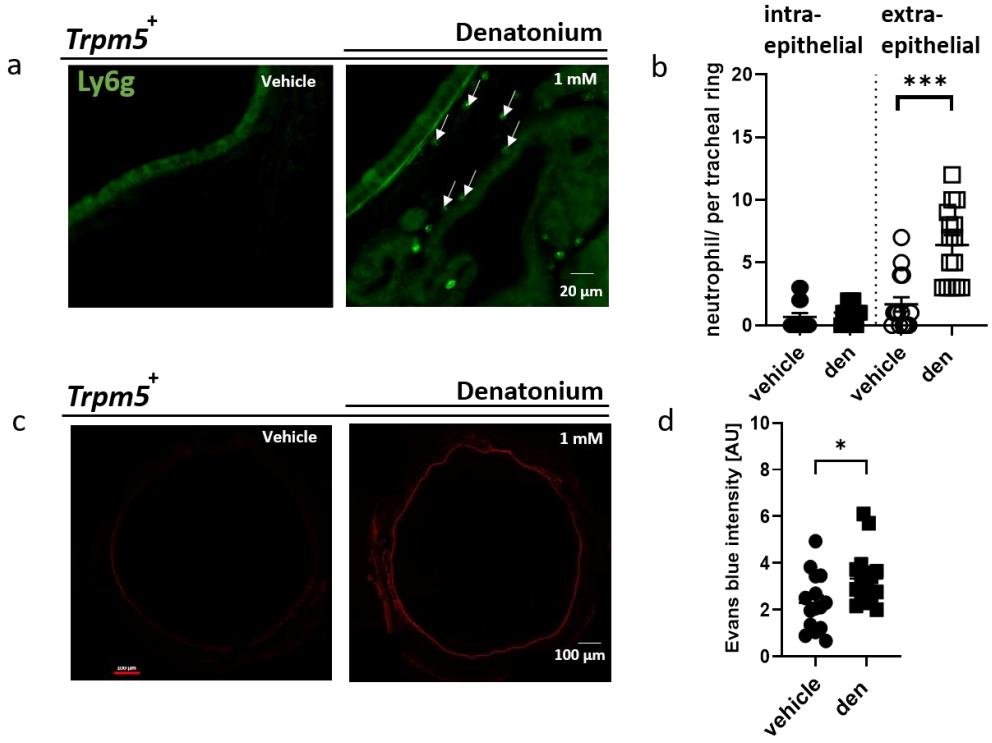

Figure 3.3: Experimental outline of a neurogenic inflammation model to study plasma and neutrophil extravasation in the trachea. a: Immunohistochemistry for Ly6G displaying different neutrophil distribution after tracheal inhalation of the vehicle or 1 mM denatonium (den). b: A significant number of extra-epithelial neutrophils are recruited after 1 mM den stimulation compared to the vehicle inhalation. The number of intraepithelial neutrophils was comparable in treated and not-treated mice. c: Images from tracheal sections showing no Evans blue extravasation in the vehicle group. Stimulation with 1 mM den led to an increase in fluorescence intensity estimated using a Texas red filter. d: Quantification of Evans blue intensity in the vehicle and den group. n=15 sections/3 mice shown as mean ± SEM. P-values were determined by the unpaired two-tailed Student's T-test (* $p < 0.05$, *** $p < 0.001$).

A significant number of extra-epithelial neutrophils were recruited to the trachea in denatonium-treated mice compared to the vehicle-treated group (Figure 3.3, a and b). Moreover, the fluorescence intensity of the Evans blue dye that extravasated after denatonium stimulation was significantly higher compared to the vehicle group (Figure 3.3, c and d).

3.4 Inhibiting cholinergic signaling affects the progression of neurogenic inflammation

BC are cholinergic (Kummer and Krasteva-Christ, 2014b; Kandel *et al.*, 2018; Hollenhorst *et al.*, 2020b), therefore it can be expected that upon stimulation, they would release ACh. On the other hand, AChR inhibition and epithelium removal abolish breathing responses when bitter substances are inhaled. Thus, to investigate whether the denatonium effects result from cholinergic transmission of BC-released ACh, atropine and MEC were either injected (*i.p.*) or inhaled before stimulation with denatonium in an the previously described neurogenic inflammation *in vivo* mouse model (Figure 3.3).

3.4.1 The *i.p.* application of atropine and MEC inhibits the denatonium-induced neurogenic inflammation

Here, the mice were injected with atropine (1 mg/kg body weight, *i.p.*), an inhibitor for muscarinic ACh receptors, and with MEC (1 mg/ kg body weight, *i.p.*), a general inhibitor for nAChRs. Thirty minutes later, the tracheae were stimulated *in vivo* with different denatonium concentrations (1, 10, and 20 mM). The fluorescence intensity of the Evans blue dye that extravasated after 1 and 10 mM denatonium stimulation was similar to the vehicle group (Figure 3.4, a and c), whereas, following stimulation with 20 mM denatonium, Evans blue dye extravasated with a higher significant intensity compared to the vehicle group. Based on our findings, we hypothesize that, unlike the effect of the 1 and 10 mM denatonium, the 20 mM denatonium increased effect is not specific to bitter taste signaling (Figure 3.4 c).

3.4.2 The application of atropine and MEC locally in the trachea didn't inhibit neurogenic inflammation

For this experiment, 1 mg/kg body weight of both atropine and MEC were inhaled using a tube incised carefully in the trachea. Five minutes later, each mouse inhaled a different denatonium concentration (1, 10, and 20 mM). The mice were sacrificed after 30 min and the tracheas were handled for immunohistochemistry (Figure 3.4 b). The fluorescence intensity of the Evans blue dye that extravasated after denatonium stimulation was significantly higher compared to the vehicle group and the denatonium-induced effect was not inhibited. Notably, 4 mice out of all (n = 20 died 28 to 30 minutes after surgery. Mice were coughing out the substances given. Contrary to the *i.p.* application of atropine and MEC, the local inhibition of cholinergic signaling led to an increase in plasma extravasation in all three different denatonium concentrations.

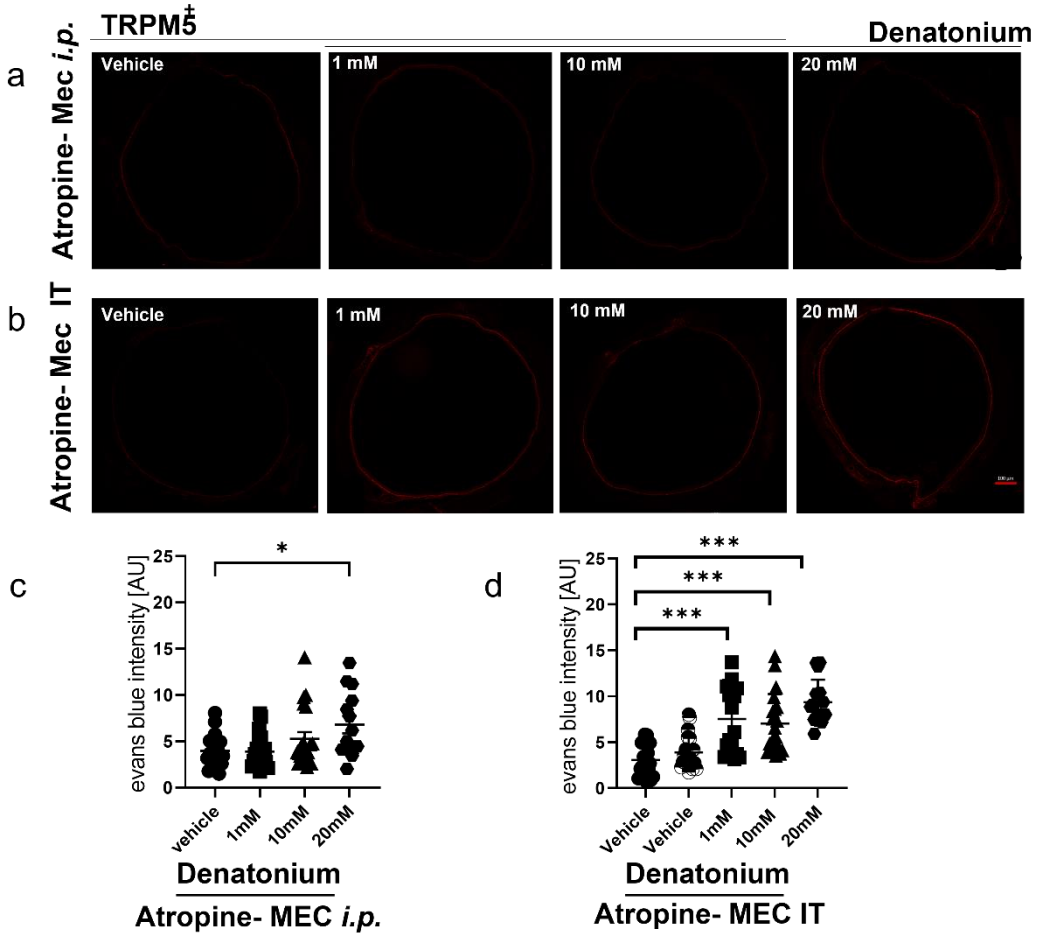

Figure 3.4: Inhibiting cholinergic signaling via the *i.p.* application of atropine and MEC suppressed blood vessel dilation in the trachea. a and b: Images from tracheal sections showing no Evans blue extravasation in the vehicle group. a: Stimulation with 1 and 10 mM den after Atropine-MEC *i.p.* treatment showed similar fluorescence intensity to the vehicle, while stimulation with 20 mM den after the Atropine- MEC *i.p.* treatment showed significant fluorescence intensity compared to the vehicle. b: Stimulation with 1, 10, and 20 mM den after the Atropine- MEC IT treatment showed significant fluorescence intensity compared to the vehicle. c and d: Quantification of Evans blue intensity in the vehicle and den group. n=15 sections/3 mice shown as mean ± SEM. P-values were determined by ANOVA test (* $p < 0.05$, *** $p < 0.001$).

3.4.3 The *i.p.* application of atropine and MEC abolished neutrophil recruitment

Previously (Figure 3.3), we found a significant extraepithelial neutrophil recruitment in the trachea of denatonium-treated mice compared to vehicle-treated mice. Here (Figure 3.5 a), the number of extra-epithelial neutrophils recruited in the trachea of a vehicle was similar to the number of extra-epithelial neutrophils recruited to the trachea in (1 and 10 mM) denatonium-treated mice after atropine and MEC *i.p.* injections. However, the mice that received 20 mM denatonium concentration had a significant increase in the number of extraepithelial recruited neutrophils compared to the vehicle-treated group. On the other hand

(Figure 3.5 b), the number of extraepithelial neutrophils recruited in the trachea of the vehicle was similar to the number of extraepithelial neutrophils recruited to the trachea after the local introduction of atropine and MEC intratracheally, followed by 1 mM denatonium, whereas the mice (from the same group) that received a concentration of (10 and 20 mM) denatonium had a significant increase in the number of extraepithelial recruited neutrophils compared to the vehicle-treated group, with an indication that this treatment didn't abolish the extraepithelial neutrophil recruitment.

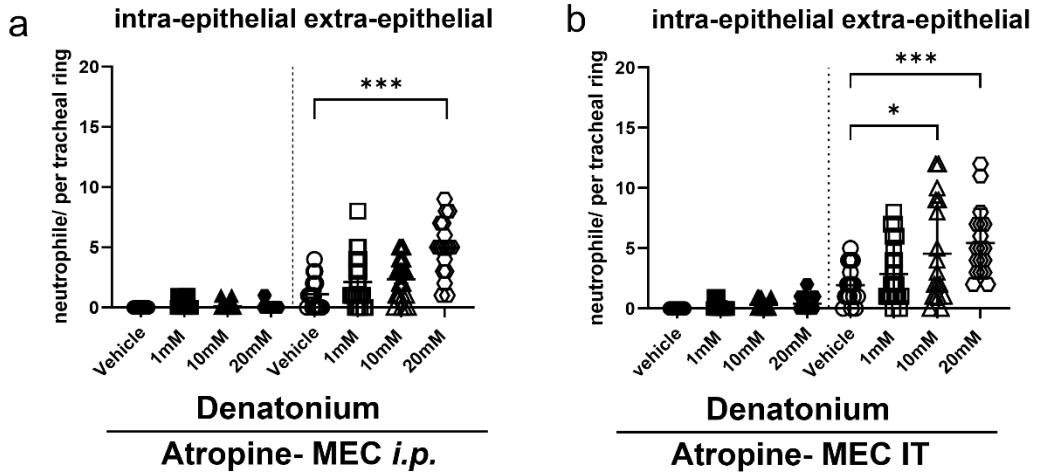

Figure 3.5: The *i.p.* application of atropine and MEC suppressed neutrophil recruitment in the trachea. a: After the *i.p.* application of atropine and MEC, a significant number of extraepithelial neutrophils are recruited when stimulated with 20 mM den compared to the vehicle; both (1 and 10 mM) denatonium were similar to the vehicle. The number of intraepithelial neutrophils was comparable in treated and non-treated mice. b: A significant number of extra-epithelial neutrophils are recruited after (10 and 20 mM) den stimulation compared to the vehicle. 1 mM denatonium treatment was similar to the vehicle. The number of intraepithelial neutrophils was comparable in treated and non-treated mice. 5 section/mouse, n=3 to 4 mice/group expressed as the mean ± SEM. P values were determined by one-way ANOVA-test (*, $P < 0.01$, ***, $P < 0.005$).

3.5 *Trpa1* depletion inhibits denatonium-induced neurogenic inflammation

To explore the involvement of the sensory nerve fibers in inducing neurogenic inflammation in the airways, mice that express the diphtheria toxin receptor (DTR) in the *Trpa1*+ neurons were generated by crossing *TRPA1*-tauGFP-IRES-Cre mice with Rosa26iDTR (Hollenhorst *et al.*, 2022). Mice were injected *i.p.* with the diphtheria toxin (DT) (20 ng/kg body weight) on three consecutive days. *Trpa1*+ nerve fiber depletion was characterized by immunohistochemistry and RT-PCR. Next, mice with depleted *Trpa1* nerve fibers received *i.v.* Evans's blue (EB, 20-mg/kg). Thirty min after inhalation of 1, 10, and 20 mM denatonium (4 µl), the tracheas were explanted, and EB and neutrophil extravasation were estimated.

3.5.1 The depletion of *Trpa1*+ neurons was first confirmed with immunohistochemistry

Ten days after three daily doses of 20 ng/kg DT injections, *Trpa1*tauGFP-DTR mice were sacrificed and the sensory neurons of the DRG were carefully extracted, after which immunohistochemistry was performed (Figure 3.6, a and b), which show the difference in GFP positive signals (*Trpa1*+ neurons). The pictures are correspondingly also showing a difference in TRPV1 + signal, indicating the overlapping of both channels in the sensory neurons. *Trpa1*+ neurons from the vehicle (mean = 27%) and *Trpa1*-depleted mice were counted (mean = 0.34%) (Figure 3.6, c), as well as *Trpv1*+ neurons from the vehicle (mean = 35%) and *Trpa1*-depleted mice (mean = 12%) (Figure 3.6, d).

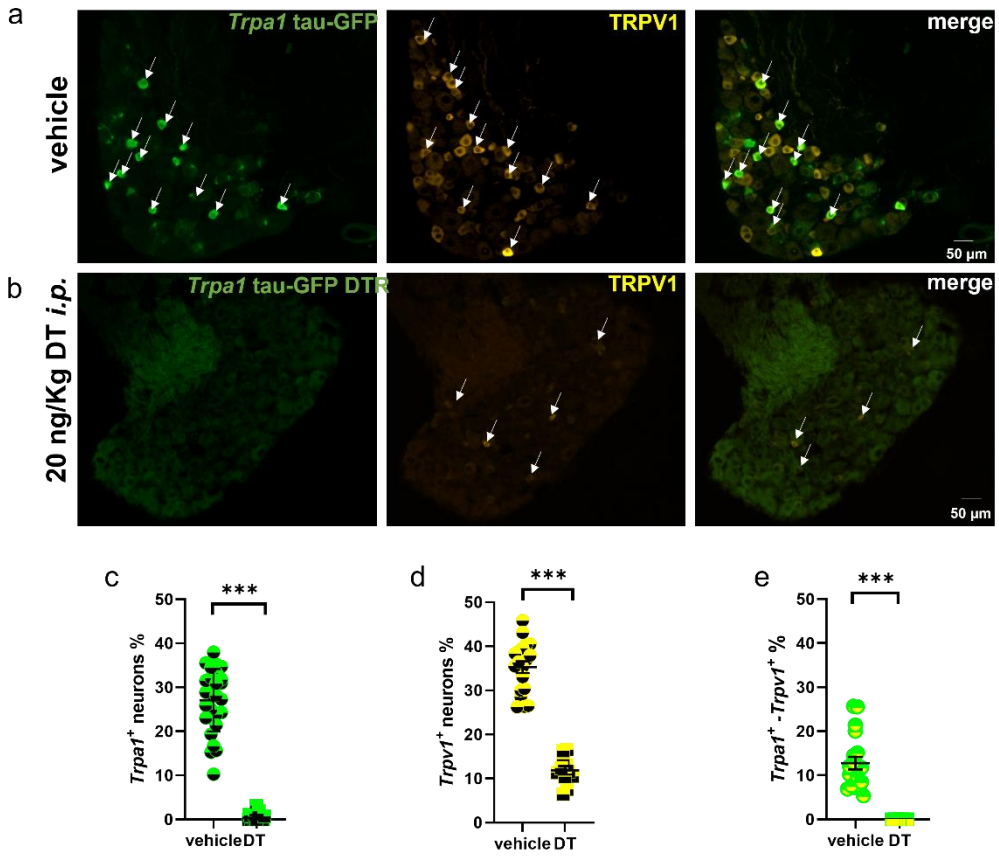

Figure 3.6: Characterization of the depletion of *Trpa1*+ and *Trpv1*+ neurons as confirmed by immunohistochemistry. The *Trpa1*+ neurons in *Trpa1*tauGFP-DTR mice were depleted via the *i.p.* injection of a 20ng/kg DT for three constitutive days. Ten days later, the mice were sacrificed and the DRG were collected. a: A cross-section of DRG showing positive *Trpa1*+ neurons enhanced GFP signal (green), in yellow *Trpv1*+ neurons. b: A cross-section of depleted DRG *Trpa1*+ neurons (green) also shows a reduced TRPV1 signal (yellow). c: Percentage count of *Trpa1*+ neurons in the vehicle and depleted mice. d: Percentage count of *trpv1*+ neurons in depleted mice compared to the vehicle. e: Percentage count of *Trpa1*+ and *Trpv1*+ double-positive neurons in the vehicle and depleted mice, n=3 to 4 mice/group expressed as the mean ± SEM. P values were determined by the unpaired two-tailed Student's T-test (***, $P < 0.001$).

3.5.2 *Trpa1* and *Trpv1* relative gene expression depletion confirmed via RT-PCR

After DT systemic treatment that led to *Trpa1*+ sensory neuron depletion, quantitative RT-PCR in regard to the gene expression of b-micro globulin (b-MG) in the DRG and JNC was prepared to investigate the gene expression for both *Trpa1* and *Trpv1* genes in the vehicle-treated and *Trpa1*-depleted mice. The relative gene expression of the *Trpa1* gene was significantly reduced compared to the vehicle (vehicle mean ΔCT = 0.024 to DTR mean ΔCT = 0.0039) in the DRG (vehicle mean ΔCT = 0.018 to DTR mean ΔCT = 0.0031) and in the JNC. Interestingly, the relative gene expression of the *Trpv1* gene was also significantly reduced in the DRG (vehicle mean ΔCT = 0.195 to DTR mean ΔCT = 0.0025) and in the JNC (vehicle mean ΔCT = 0.12 to DTR mean ΔCT = 0.0025), compared to the vehicle-treated group. The significant down-regulation of both *Trpa1* and *Trpv1* gene expressions in the sensory ganglia is another indication of the successful depletion of *Trpa1*/*Trpv1* sensory neurons in the ganglia (Figure 3.7, a and b).

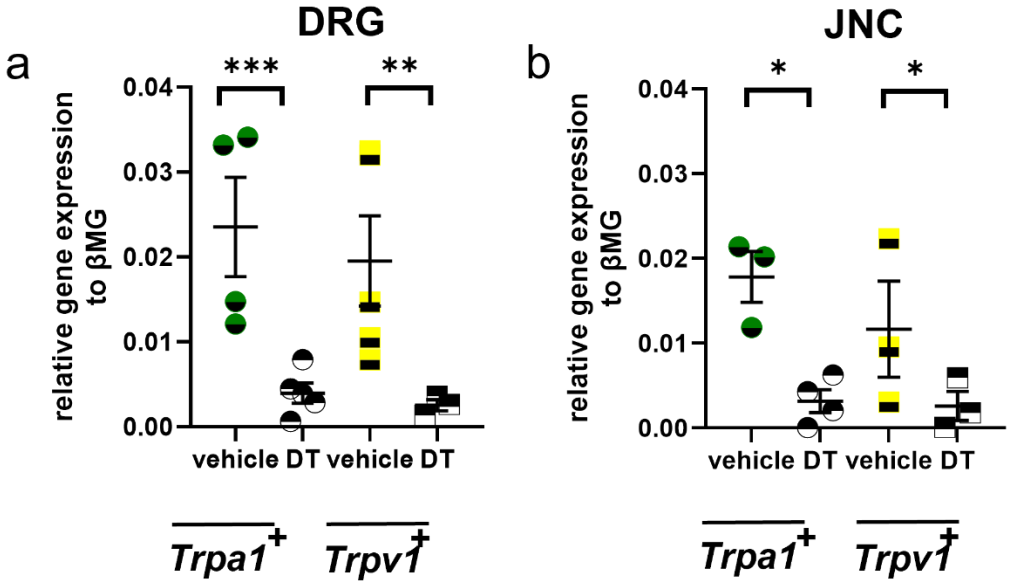

Figure 3.7: *Trpa1* and *Trpv1* relative gene expression confirmed via RT-PCR. The TRPA1 channel in *Trpa1*tauGFP-DTR mice was depleted by the intra-tracheal application of 20 ng/kg DT every day for three days. Ten days later, the mice were sacrificed and the JNC and DRG were collected for RNA extraction. a: Quantitative PCR confirming *Trpa1*+ neuron depletion in the DRG of DTR mice compared to the vehicle. b: Quantitative PCR to confirm the changes in *Trpv1*+ neurons in the vehicle and depleted mice. n=3 to 4 mice/group expressed as the mean ± SEM. P values were determined by the unpaired two-tailed Student's T-test (*, P < 0.05, **, P < 0, 01, ***, P < 0.0001).

3.5.3 *Trpa1* depletion led to CGRP and SP reduction in the sensory neurons

In the DRG, 11.1% of neurons were double-positive for SP and CGRP. Only 4% were solely positive for CGRP and less than 0.5% were solely positive for SP (Figure 3.8, a and c). After *Trpa1* depletion, these percentages dramatically decreased to less than 3% CGRP/SP double-positive, 1.76% only CGRP-positive, and 0.15% only SP-positive (Figure 3.8, b and c).

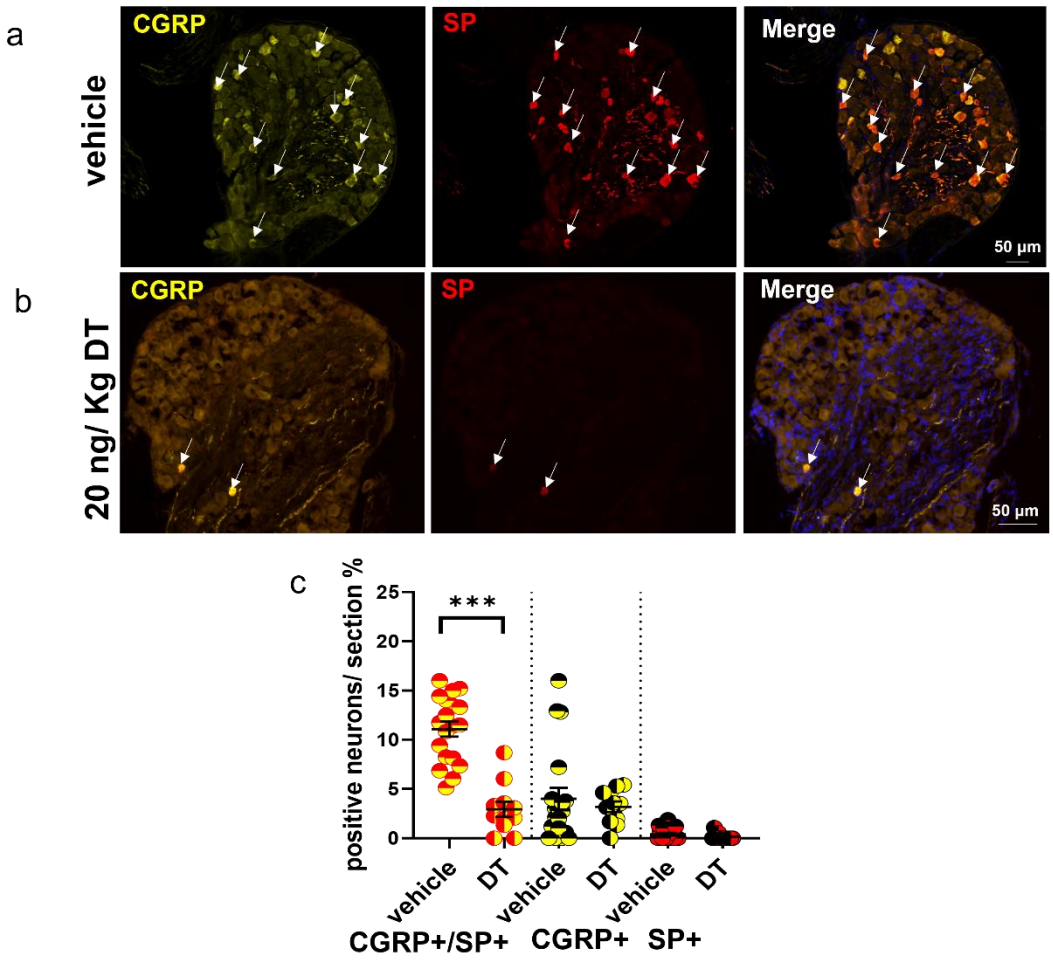

Figure 3.8*:* Reduction of CGRP and SP positive neuronal fibers accompanies *Trpa1* depletion. a: Immunohistochemistry for CGRP in yellow and SP in red, displaying CGRP and SP+ neurons in a DRG cross-section of a vehicle. b: A cross-section of DRG from *Trpa1*-DTR mice showing a reduction in CGRP and SP+ neurons compared to the cross-section in (a). c: Percentage count of CGRP/SP, CGRP, and SP positive neurons in the vehicle and depleted DRG showing a significant decrease in the number of CGRP/SP+ neurons of the *Trpa1*-DTR mice compared with the vehicle. n=6 to 8 mice/group expressed as the mean ± SEM. P values were determined by the unpaired two-tailed Student's T-test (***, $P < 0.001$).

3.5.4 *Trpa1* depletion led to CGRP and SP reduction in the trachea

To demonstrate the reduction of CGRP and SP+ sensory neuronal fibers in the trachea of the *Trpa1*-DTR mice, immunohistochemistry (Figure 3.9, a) was illustrated for tracheal cross-sections and whole-mount tracheal preparations from both vehicle and *Trpa1*-DTR mice (Figure. 3.9, c). The alteration in CGRP/SP+ (yellow/red respectively) neurons in the vehicle and after depletion is very noticeable in the pictures. For more precise confirmation, IMARIS software was used to measure the fluorescence intensity for the CGRP and SP signals in a defined image stack volume. Vehicle treated mice relative volume mean = 1.256 compared to 0.1285 in DT treated mice, and vehicle treated mice relative volume mean = 1.563 compared to 0.207 in DT treated mice for SP and CGRP, respectively (Figure. 3.9, b).

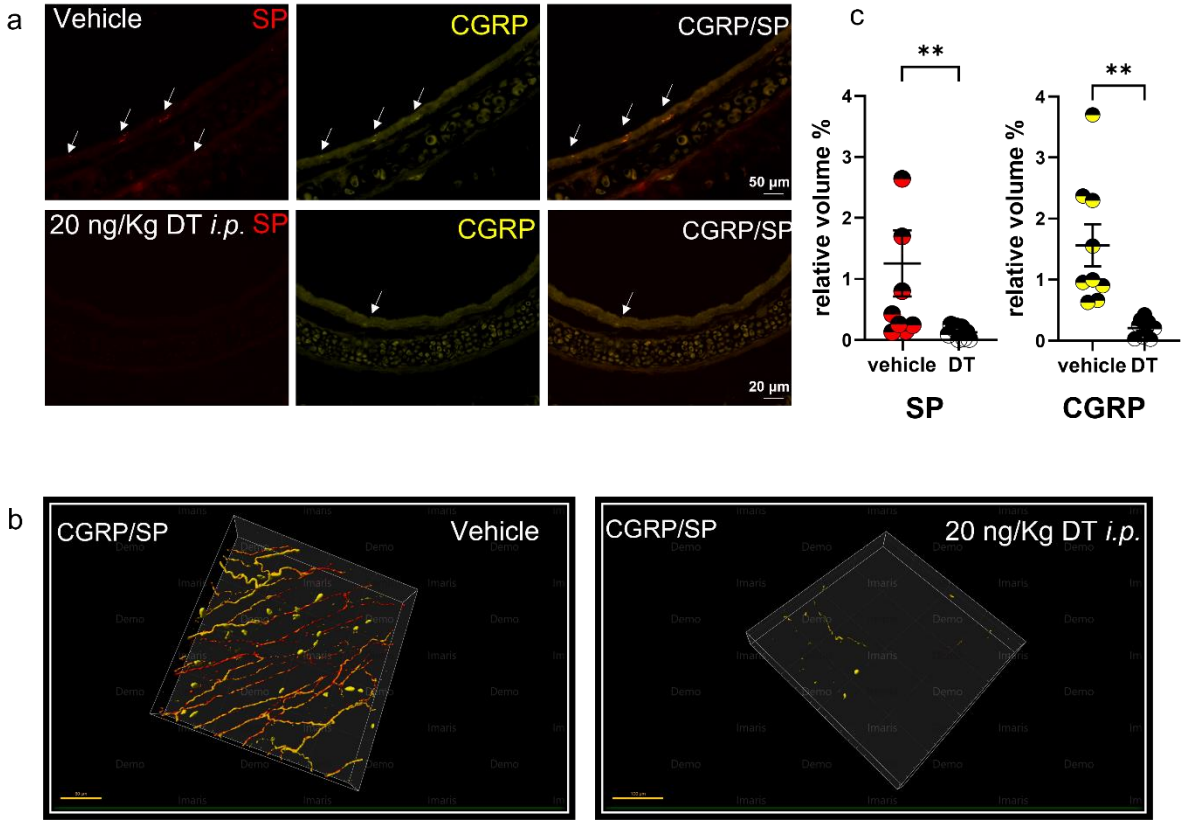

Figure 3.9: Depletion of CGRP+ and SP+ sensory neuronal fibers accompanied the *Trpa1* depletion in the trachea. a: A tracheal cross-section showing, in yellow CGRP+ fibers, in red SP+ fibers in the vehicle, and after DT treatment. b: Percentage of the relative volume intensity of SP and CGRP in the vehicle and depleted mice. c: Tracheal whole-mount preparations of the vehicle and *Trpa1*-DTR mouse showing CGRP and SP fiber reduction in the DT-treated mice. Whole-mount pictures were taken using a confocal microscope showing SP+ in red, and CGRP in yellow in both vehicle and depleted mice. n=3 mice/group, two sections each, expressed as the mean ± SEM. P values were determined by the unpaired two-tailed Student's T-test (**, P < 0, 01).

3.5.5 *Trpa1* depletion led to the inhibition of denatonium-induced neurogenic inflammation

Firstly, to exclude the involvement of the DT in inducing neurogenic inflammation in the airways, vehicle mice (without the DTR) were injected *i.p.* with the (DT) (20 ng/kg body weight) on three consecutive days. Then, the neurogenic inflammation model described earlier was used to compare these mice to the vehicle mice that didn't receive any treatment, both after inhalation of 1 mM denatonium. The two groups were significantly similar in EB mean intensity (mean vehicle = 3.3, mean vehicle + DT = 3.1. Figure 3.10, a and b). Regarding neutrophil recruitment, both groups had comparable intra-epithelial (mean vehicle = 1, mean vehicle + DT = 1.6) and extra-epithelial (mean vehicle = 6.4, mean vehicle + DT = 7.5) neutrophil numbers (Figure 3.10, b). Secondly, the *Trpa1*-DTR mice were stimulated with different denatonium concentrations: 1, 10, and 20 mM. The first two concentrations were similar to the vehicle (mean of Evans blue = 1.842 1.63, and 1.45, respectively). However, for 20 mM denatonium-treated mice, the mean of Evans blue intensity was significantly different at 2.54.

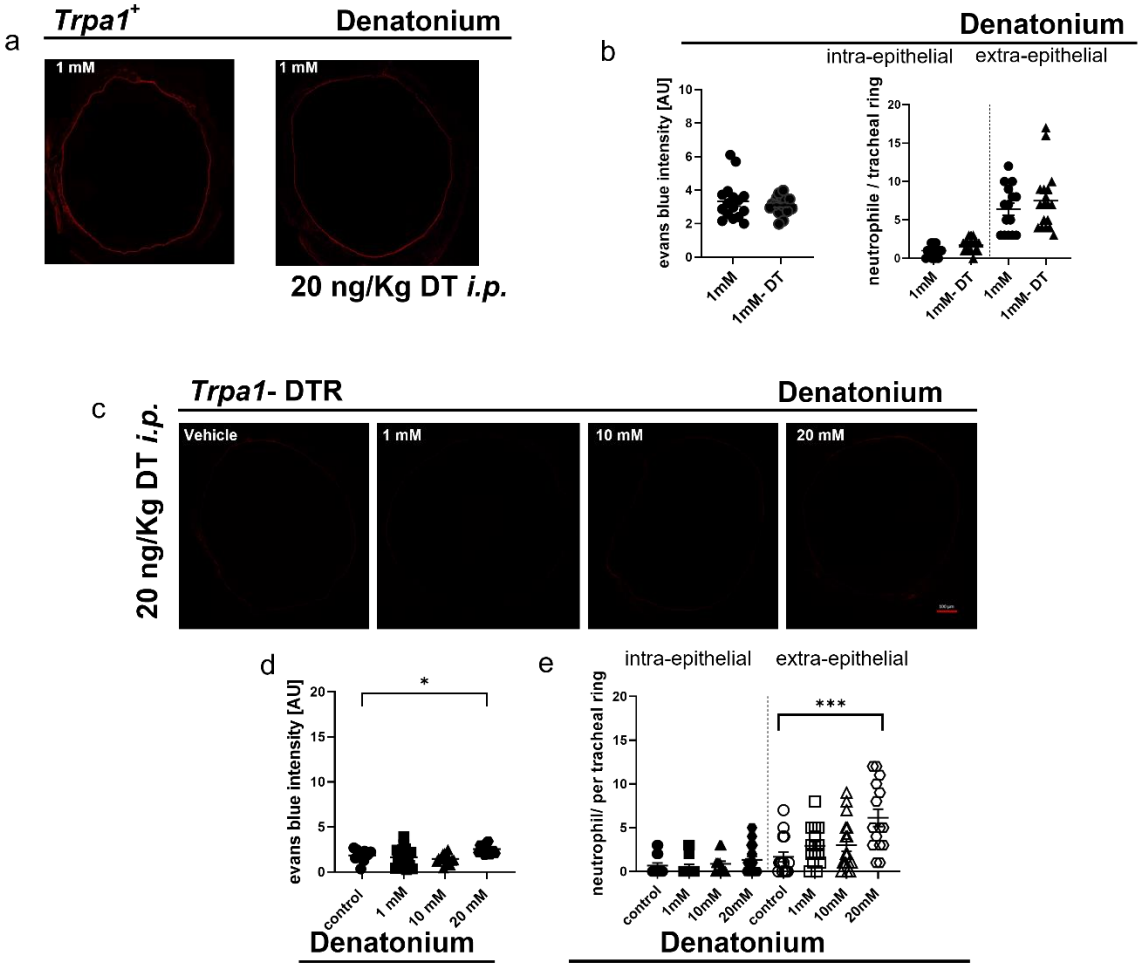

Figure 3.10: Experimental outline of plasma extravasation and neutrophil recruitment in the vehicle, vehicle+ DT, and *Trpa1*- DTR mice. a: Images from tracheal sections showing similar Evans blue extravasation in both groups.

b: The stimulation with 1 mM den led to an increase in fluorescence intensity estimated using a Texas red filter. The DT treatment in the second group didn't affect the intensity of the Evans blue dye. c: Tracheal cross-sections showing significantly reduced plasma extravasation in the vehicle: 1, 10, and 20 mM den stimulation after the *i.p.* injecting the *Trpa1*-DTR mice with 20 ng /Kg DT. d: Evans blue intensity measurements in the depleted *Trpa1*-DTR mice. e: Neutrophil count in the vehicle: 1, 10, and 20 mM den stimulation after *Trpa1*-DTR depletion illustrating a significant number of extra-epithelial neutrophils recruited after 20 mM denatonium stimulation compared to the vehicle. Both (1 and 10 mM) denatonium-treated mice were similar to the vehicle. The number of intraepithelial neutrophils was comparable in treated and not-treated mice (*, $P < 0.05$; ***, $P < 0.001$).

Alongside Evans blue intensity, recruited neutrophils were counted per section. Similar results were compatible with the intensity of the EB dye extravasation: 1 mM and 10 mM were similar to the vehicle, while 20 mM was significantly different (mean neutrophil per ring: vehicle = 0.667,1 mM = 0.53 10 mM = 0.86 and 1.3 for 20 mM) for the intra-epithelial (mean neutrophil per ring: vehicle = 1.667,1 mM = 2.9 10 mM = 3 and 6.1 for 20 mM) and extra-epithelial (Figure 3.10 e). The remaining effect in the 20 mM den concentration is believed to be conducted through the residual un-depleted *Trpv1*+ neurons. The depletion of most *Trpa1*+ nociceptor neurons was complemented by an 80% depletion of *Trpv1*+ neurons and 73% of SP/CGRP double-positive neurons. This all led to a neurogenic inflammation inhibition in the airways at least in the 1 and 10 mM denatonium.

3.5.6 Denatonium treatment leads to blood vessel dilation in WT mice

To investigate the effect of denatonium on blood vessel tone in each of our animal models, tracheal whole-mount preparations were performed. The tracheas were stimulated with 1 mM denatonium. WT, *Trpm5*-deficient, and *Trpa1*-DTR mice were sacrificed 30 min after stimulation. CD31 antibody was used for the staining of endothelial cells of the blood vessels. Images were taken using a confocal microscope (Leica TCS SP5), while Image J software was used for the image analyses which included measurements of the diameter of different types of small blood vessels (Figure 3.11, b). These vessels play an important role in the cardiovascular system. By constricting or dilating in response to various signals, arterioles regulate blood flow in the trachea. Venules collect blood from capillaries and return it to the larger veins, whereas a capillary connects an arteriole and provides nutrients, oxygen, carbon dioxide, and waste exchange between the bloodstream and tissue. These vessels can be easily identified in whole-mount preparations. An arteriole is a relatively straight, narrow vessel with elongated, spindle-shaped endothelium and elongated smooth muscle cells around the circumference. Venules are more prominent, more branched, more variable in size, and irregularly shaped. The lymphatics are situated between cartilage rings. They are composed of initial lymphatic vessels collecting lymphatics (Ni *et al.*, 2010; Baluk and McDonald, 2018, 2022). In this experiment, the WT mice had an increase in diameter after denatonium stimulation compared to the vehicle mice. *Trpm5*-KO mice and *Trpa1*-DTR mice were similar to the vehicle after denatonium treatment (Figure 3.11, a).

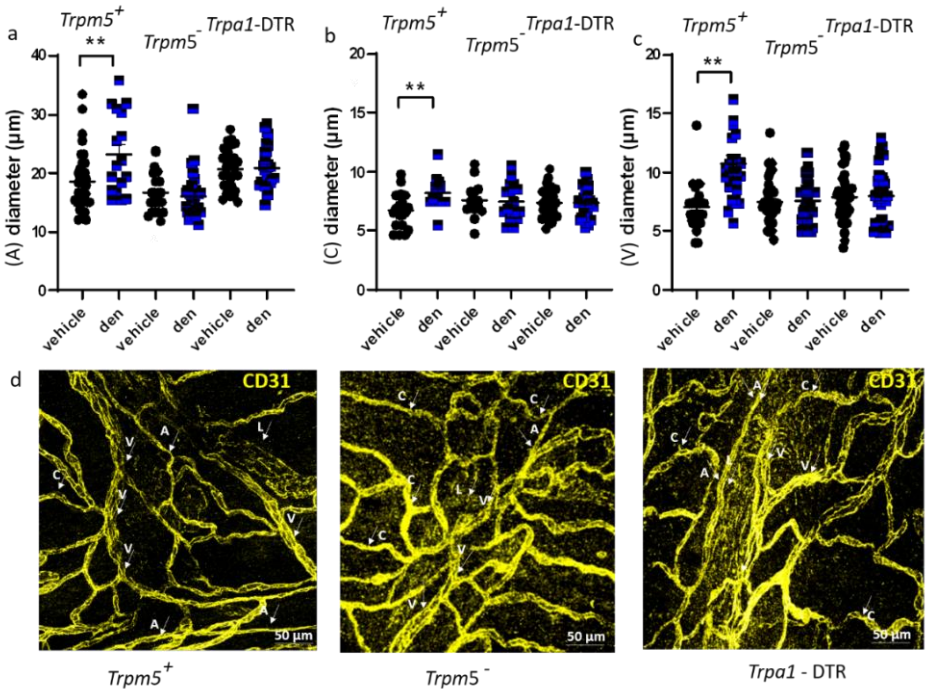

Figure 3.11*:* BC activation with 1 mM denatonium dilated vessels in the WT mice. a: A significant difference is seen in the diameter of the arterioles between the WT vehicle and after 1 mM denatonium stimulation: denatonium-stimulated *Trpm5*-KO mice and *Trpa1*- DTR mice were similar to their vehicle. b: The diameter of the capillaries in denatonium-stimulated WT were different from the treated vehicle, whereas *Trpm5*-KO mice and *Trpa1*- DTR mice were similar to the vehicle. c: The diameter of venules from the WT showed a significant change between the vehicle and stimulated WT mice: the *Trpm5*-KO mice and the *Trpa1*- DTR mice were similar to the vehicle. d: The pictures of whole-mount tracheal preparations for CD31 (in yellow) display different vessel distribution in the trachea (venules (v), arterioles (A), capillaries (C), and lymphatics (L) in WT, *Trpm5*-KO, and *Trpa1*- DTR. The pictures were taken using a Lecia SP5 confocal microscope. n=3 mice/group expressed as the mean ± SEM. P values were determined by the one-way ANOVA-test (**, $P < 0.01$).

3.6 The TRPM5 channel is not expressed in the sensory ganglia, and neither TRPA1 nor TRPV1 are affected by this

Here, the aim is to discover the role of the TRPM5 channel in the sensory neurons. Firstly, in order to detect the abundance of the TRPM5 channel in the sensory ganglia, Western blotting was performed with total protein lysates from DRG, JNC, WT HEK293 cells and HEK293 cells transfected with *Trpm5* (positive control) using antibodies against TRPM5 and b-tubulin, and expression levels at 131kDa and 55 kDa, respectively (Figure 3.12, a).

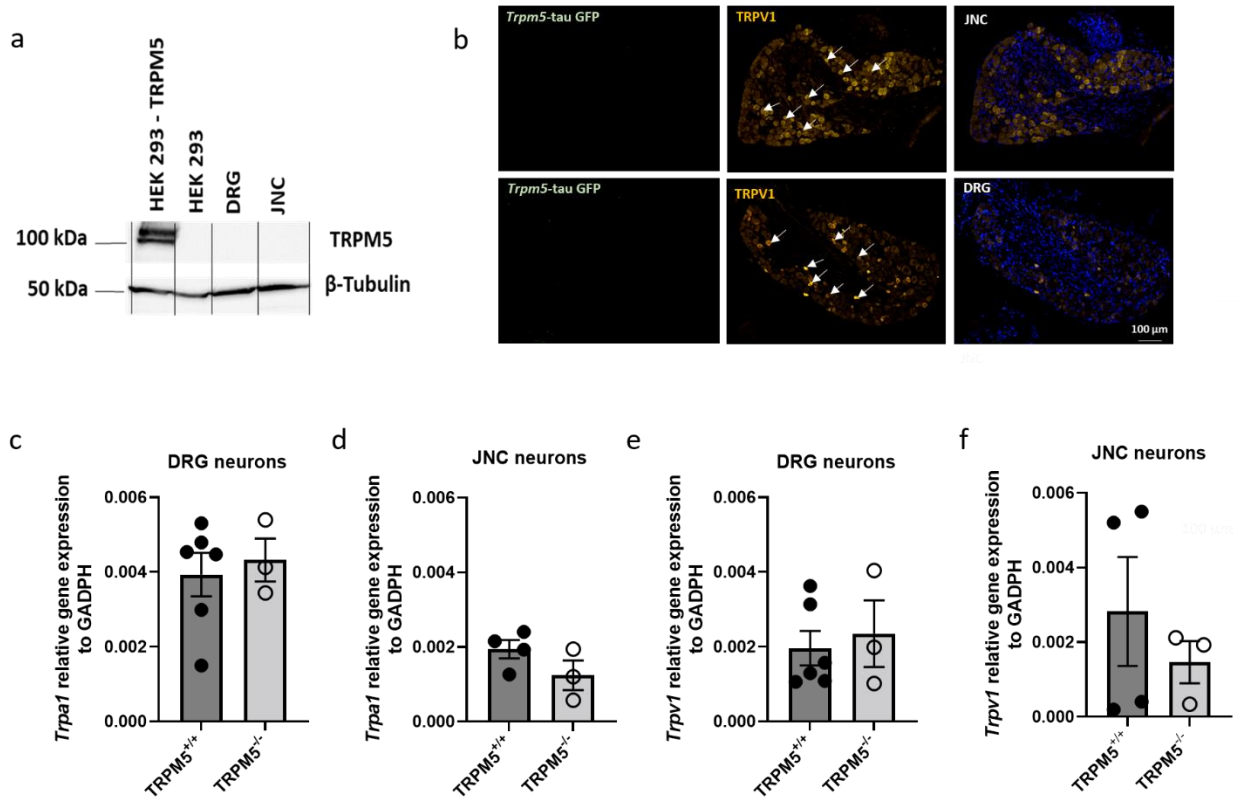

Figure 3.12*: Trpm5* is not expressed in the sensory ganglia and the *Trpm5*-deficiency does not affect the *Trpv1* and *Trpa1* content. a: Total protein lysate from DRG, JNC, and HEK293 cells were used in this Western blot. b: Neuronal cross-sections from *Trpm5*- tau GFP mice: no *Trpm5* positive neurons were found in the DRG or JNC neurons enhanced the GFP signal (green), in yellow *Trpv1*+ neurons. c, d, e, and f: The DRG and JNC from WT and *Trpm5*-KO mice were collected for RNA extraction. Then, qPCR was employed to investigate *Trpa1* and *Trpv1* gene expression in the sensory ganglia of both genotypes. All comparisons were similar to the vehicle. n=3 to 5 mice/group expressed as the mean ± SEM. P values were determined by the unpaired two-tailed Student's T-test.

The first row shows that the TRPM5 channel was not detected in either one of the sensory ganglia compared to the positive control (first lane). The blot is also showing equal amounts of protein loaded using the β-tubulin antiserum as a housekeeping gene in the second positive row of each lane. Secondly, using immunohistochemistry, we showed that the channel is not expressed in sensory DRG and JNCs (Figure 3.12, b). Sensory ganglia (DRG and JNC) were collected from *Trpm5*-tau GFP mice, sections were made and stained, the GFP signal (green) was enhanced to investigate the occurrence of the TRPM5 channel and the TRPV1 antiserum (yellow) was used as a positive control. Furthermore, quantitative RT-PCR was used to investigate whether there was any difference in the expression of *Trpa1* and *Trpv1* between the WT and the *Trpm5* deficient mice (Figure 3.12, c, d, e and f). Total RNA was extracted from the sensory ganglia (DRG and JNC) of both mice models and equal amounts of cDNA were used in each qPCR reaction tube. Relative expression was normalized to the relative *GADPh* gene expression. Interestingly, the results

indicated no significant difference in the expression of these genes in the WT compared with the KO. *Trpa1* relative gene expression in the DRG (Figure 3.12, c) shows no significant difference between the vehicle (mean Δ CT = 0.003932) and *Trpm5* deficient mice (mean Δ CT = 0.004322). *Trpa1* relative gene expression in the JNC (Figure 3.12, d) is also showing no significant difference between the vehicle (mean Δ CT = 0.001937) and *Trpm5* deficient mice (mean Δ CT = 0.001240). Furthermore, *Trpv1* relative gene expression in the DRG (Figure 3.12, e) shows no significant difference between the vehicle (mean Δ CT = 0.001963) and *Trpm5* deficient mice (mean Δ CT = 0.002351). *Trpv1* relative gene expression in the JNC (Figure 3.12 f) is also showing no significant difference between the vehicle (mean Δ CT = 0.002823) and *Trpm5* deficient mice (mean Δ CT = 0.001462).

3.7 *Trpm5*-deficiency negatively regulates $[Ca^{2+}]$i-dependent responses in capsaicin and CA-stimulated DRG neurons

Previously (Figure 3.12), we confirmed that *Trpm5* is not expressed in the sensory neurons. Here, we studied the effect of *Trpm5* deficiency on the function of the sensory nerve-mediated responses. To study the function, two of the most abundant TRP channels in the DRG and JNC, TRPA1 and TRPV1, were chosen for our investigation. First, we chose specific selective agonists for both channels and calculated EC_{50} for each via $[Ca^{2+}]$i imaging on DRG dissociated neurons in the WT and the *Trpm5*-deficient mice. Capsaicin is a selective TRPV1 channel agonist, using the $[Ca^{2+}]$i imaging technique. EC_{50} was calculated in the vehicle as 50.1 nM (Figure 3.23, a). Strangely, in the *Trpm5*-deficient mice, the EC_{50} for capsaicin was decreased by more than half, to 18.36 nM. (Figure 3.13, b). Then again, CA is a selective TRPA1 channel agonist, using $[Ca^{2+}]$i imaging. EC_{50} was calculated in the vehicle as 203.7 μM Figure 3.13, c). Oddly, in the *Trpm5*-deficient mice, the EC_{50} for CA was decreased by more than half, to 96.6 μM (Figure 3.13, d).

Starting from this experiment, we considered all neurons that responded to CA in $[Ca^{2+}]$i imaging as *Trpa1*+ neurons. Additionally, we considered all neurons that react to capsaicin as *Trpv1*+ neurons.

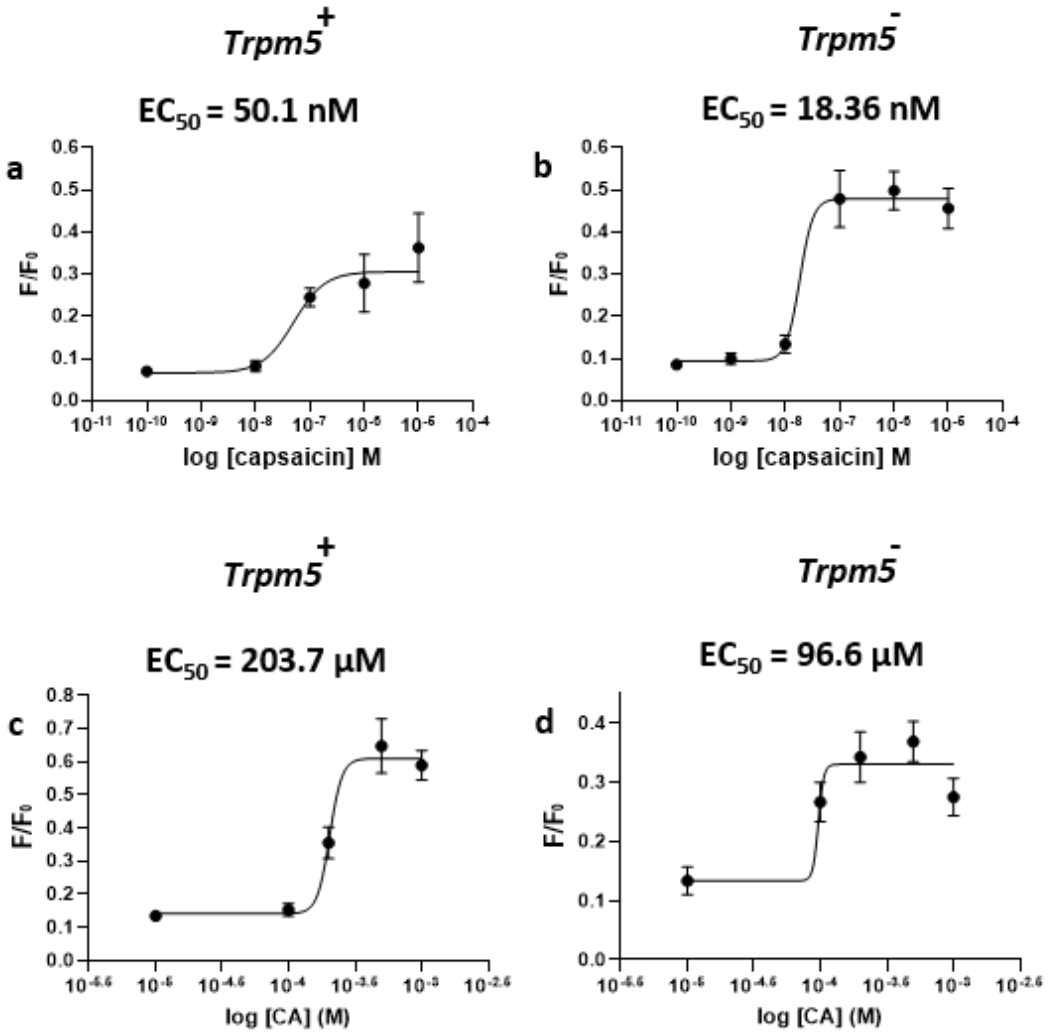

Figure 3.13: *Trpm5* deficiency affected the sensitivity of the TRPA1 and TRPV1 channels in the DRG. a: EC_{50} for capsaicin in the WT is 50.1 nM based on $[Ca^{2+}]i$ imaging measurements. b: *Trpm5*-KO mice had an almost 50% decrease in sensitivity to capsaicin with an EC_{50} of 18.36 nM. c: CA EC_{50} in the WT is 203.7 µM. d: *Trpm5*-KO had an almost 50% decrease in the sensitivity to CA with EC_{50} = 96.6. n=3 to 5 mice/group expressed as the mean ± SEM.

3.8 *Trpm5* deficiency negatively regulates $[Ca^{2+}]i$-dependent responses in capsaicin and CA-stimulated JNC neurons

Having confirmed an effect of *Trpm5* deficiency on in the DRG, it's reasonable to investigate whether the effect is true in the JNC. In this case, JNC dissociated neurons were used in $[Ca^{2+}]i$ imaging experiments to calculate the EC_{50} for both TRPA1 and TRPV1 EC_{50}. As with the EC_{50} results from the DRG neurons, the EC_{50} results from the JNC were affirmative (Figure 3.14, a and b). The sensitivity of TRPA1 in the JNC increased from EC_{50} = 203 µM in the WT to EC_{50} = 96.58 µM in the KO (Figure 3.14, a). Additionally, the

sensitivity of the TRPV1 in the JNC increased from EC_{50} = 51.4 nM in the WT to EC_{50} = 5.3 nM in the *Trpm5*-KO (Figure 3.14, b).

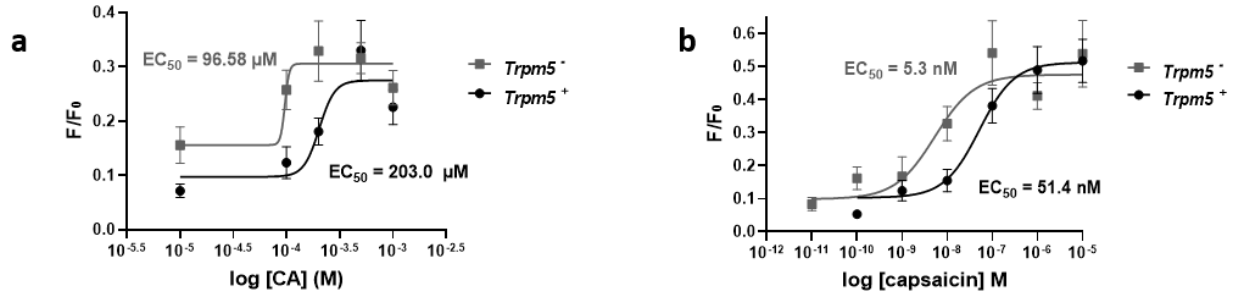

Figure 3.14*:* The TRPM5 channel deficiency affects the activity of TRPA1 and TRPV1 in the JNC but is almost equal to the DRG in the WT. $[Ca^{2+}]i$ imaging from JNC dissociated neurons in WT and *Trpm5*-KO mice was used to calculate EC_{50} for CA and capsaicin. a: CA EC_{50} is 203 µM in the WT, and 96.58 µM in the *Trpm5*-KO. b: Capsaicin EC_{50} in the WT is 51.4 nM while it is 5.3 nM in the *Trpm5*-KO mice. n=3 to 5 mice/group expressed as the mean ± SEM.

3.9 Local depletion of tracheal BC negatively regulates $[Ca^{2+}]i$-dependent responses in capsaicin and CA-stimulated sensory ganglia

In the previous experiment, we evidenced a difference in the sensitivity of sensory neurons between the WT and the *Trpm5*-deficient mouse model which had a systemic *Trpm5* deficiency. However, we are interested in the effect of the tracheal-*Trpm5*+ BC on the sensory nerve-mediated responses. Here, we used a different mouse model, in which *Trpm5* cells are targeted and depleted in the trachea after DT local application. The tracheae of *Trpm5*-DTR mice received an amount of 40 µl of DT (200 ng). 48h after the treatment, the DRG were explanted, and $[Ca^{2+}]i$ imaging was employed to calculate the EC_{50} of TRPV1 and TRPA1. A predictable result in both experiments was acquired. Both EC_{50} were reduced in the DRG of *Trpm5*- DTR mice. The EC_{50} was estimated at 14.84 nM capsaicin, and 144.2 µM CA (Figure 3.15, a, c). The change in $[Ca^{2+}]i$ was not the only difference after depletion: more cells were reacting to different concentrations; for example, a mean of 34% of DRG neurons reacted to 100 nM capsaicin in comparison to a mean of 58% from the *Trpm5*-DTR mice (Figure 3.15, b). As per 500 µM CA, a mean of 23% DRG neurons reacted in vehicle mice compared to a mean of 55% from neurons of the *Trpm5*-DTR mice (Figure 3.15 d). The change in EC_{50} of both TRPA1 and TRPV1 channels in the *Trpm5*- DTR model demonstrate the important effect of BC on the sensitivity of sensory neurons.

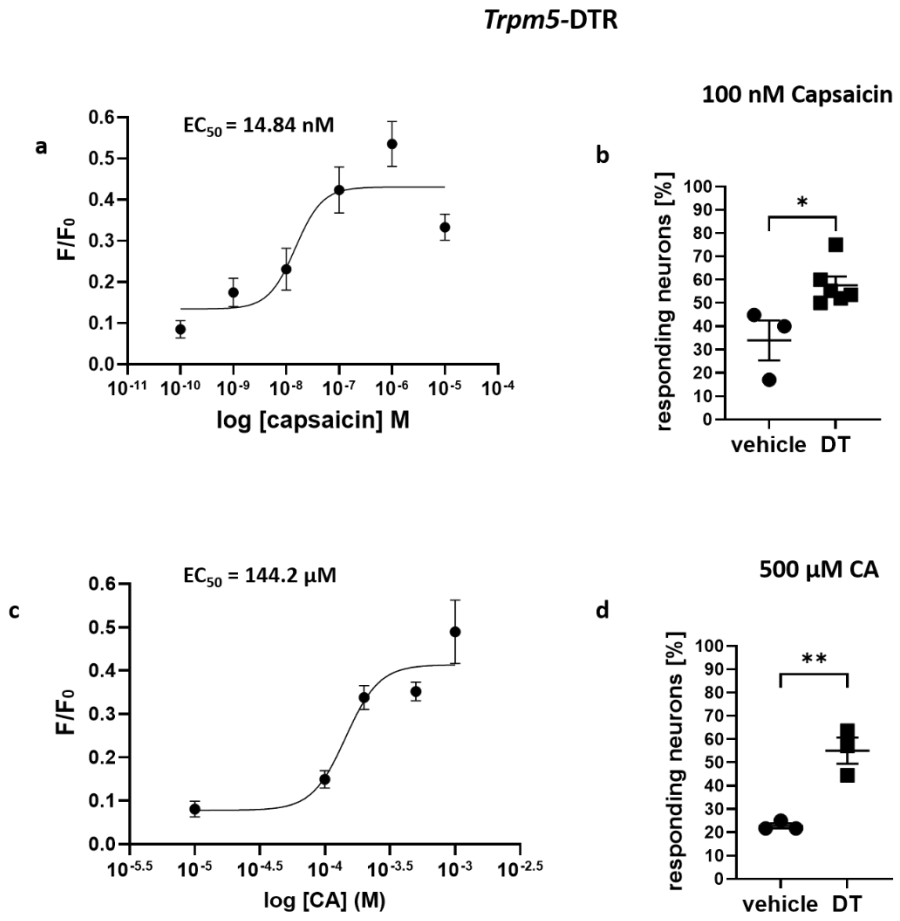

Figure 3.15: Local tracheal BC depletion affects the activity of the TRPA1 and TRPV1 in the DRG. BC in the *Trpm5*-DTR mice were depleted via the intra-tracheal application of 200 ng DT. 48h later, the mice were sacrificed and the DRG were collected. a: The capsaicin EC_{50} in the DRG neurons of *Trpm5*- DTR mice is 14.84 nM. b: In the percentage of reacted neurons to 100 nM capsaicin, the WT was significantly different than the *Trpm5*-depleted mice. c: The CA EC_{50} in the DRG neurons of *Trpm5*- DTR mice is 144.2 µM. d: The percentage of responding DRG neurons to 200 µM CA in the WT was significantly different to the *Trpm5*-DTR mice. n=3 to 5 mice/group expressed as the mean ± SEM. P values were determined by the unpaired two-tailed Student's T-test (*, $P < 0.05$, **, $P < 0.01$).

3.10 Local depletion of tracheal BC negatively regulates $[Ca^{2+}]$i-dependent responses in sensory neurons of the JNC

In this experiment, the JNC from the mice after 48h of tracheal application of 40 µl of DT (200 ng) were explanted and dissociated for $[Ca^{2+}]$i imaging. A similar outcome to the DRG results was observed: more neurons from the *Trpm5*-DTR mice were reacting to 50 nM capsaicin (mean = 38% in vehicle to mean = 52% in *Trpm5*-DTR) and 200 µM CA (mean = 38% in vehicle to mean = 61% in *Trpm5*-DTR) (Figure 3.16 a, c). Nevertheless, many studies suggested that DT injections caused an inflammatory response due to cell death, so we cannot conclude whether these outcomes were due to depletion.

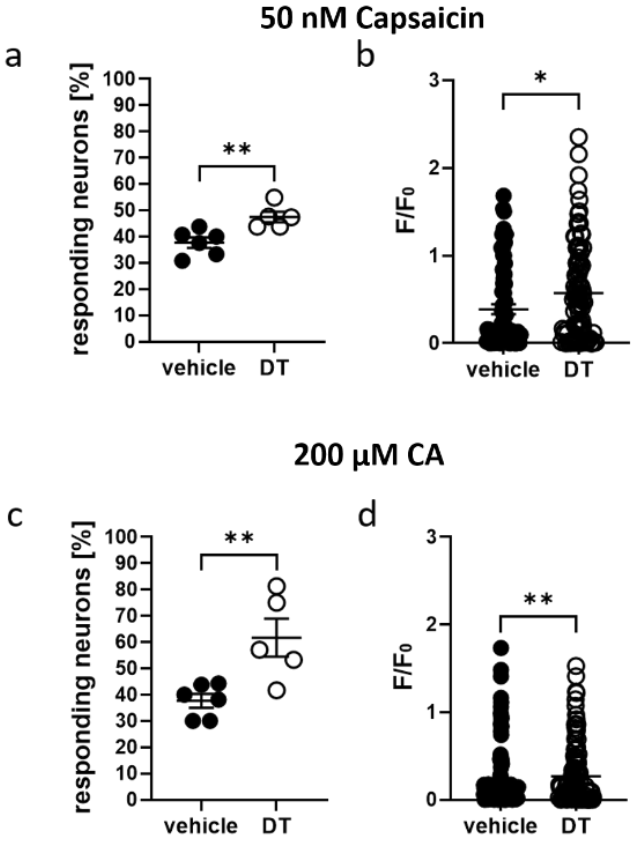

Figure 3.16*:* Local BC depletion in the trachea affects the activity of TRPA1 and TRPV1 in the JNC. BC in *Trpm5*-DTR mice were depleted by the intra-tracheal application of 200 ng /kg DT. 48h later, the mice were sacrificed and the JNC were collected. a: Percentage of reacted neurons to 50 nM capsaicin: the WT was significantly different to the *Trpm5*-DTR mice. b: Difference in $[Ca^{2+}]i$ after capsaicin stimulation: a significant number of neurons had an increase in $[Ca^{2+}]i$ from *Trpm5*-DTR mice compared to the WT; n=72 and 92 neurons respectively. c: Percentage of reacted neurons to 200 µM CA: the WT was significantly different from *Trpm5*-depleted mice. d: Difference in $[Ca^{2+}]i$ after CA stimulation: *Trpm5*-depleted mice were significantly different from the WT; n=130 and 170 neurons, respectively. n=5 to 6 mice/group expressed as the mean ± SEM. P values were determined by the unpaired two-tailed Student's T-test (*, $P < 0.05$, **, $P < 0, 001$).

3.11 Confirmation of the depletion of tracheal BC in *Trpm5*-DTR mice

To confirm the success of the tracheal BC depletion, immunohistochemistry was applied for trachea and colon cross-sections from the vehicle and the *Trpm5*-tauGFP-DTR mice. The images (Figure 3.17) show the results. The green signal designates the tauGFP enhanced signal while the TRPM5 signal is in yellow. In the vehicle, the double-immunoreactive cells are the tracheal BC (Figure 3.17, a). However, a complete depletion of the TRPM5 positive signal in the tracheal epithelia after the local application of 200 ng/kg DT is observed (Figure 3.17, b). On the other hand, the occurrence of the TRPM5 channel in the colon was

investigated as well. Cells expressing the *Trpm5* were not depleted after the tracheal application of DT. The immunohistochemistry images in both mice models looked similar (Figure 3.17, c and d). The remaining *Trpm5*+ cells in organs other than the trachea may explain the changes in EC_{50} between *Trpm5*-deficient mice and depleted mice since both models didn't have *Trpm5*+ cells in the trachea. Both capsaicin and CA EC_{50} from the *Trpm5*-deficient mice were less than that of the *Trpm5*-depleted mice, although both were significantly different from the vehicle.

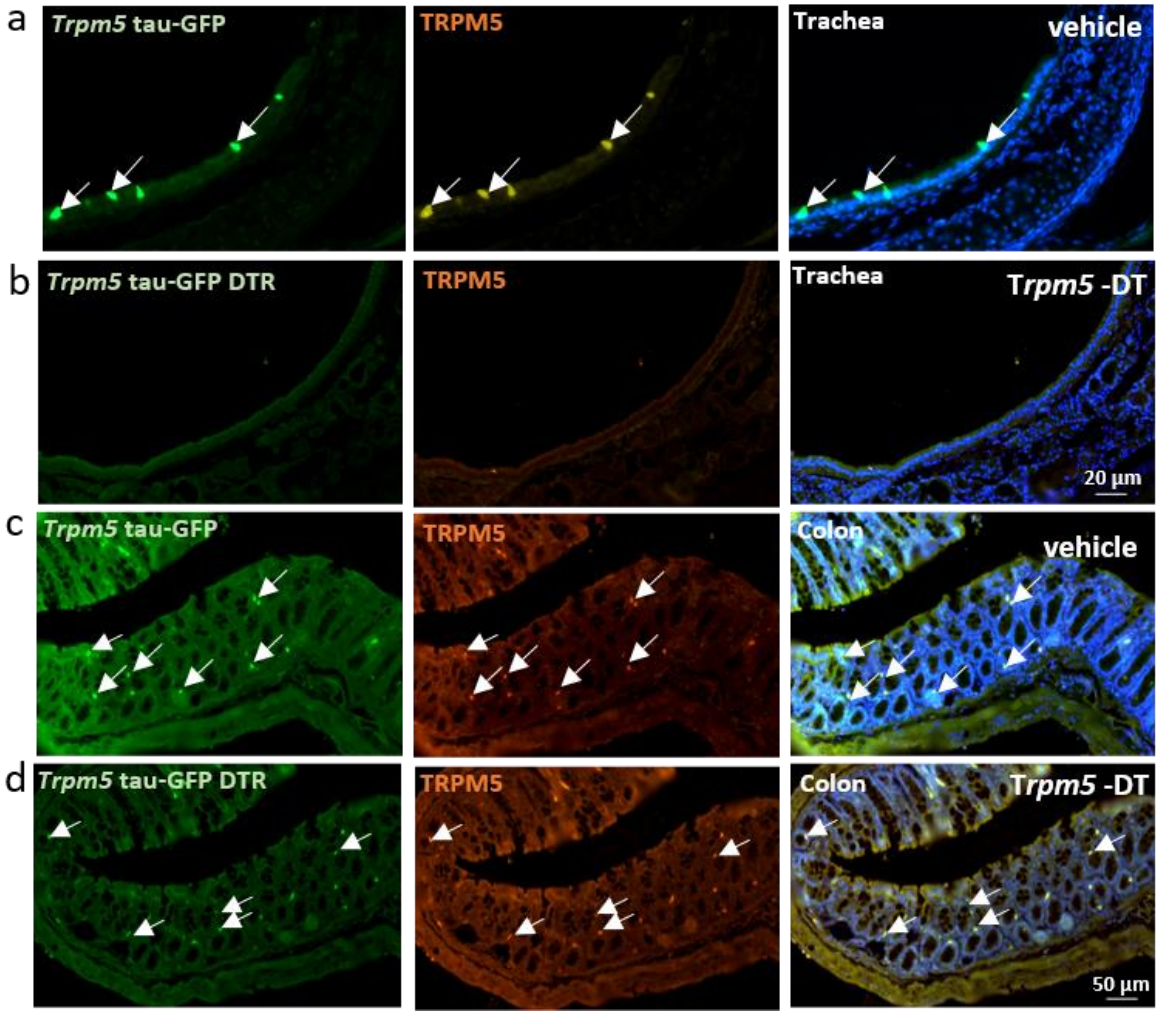

Figure 3.17*:* Local tracheal DT application depletes *Trpm5* cells in the trachea only. a: Immunohistochemistry images of tracheal sections showing epithelial cells of a *Trpm5*-tauGFP mouse, with the enhanced GFP signal in green, and TRPM5 in yellow. b: After 200 ng/kg DT was applied in the trachea, no TRPM5 positive signal was observed in green or in yellow in the trachea of a *Trpm5*-tauGFP-DTR mouse. c and d: colon cross-section showing positive TRPM5 signal in both vehicle and *Trpm5*-tauGFP-DTR mice.

3.12 Tracheal BC activation using CNO altered the activity of the *Trpv1* and *Trpa1*+ neurons in the DRG

In this experiment, we generated mice that express the receptor (DREADD) in *Trpm5*+ cells by cross-breeding the *Trpm5*-IRES-Cre mice with the mouse strain ROSA26NLSiRFP720-2A-Rq. To activate the DREADD receptor, mice were treated with one dose of 100 µM clozapine-N-oxide (CNO) which was inhaled locally by a tube inserted in the trachea. Being able to activate the DREADD receptor in *Trpm5*+ cells means the ability to control the activity of BC.

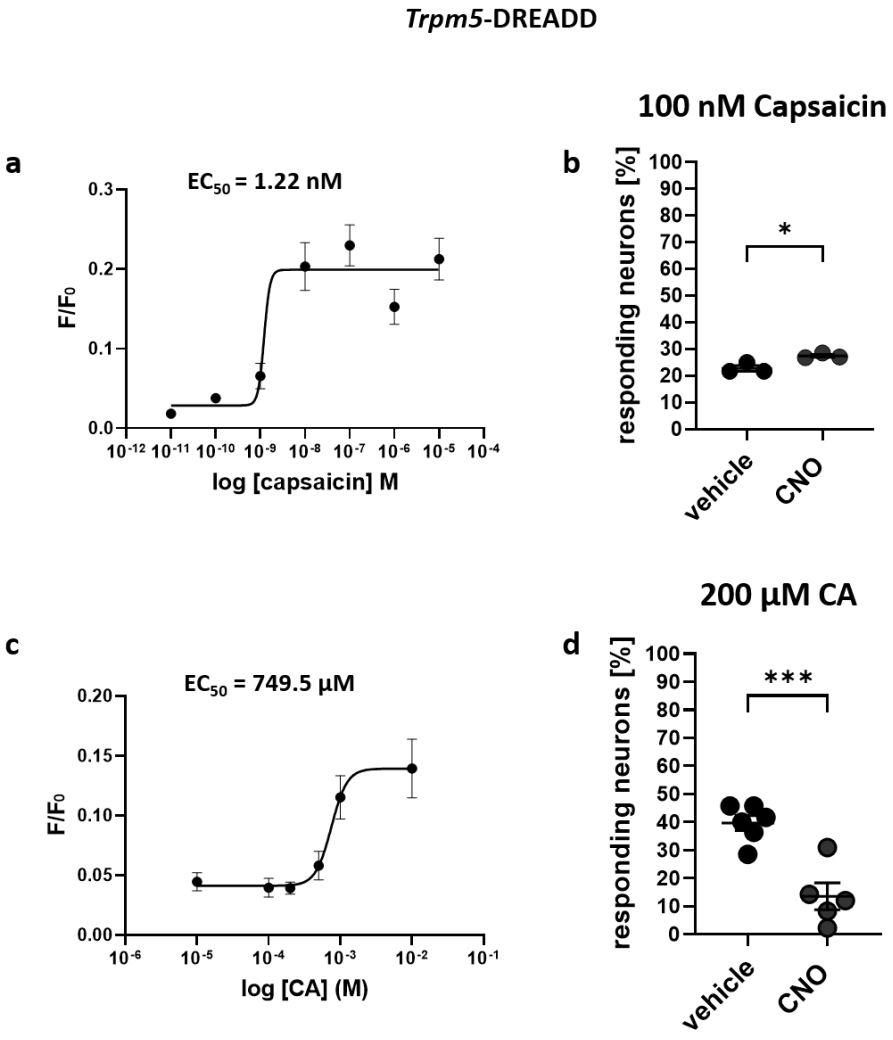

Figure 3.18: Tracheal BC activation affects the sensitivity of sensory neurons in the DRG. Tracheal BC in the *Trpm5*+ DREADD mouse were activated locally using CNO. Thirty minutes later, the mice were sacrificed and DRG were collected. a: $[Ca^{2+}]i$ c of in the *Trpm5*-DREADD mice resulted in EC_{50} of 1.22 nM. b: The percentage of reacted neurons to 100 nM capsaicin in the *Trpm5*-DREADD mice - neurons were significantly more sensitive to capsaicin stimulation than the WT. c: CA $[Ca^{2+}]i$ imaging-based EC_{50} in the *Trpm5*-DREAD mice is 749.5 µM. d: Percentage of reacted neurons to 200 µM CA - WT neurons were significantly less sensitive to CA stimulation than the *Trpm5*-

DREADD mice. Values were determined by the unpaired two-tailed Student's T-test. n=3 to 5 mice/group expressed as the mean ± SEM (*, P < 0.05, ***, P < 0, 001).

In theory, the upstream activation of the DREADD receptor leads to the activation of all BC abundant in the trachea. Thus, to further investigate the influence of tracheal TRPM5 on TRPV1 and TRPA1 in the sensory ganglia, *Trpm5*-DREADD mice inhaled 4 µl of 100 µM CNO. 30 minutes later, the mice were sacrificed. An EC_{50} diagram was made after $[Ca^{2+}]i$ imaging was used. Dissociated neurons from the DRG were stimulated with different capsaicin concentrations (Figure 3.18, a). Surprisingly, the EC_{50} value changed from 50.1 nM in the vehicle to 1.22 nM in the *Trpm5*-DREADD mice. This indicates an increase in the sensitivity of the TRPV1 channel after the activation of BC. Additionally, the mean percentage of responding DRG neurons to 100 nM capsaicin after BC activation was significantly higher than in the vehicle (mean = 22.8% in vehicle, to mean = 28% in *Trpm5*-DREADD) (Figure 3.18, b). On the other hand, the EC_{50} diagram was made to study the effect of BC activation on the *Trpa1*+ neurons. $[Ca^{2+}]i$ imaging was applied to the dissociated neurons using different CA concentrations. Here, *Trpm5*-DREADD mice had a much higher EC_{50} value compared to the vehicle (Figure 3.18, c). The EC_{50} value changed from 203.7 µM in the vehicle to 749.5 µM in the *Trpm5*-DREADD mice, indicating a sharp decrease in the sensitivity of the TRPA1 channel after BC activation. Additionally, the mean percentage of responding neurons to 200 µM CA after BC activation was significantly decreased compared to the vehicle (mean = 40% in the vehicle, to mean = 14% in *Trpm5*-DREADD) (Figure 3.18, d).

3.13 Local activation of BC in the trachea using CNO altered the activity of the *Trpv1* and *Trpa1*+ neurons in the JNC

In this experiment, we aimed to study the change in sensitivity of the JNC neurons after selectively activating BC using the previously explained DREADD receptor. One dose of a 100 µM CNO was applied locally in the trachea of a *Trpm5*-DREADD mouse. Thirty minutes later, the JNC were carefully dissected and the neuronal tissue was dissociated into single neurons. $[Ca^{2+}]i$ imaging was studied after stimulating the JNC dissociated neurons with different concentrations of capsaicin or CA. This is vital to study the change in the activity of TRPV1 and TRPA (Figure 3.19). The precise activation of BC led to a significant increase in the mean number of *Trpm5*-DREADD JNC neurons sensitive to a concentration of 50 nM capsaicin compared to the vehicle (mean = 38% in the vehicle, to mean = 45% in the *Trpm5*-DREADD) (Figure 3.19, a). The previous result was confronted by a significant decrease in the activity of TRPA1. A lower percentage of reacted *Trpm5*-DREADD JNC neurons responded to stimulation with 200 µM CA

compared to the vehicle (mean = 38% in the vehicle, to mean = 16% in the *Trpm5*-DREADD) (Figure 3.19, c).

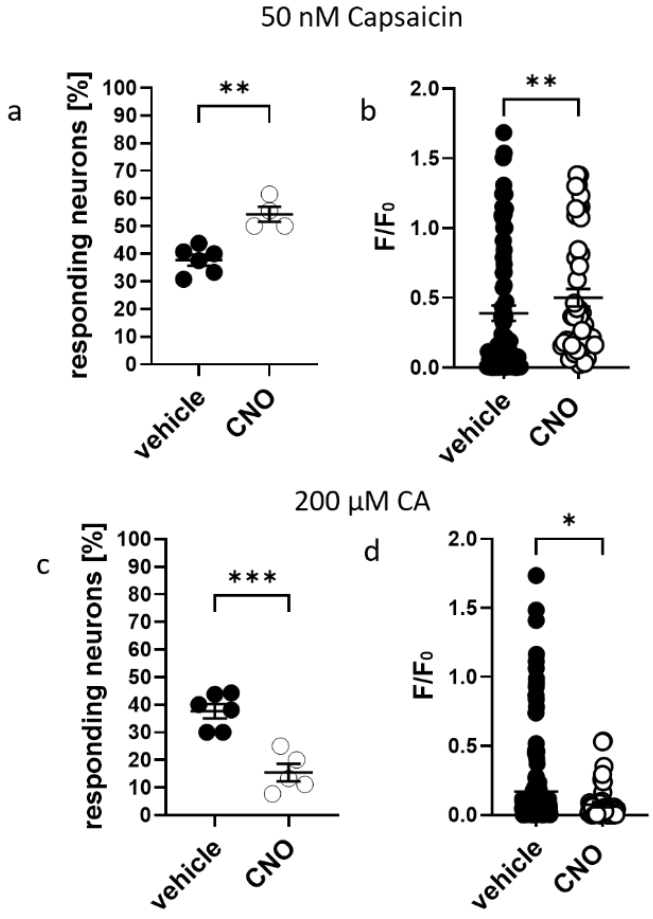

Figure 3.19: Tracheal BC selective activation alters the sensitivity of *Trpv1* and *Trpa1*+ neurons in the JNC. Tracheal BC in the *Trpm5*-DREADD mouse model were activated locally using CNO. Thirty minutes later, the mice were sacrificed and the JNC were collected. a: Percentage of reacted neurons to 50 nM capsaicin. WT was significantly different than the CNO treated DREADD mice. b, Change in $[Ca^{2+}]i$ after stimulation. A significant difference was observed between the vehicle and the CNO-treated *Trpm5*-DREADD mouse. c: Percentage of reacted neurons to 200 µM CA. The WT was significantly different than the CNO treated *Trpm5*-DREADD mouse model. d: Change in $[Ca^{2+}]i$ after stimulation with CA. A significant difference was observed between the vehicle and the CNO-treated DREADD mouse. n=4 to 6 mice/group expressed as the mean ± SEM. P values were determined by the unpaired two-tailed Student's T-test (*, P < 0.05, **, P < 0, 01, ***, P < 0, 001).

3.14 Tracheal BC stimulation via 1 mM denatonium altered the sensitivity of *Trpv1*+ and *Trpa1*+ neurons

Previously we demonstrated several experiments where we proved that the BC-induced protective neurogenic inflammation depends on the transmission to and from sensory nerve fibres. Additionally, we found out that the *Trpv1*+ and *Trpa1*+ sensory neurons had a change in sensitivity after activating BC with

CNO in the *Trpm5*-DREAD mouse model. In this experiment, in order to confirm the effect on sensory neurons after BC activation using CNO and the *Trpm5*-DREAD mouse model, mice from vehicles and *Trpm5*-KO were stimulated *in vivo* with denatonium. For each mouse, a volume of 4 µL of vehicle or 1 mM denatonium was inhaled in the trachea. Mice from both genotypes were sacrificed at different time points after denatonium inhalation, after 30 min, 24h, and one week (Figure 3.20). The JNC from each mouse was collected for neuronal dissociation. $[Ca^{2+}]$i imaging on single neurons was performed. The results were unsurprisingly consistent with the *Trpm5*-DREAD mouse model. In the denatonium-treated mice, a significant number of WT neurons responded to a 50 nM capsaicin stimulation compared to the vehicle after 30 minutes of local denatonium stimulation with P-value <0.0001. The effect decreased significantly after 24h to become similar to the vehicle with P-value = 0.4942, and no effect was seen after one week with P-value = 0.8742. No significant difference was seen in the knockout-treated compared to the vehicle. The P-value > 0.9999, 0.9999, and 0.9988 respectively. The unpaired t-test between each group was also applied, and the test found the 30 min denatonium-treated WT to be significantly different from the *Trpm5*-KO, with P-value = 0.0004. The 24h and one-week t-test comparison found no difference between the treated mice, with P-value = 0.1590 and 0.6450, respectively (Figure 3.20, a).

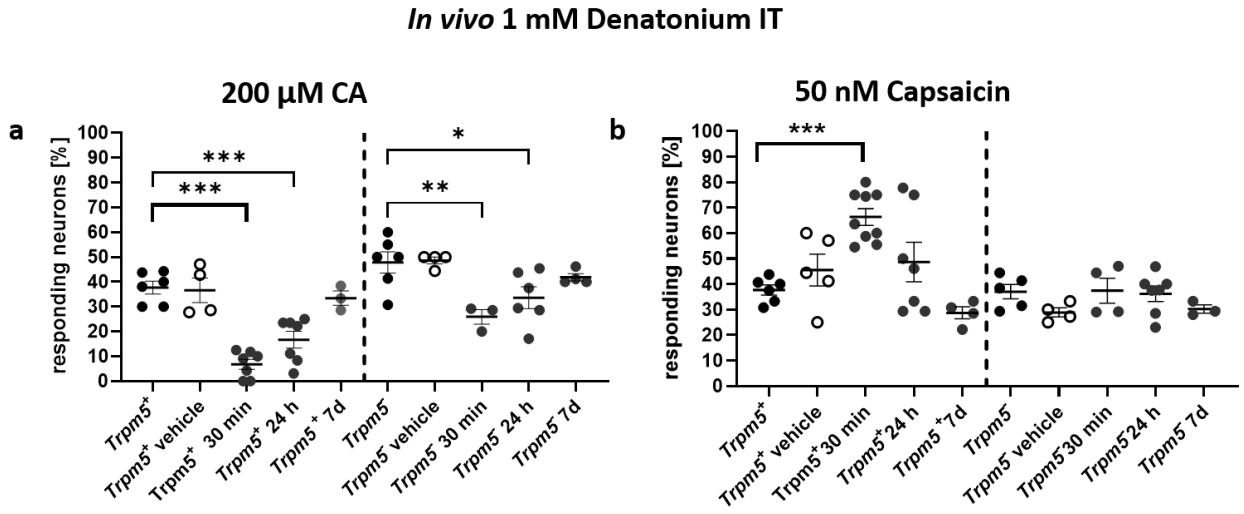

Figure 3.20*:* The activation of tracheal BC via 1 mM denatonium alters the sensitivity of *Trpv1* and *Trpa1*+ JNC neurons. Tracheas in WT and *Trpm5*-KO mice were treated locally via 1 mM denatonium. The mice were sacrificed at three different time points and the JNC were collected for dissociation and $[Ca^{2+}]$i imaging. a: Mean percentage of neurons responding to 50 nM capsaicin. Denatonium-stimulated WT mice were significantly different from the vehicle only at the 30 min time point. Denatonium stimulation of the *Trpm5*-KO was similar to the *Trpm5*-KO vehicle. b: Percentage of reacted neurons to 200 μM CA. The mean percentage of the WT neurons was significantly less than the vehicle at 30 min as well as after 24h. Another significant difference was observed between the *Trpm5*-KO vehicle and denatonium-treated mice at both time points. No significance was seen in either treatment at the one-week time point. n=3 to 7 mice/group expressed as the mean ± SEM. P values were determined by the one-way ANOVA test. (*, P < 0.05, **, P < 0, 01, ***, P < 0.001).

In the case of the TRPA1, dissociated neurons from the JNC were stimulated with 200 μM. A significant decrease in the percentage of reacted neurons was seen 30 minutes after activation with P-value <0.0001 compared to the vehicle. Additionally, a significant difference was seen 24h after denatonium stimulation with P-value = 0.0002. Nevertheless, similar to the *Trpv1+* neurons, no effect was seen after one week with P-value = 0.9950. In the *Trpm5*-KO mice, stimulation with 200 μM CA demonstrated a decrease in the mean number of responding neurons after 30 mins and one day compared to the KO vehicle with P-value = 0.0024 and 0.0257, respectively. However, the effect of the denatonium stimulation in WT mice was significantly different after 30 minutes than the KO with P-value = 0.0008 and the same after 24h with P-value = 0.0098 (Figure 3.20, b). The surgery itself had no significant difference and NaCl-treated WT and *Trpm5*-KO mice were similar to vehicle non-treated mice.

3.15 Infection with the gram-negative bacteria *Pseudomonas Aeruginosa* altered neuronal *Trpa1+* sensitivity

Infection with gram-negative bacteria is a main health concern to humans. BC are activated via bitter substances as shown previously (Hollenhorst *et al.*, 2020). Many studies have shown that *Pseudomonas aeruginosa* QSM activate BC. This activation provokes respiratory reflexes causing the elimination of inhaled pathogens via neutrophil recruitment. Therefore, to learn more about BC activation's effects on sensory neurons, an infection model was developed in which animals of different genotypes inhale bacteria and supernatants of *Pseudomonas aeruginosa* using a tracheal cannula passing through their mouths. Infected mice were kept at optimum conditions for different time points. Animals were sacrificed after 4h, 48h, 72h, and 7 days. This procedure is different from the other mentioned protocols with DT, CNO and den, because the infection protocol does not include surgery. Any results found should be solely due to bacteria and its QSM. On a killing day, the JNC from each mouse is collected, the neurons are dissociated for $[Ca^{2+}]i$ imaging, and the neurons are first stimulated by 200 μM CA followed by 50 nM capsaicin and KCL lastly to determine each neuron's viability. WT mice exhibited an increase in the sensitivity of *Trpv1+* neurons, whereas the sensitivity of the *Trpa1+* neurons was significantly decreased (Figures 3.21 and 3.22). The infected *Trpm5*-KO mice had quite similar results after stimulation with 200 μM CA. The change in sensitivity decreased simultaneously faster in the WT *Trpa1+* neurons compared to the infected *Trpm5*-KO which remained with a significant difference at 7 days compared to the *Trpm5*-KO vehicle with P-value = 0.0037, while the WT was similar to the WT vehicle at the same time point with P-value = 0.1798 (Figure 3.21, a). After stimulation with 200 μM CA, JNC neurons at different time points had a significant decrease in the percentage of reacted neurons. This was seen 4h after infection with P-value <0.0001 compared to the vehicle (mean responding neurons per mouse in WT vehicle = 40% to mean responding neurons per

mouse in 4h infected WT = 5%). The effect in the infected WT continued until 48h and 72h after infection with P-value = 0.0024 and 0.0044, respectively (mean responding neurons per mouse after 48h and 72h per mouse is 18% and 20% respectively). As for the *Trpm5*-KO mice, $[Ca^{2+}]i$ imaging after 200 µM CA stimulation demonstrated a decrease in the number of responding neurons in all of the time points compared to the KO vehicle, with P-value <0.0001 at 4h, 0.0003 after 48h and 0.0037 after 72h (mean responding neurons per mouse in the vehicle and after 4, 48h, and 72h infection per mouse is 50%, 17%, 18%, and 25% respectively) (Figure 3.21 a).

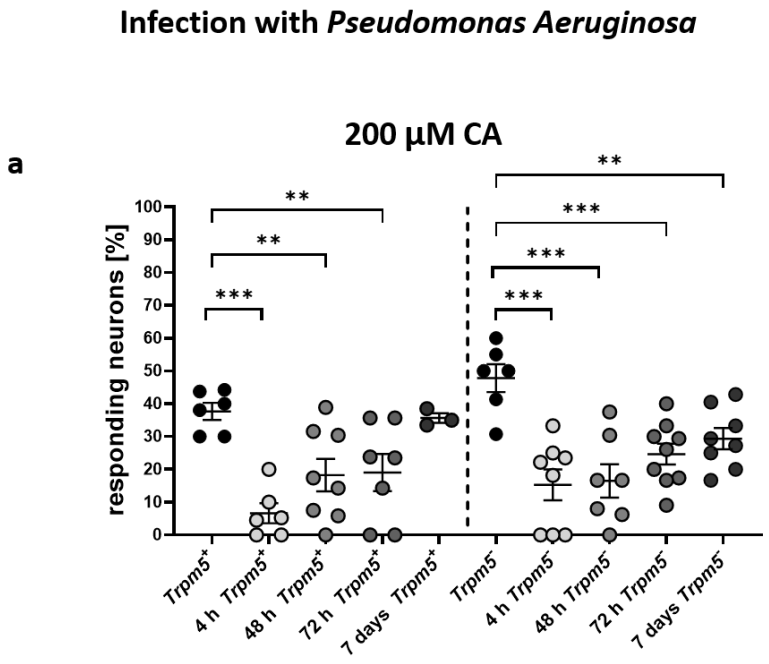

Figure 3.21: Infection with gram-negative bacteria *Pseudomonas aeruginosa* led to a decrease in the sensitivity of *Trpa1*+ JNC neurons in WT and *Trpm5*-KO mice. Infected mice from both genotypes (WT and *Trpm5*- KO) were sacrificed at four different time points and the JNC were collected for dissociation followed by $[Ca^{2+}]i$ imaging. a: Mean percentage of reacted neurons to 200 μM CA after infection. The percentage of the neurons of the WT was significantly less than the vehicle at 4h, 48h, and 72h, while the one-week time point in the WT was similar to the vehicle. A significant difference was also observed between the *Trpm5*-KO vehicle and treated KO at all the different time points. n=3 to 7 mice/group expressed as the mean ± SEM. P values were determined by the one-way ANOVA-test (*, P < 0.05, **, P < 0, 01, ***, P < 0.001).

3.16 Infection with gram-negative bacteria *Pseudomonas Aeruginosa* led to the alteration in the sensitivity of the *Trpv1*+ neurons

In the previous section showed the effect of infection with *Pseudomonas Aeruginosa* on *Trpa1*+ neurons. Conversely, at all the different time points, T*rpv1*+ neuron activity was boosted by more than 20% after

infection in both genotypes (WT and *Trpm5*- KO). However, over time, the channel-increased sensitivity was gradually reduced. In the WT and the *Trpm5*- KO, the bacterial infection effect was demolished at 7 days with P-value = 0.3917 in the WT and P-value = 0.05371, compared to the vehicle from each genotype (Figure 3.22). A significant increase in the mean percentage of reacted neurons was seen in the WT at 4h after infection with P-value = 0.0311 compared to the vehicle. The effect increased after 48h and 72h after infection with P-value = 0.0057 and 0.0018. respectively (mean responding neurons per mouse in the vehicle and after 4, 48h and 72h infection is 37%, 48%, 54% and 59% respectively). As for the *Trpm5*-KO mice, $[Ca^{2+}]i$ imaging after50 nM capsaicin demonstrated an increase in the number of responding neurons to stimulation in all of the time points, with P-value <0.0001 at 4h, <0.0001 after 48h, and 0.0010 after 72h compared to the KO vehicle (Figure 3.22 a) (mean responding neurons per mouse in the vehicle and after 4, 48h and 72h infection is 35%, 65%, 70% and 59% respectively). On two occasions, there was a difference between infected WT and *Trpm5*- KO. The *Trpv1+* neurons were more sensitive to capsaicin stimulation in the *Trpm5*- KO, 4h and 48h after infection with P- values = 0.0179 and 0.0160 respectively, which indicates an important rule for the TRPM5 channel for regulation and recovery of immune responses during lung infection.

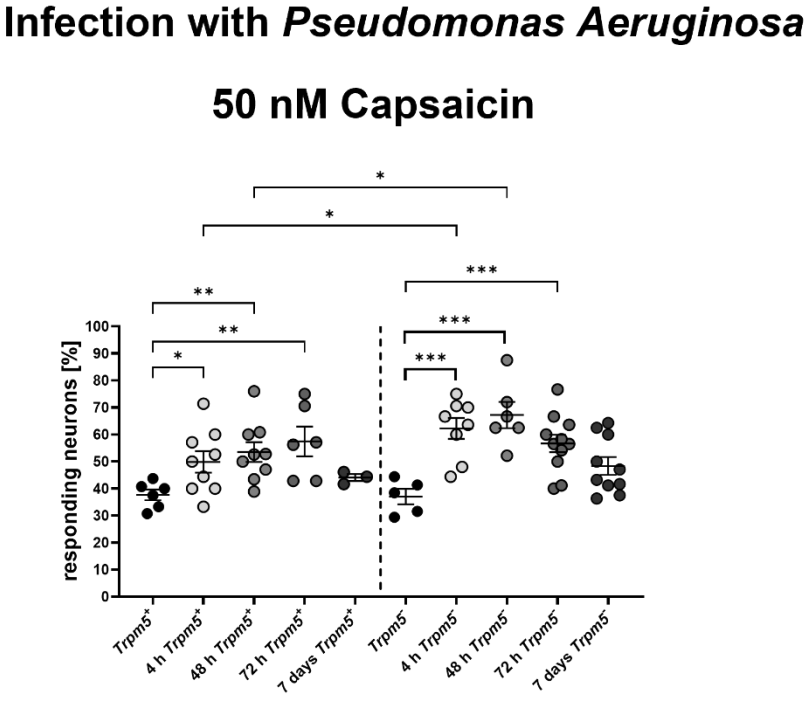

Figure 3.22: Infection with gram-negative bacteria *Pseudomonas aeruginosa* led to a surge in the sensitivity of the *Trpv1+* JNC neurons in WT and *Trpm5*-KO mice. Infected mice from both genotypes were sacrificed at four different time points and the JNC were collected for dissociation and $[Ca^{2+}]i$ imaging. a: Mean percentage of reacted

neurons to 50 nM capsaicin. The percentage of the reacting sensory neurons in the WT was significantly higher than the vehicle at 4h, 48h, and 72h minutes. A significant difference was observed between the *Trpm5*-KO vehicle and infected KO at all the different time points. n=3 to 8 mice/group expressed as the mean ± SEM. P values were determined by the one-way ANOVA-test (*, P < 0.05, **, P < 0, 01, ***, P < 0.001).

3.17 Chronically infected mice with *Pasteurella Pneumotropica Heyl / Rodentobacter Heylii* altered the sensitivity of *Trpa1*+ neurons

The bacterium *Rodentobacter heylii* is a common animal pathogen that can transfer to humans by animal bites and scratches. Nonetheless, we have found mice infected with these bacteria in our animal facility. After confirming that each animal we used in these experiments is positive for the infection with this bacterium using a tracheal swap, animals were sacrificed. Then, the JNC ganglia were collected for dissociation and $[Ca^{2+}]i$ imaging. Single neurons were stimulated by 200 µM CA followed by 50 nM capsaicin and KCL at the end to determine each neuron viability (Figure 3.23). For the capsaicin stimulation (Figure 3.25 a), all results were similar. The mean percentage of reacted neurons in the sick mice was similar to the vehicle from each genotype, and the sick mice were similar to each other. Conversely, the CA stimulation *on Trpa1*+neurons (from both the WT and the *Trpm5*-KO sick mice) resulted in a decrease in the sensitivity in both genotypes with more decline in the WT compared to the WT vehicle and the sick *Trpm5*-KO with P-value = 0.0007 and 0.0447, respectively (Figure 3.23 b).

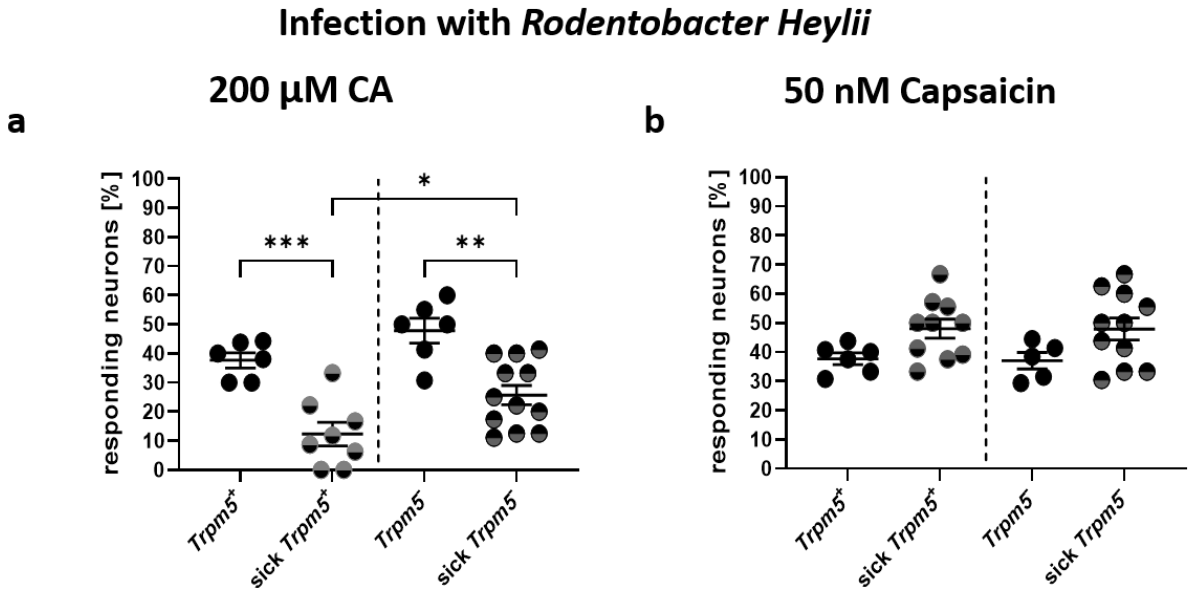

Figure 3.23: Chronically infected mice with the bacteria *Pasteurella pneumotropica Heyl/Rodentobacter heylii* led to the alteration of *Trpa1+* neuron sensitivity. Chronically infected mice were sacrificed, after which the JNC were collected for dissociation and $[Ca^{2+}]i$ imaging. a: Percentage of reacted neurons to 50 nM capsaicin. The percentage of the neurons of the WT was similar to the *Trpm5*- KO, and all were similar to the vehicle from each genotype. b: Mean percentage

of reacted neurons to 200 μM CA. The percentage of the neurons of the WT was significantly different from the *Trpm5*-KO, and all were different to the vehicle from each genotype. n=5 to 12 mice/group expressed as the mean ± SEM. P values were determined by the one-way ANOVA-test (*, P < 0.05, **, P < 0, 01, ***, P < 0.001).

3.18 Acetylcholine regulates *Trpa1* and *Trpv1+* neuron activity

Altogether, the previously introduced experiments used different animal models and the results presented above recognized a modulatory influence on the *Trpa1* and *Trpv1+* neurons once BC are activated. In the introduction of this thesis, research from peer-reviewed articles established that BC are cholinergic and release ACh once activated via bitter substances such as bacterial QSM and denatonium (Hollenhorst *et al.*, 2020a; Perniss *et al.*, 2020), so it was the first logical chemical to study in our pursuit of finding a convincing explanation for these results.

3.18.1 Acetylcholine led to a change of intracellular [Ca^{2+}]i in dissociated JNC neurons

For these experiments, WT mice were sacrificed and the JNC neurons were dissociated for [Ca2+]i imaging experiments. An end concentration of 100 µM ACh was used and around 50% of all neurons responded to this concentration. However, the effect of ACh was demolished after incubating the neurons with a mix of the cholinergic inhibitor atropine, and MEC with an end concentration of 100 µM and 50 µM, respectively. All included neurons were tested as viable using KCl (Figure 3.24, a and b).

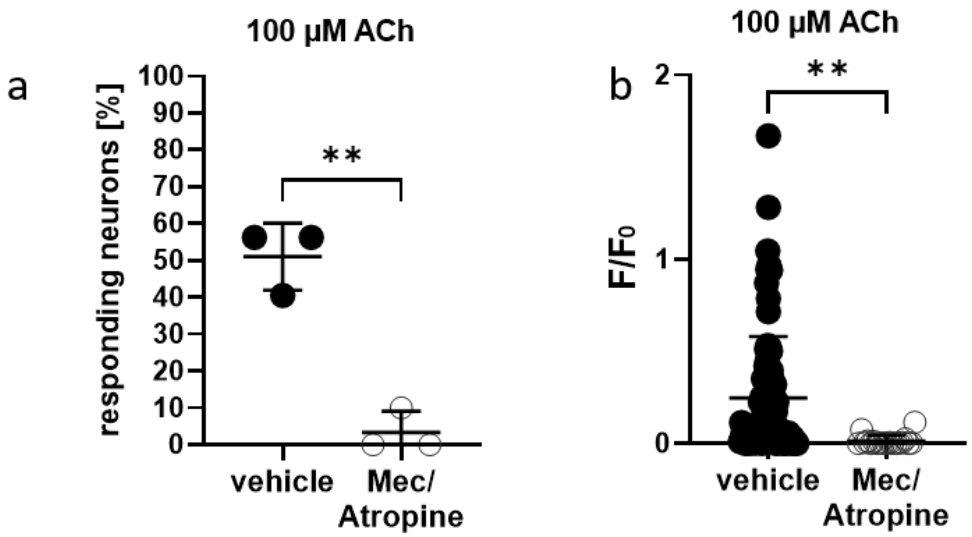

Figure 3.24: **About 50% of JNC neurons respond to ACh**. a: In [Ca^{2+}]i imaging, together, atropine and MEC (100 µM and 50 µM respectively) significantly inhibited the neuronal ACh response. b: The results show a significant difference in [Ca^{2+}]i change in (a). n=3 mice/group expressed as the mean ± SEM. 104 neurons were studied. P values were determined by the two-tailed Student's T-test (**, P < 0, 01)

3.18.2 Acetylcholine inhibits CA-stimulated *Trpa1+* neurons, whereas it activates capsaicin-stimulated *Trpv1+* neurons

To calculate the effect of ACh on TRPA1 and TRPV1**,** after dissociation, neurons of the JNC were used in [Ca2+]i imaging. Each coverslip of neurons was first incubated with a different concentration of ACh. Then, neurons were incubated with the TRPA1 agonist CA (EC_{50} =200 μM) or the TRPV1 agonist capsaicin (EC_{50} = 50 nM). These data were collected and two separate EC_{50} diagrams were made for both agonists (Figure 3.25, a and b). An end concentration of 9.08 μM of ACh is needed to cause an activation of half the *Trpv1+* capsaicin-sensitive neurons. However, this diagram instigates the ACh regulation effect, which suggests the need for a sufficient amount of ACh to cause a change in TRPV1 activity (Figure 3.25, a). Conversely, when incubated with high ACh concentration, CA-sensitive neurons responded with no change of $[Ca^{2+}]i$ with EC_{50} = 9.04 nM (Figure 3.27 b), which indicates that very low concentrations of the neurotransmitter ACh would lead to the inhibition of the TRPA1 channel.

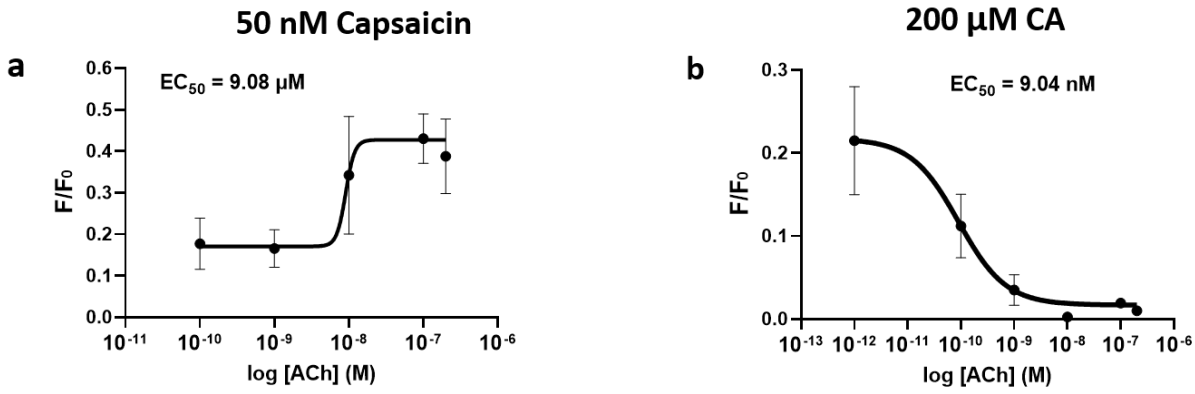

Figure 3.25*:* In the JNC, ACh inhibits *Trpa1* and activates *Trpv1+* neurons. a: To increase the activity of the TRPAV1 channel, an EC_{50} of 9.08 μM ACh is needed. b: 9.04 nM of ACh is enough to inhibit the TRPA1 channel. n=3 mice/group expressed as the mean ± SEM.

3.18.3 The ACh effect on *Trpa1* and *Trpv1+* neurons was inhibited fully via atropine and MEC

Next, in order to determine whether the ACh effect on TRPV1 and TRPA1 was mediated via the activation of AChRs, an experiment was set up where $[Ca^{2+}]i$ changes were measured on freshly dissociated JNC neurons. Single neurons were incubated with an atropine and MEC mix (100 μM and 50 μM, respectively) followed by 100 μM ACh, 200 μM CA, and 50 nM capsaicin. The results from these experiments were decisive. For the *Trpa1+* neurons, the effect of ACh was reversed after using the inhibitors (neurons responded upon CA stimulation). The mean of responding neurons to 200 μM CA declined from about 40%

to 2% after ACh application. However, the effect was overturned to a mean of 50% after the incubation with atropine and MEC (Figure 3.26, c and e). More experiments are needed to understand how ACh is regulating the TRPV1 (Figure 3.28, c and d). There was a significant increase in the number of neurons reacting to 50 nM capsaicin after stimulation with 100 µM ACh compared to the vehicle. After incubation with the atropine/ MEC inhibitor mix, neither the number of neurons reacting to capsaicin stimulation nor the $[Ca^{2+}]i$ content changed significantly (Figure 3.28, e and f).

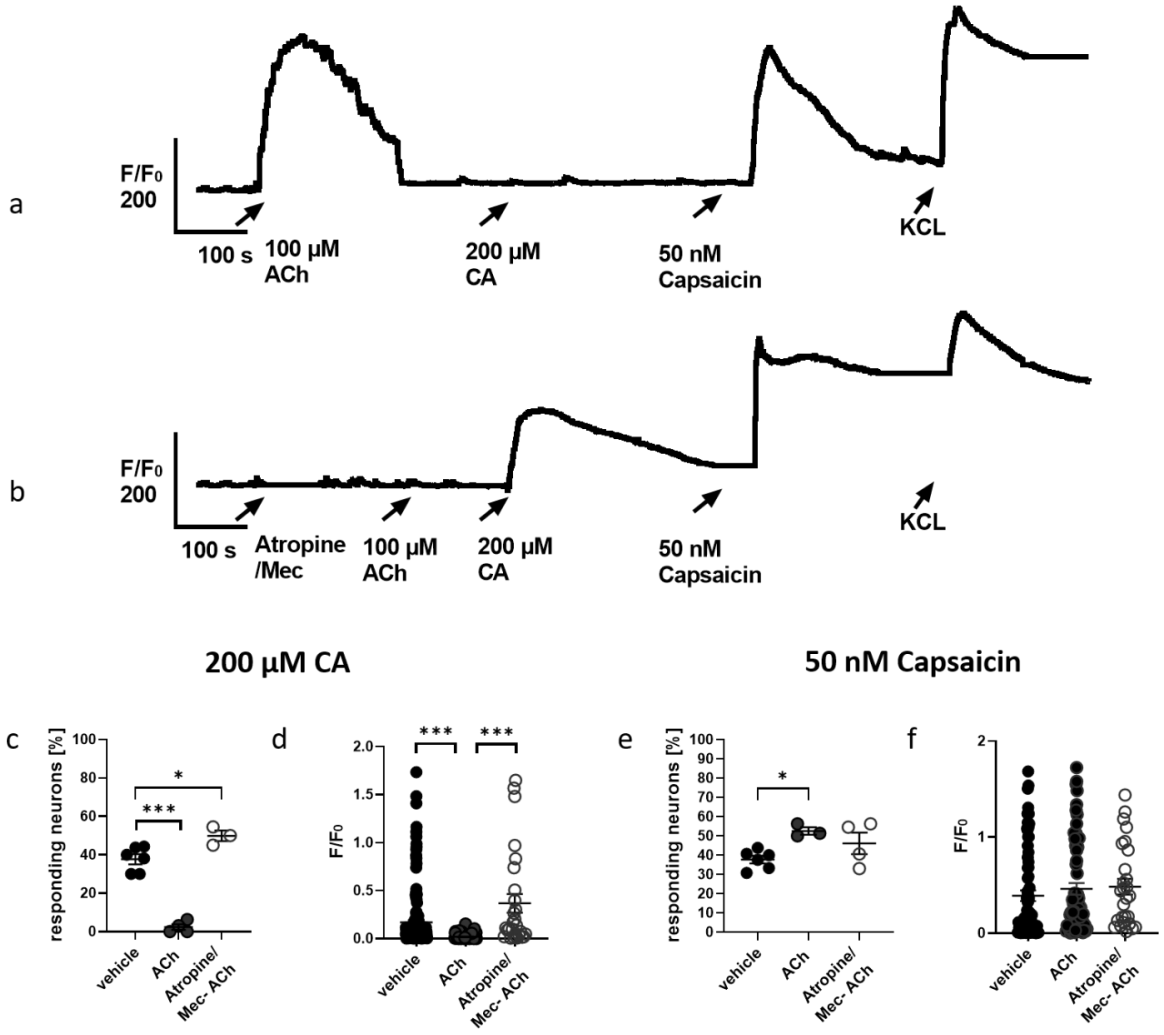

Figure 3.26: ACh regulates *Trpa1+* and *Trpv1+* JNC neurons sensitivity to agonists. In $[Ca^{2+}]i$ imaging, a simultaneous application of atropine and MEC (100 µM and 50 µM, respectively) significantly inhibited the ACh effect. a: A representative trace showing one JNC neuron responding to 100 µM ACh, 200 µM CA, and 50 nM capsaicin. b: A representative trace showing one JNC neuron firstly incubated with atropine and mec (100 µM and 50 µM, respectively) and then responding to 100 µM ACh, 200 µM CA, and 50 nM capsaicin. c: The mean percentage of neurons per mouse responding to 200 µM CA after the application of 100 µM ACh. The diagram also demonstrates the mean number of neurons per mouse responding to CA after the inhibition of AChRs with atropine and MEC (100 µM and 50 µM, respectively). d: A demonstration of the $[Ca^{2+}]i$ change in (c). e: The mean percentage of neurons per mouse responding to 50 nM capsaicin after the application of 100 µM ACh. The diagram also demonstrates the mean number of neurons per mouse responding to capsaicin after the inhibition of AChRs with atropine and MEC (100 µM and 50 µM, respectively). f: A demonstration of the $[Ca^{2+}]i$ change in (e). 288 and 170 neurons were studied in a and

b, respectively. n=3 to 6 mice/group expressed as the mean ± SEM. P values were determined by the one-way ANOVA-test (*, P < 0.05, ***, P < 0.001).

3.18.4 DMPP had a similar effect to ACh and was inhibited via hexamethonium

Pain perception is associated with nAChRs in the sensory neuron (Costa *et al.*, 2012; Papke *et al.*, 2018), as well as with the TRPA1 channel (Yoshida *et al.*, 2011; Meseguer *et al.*, 2014; Asgar *et al.*, 2015; Liu *et al.*, 2016; Souza Monteiro de Araujo *et al.*, 2020). In this experiment, $[Ca^{2+}]$i imaging measurement of JNC dissociated sensory neurons was made by first incubating the neurons with 10 µM dimethylphenylpiperazinium (DMPP) which is a nicotinic agonist that activates a nAChRs subtype consisting of α3 and β4 subunits (Brus and Jacobowitz, 1970). The outcome of this experiment was in line with the results of the ACh $[Ca^{2+}]$i imaging measurements. 20% more *Trpv1+* neurons were responding to capsaicin after DMPP application (Figure 3.27, a), while the *Trpa1+* neurons were not responding to CA. Approximately only 10% of all *Trpa1+* neurons were responding to DMPP compared to a mean of 40% in the vehicle group (Figure 3.29, b).

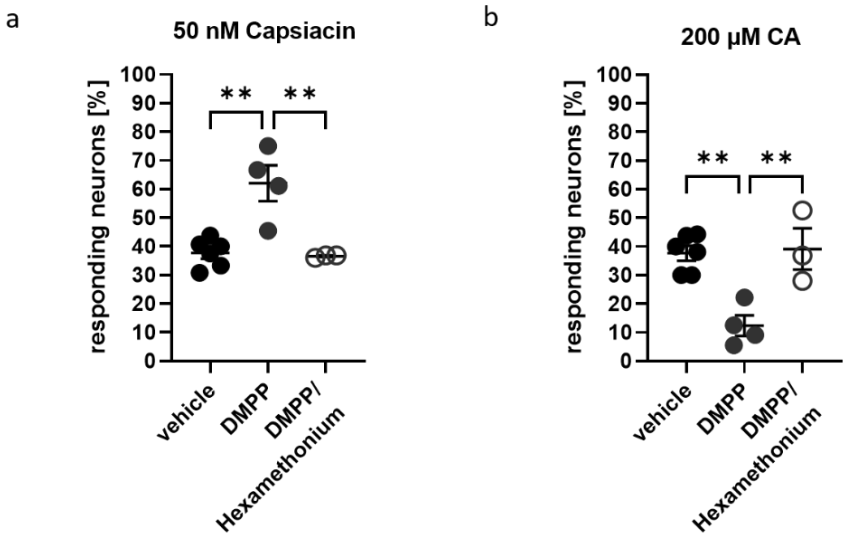

Figure 3.27: DMPP activates *Trpv1+* neurons and decreases the activity of *Trpa1+* neurons in the JNC. a: In $[Ca^{2+}]$i imaging measurements, DMPP was found to increase the activity of *Trpv1+* neurons and to decrease the activity of *Trpa1+* neurons. b: Both effects were reversed to be significantly similar to the vehicle after incubating the neurons with 3mM of the nicotinic antagonist hexamethonium. n=3 to 6 mice/group expressed as the mean ± SEM. P values were determined by the one-way ANOVA-test (**, P < 0, 01).

We then studied whether this effect was due to the activation of the nicotinic subunit α3β4. Neurons were incubated with a mix of 3 mM of the nAChRs inhibitor hexamethonium and 10 µM DMPP, followed by 200 µM CA, and 50 nM capsaicin; $[Ca^{2+}]$i measurements were also performed. The results were consistent

with the proposed theory and the effect was reversed to the level of the vehicle-treated group in both *Trpa1* and *Trpv1*+ neurons (Figure 3.29, a and b, respectively).

3.18.5 The effect of ACh was inhibited with the antagonist hexamethonium

Hexamethonium is a known inhibitor of nAChRs (BYCK, 1961; Asghar and Roth, 1971; Misu and Kubo, 1972; Malin *et al.*, 1997). To study the involvement of nAChRs in the ACh-induced increase in [Ca^{2+}]i levels in JNC sensory neurons (Figure 3.26), we performed [Ca^{2+}]i with freshly isolated JNC neurons, applying 100 µM ACh after 3 min incubation with either vehicle of 3 mM hexamethonium. Hexamethonium abolished the effect of ACh (Figure 3.28, a). The effect of ACh on the *Trpv1*+ and *Trpa1*+ neurons was similar to the vehicle without ACh stimulation (Figure 3.30 b, c). After hexamethonium incubation followed by ACh, about 45% of the *Trpv1*+ neurons responded to capsaicin compared to 40% in the vehicle-treated group (Figure 3.28, b). 38% of the neurons responded to CAin the vehicle-treated group. For comparison, the percentage of neurons that reacted to CA after the incubation with a hexamethonium and ACh mix was 45% (Figure 3.28, c).

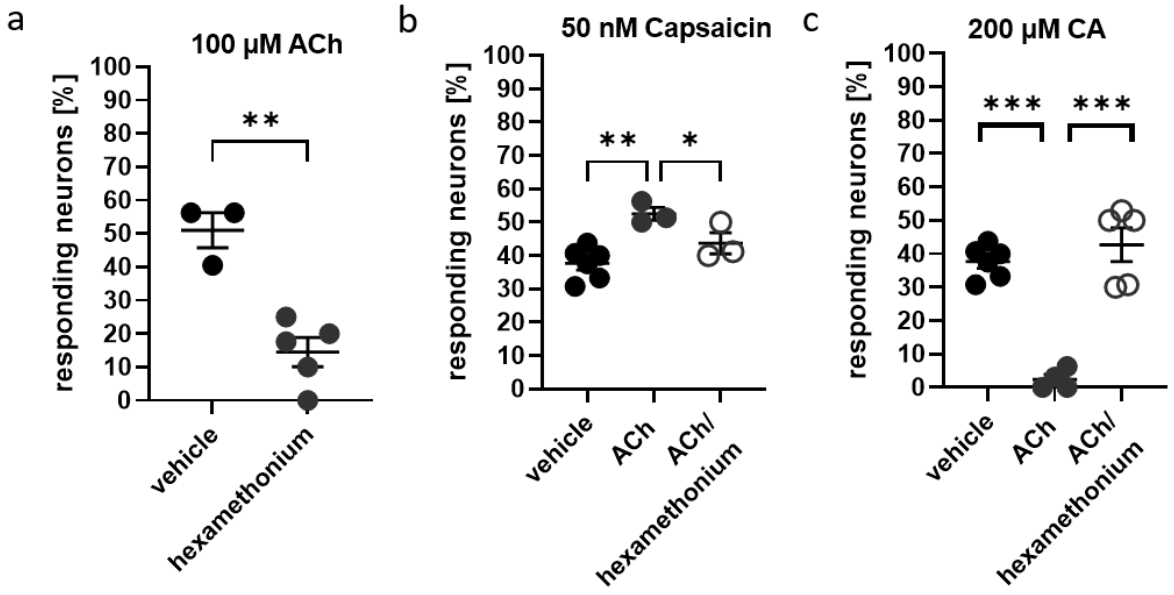

Figure 3.28*:* Hexamethonium inhibits nAChRs in sensory neurons reversing the ACH effect on the *Trpv1*+ and *Trpa1*+ JNC neurons. a: In [Ca^{2+}]i imaging measurements, hexamethonium inhibits the response to 100 µM ACh. b: Both effects were reversed to be significantly similar to the vehicle after incubating the neurons with 3 mM of the antagonist hexamethonium. n=3 to 6 mice/group expressed as mean ± SEM. P-values were determined by one-way ANOVA-test (* $p < 0.05$, ** $p < 0.01$, ***, $p < 0.001$).

In this experiment, we aimed to study the involvement of nAChRs in the ACh-induced increase in $[Ca^{2+}]i$ levels in JNC sensory neurons. We applied 100 μM ACh after a 3-minute incubation with either the vehicle or 3 mM hexamethonium, and measured the $[Ca^{2+}]i$ levels in freshly isolated JNC neurons. The results showed that hexamethonium abolished the effect of ACh on $[Ca^{2+}]i$ levels in JNC neurons. This suggests that nAChRs are involved in the ACh-induced increase in $[Ca^{2+}]i$ levels in JNC sensory neurons. Overall, the results of this experiment suggest that nAChRs play a role in modulating the response of JNC sensory neurons to both TRPV1 and TRPA1 agonists.

CHPATER 4: DISCUSSION

Brush cells (BC) are a type of cells found in the epithelium of the respiratory and digestive tracts. Previously, researchers have addressed the role of BC in chemosensation. Additionally, these cells can release ACh (Hollenhorst *et al*., 2020). BC provoke innate immune reactions once activated via different stimuli such as QSM and bacterial infections (Hollenhorst *et al.*, 2022a). This is important for the respiratory system's protection against invaders and unwelcome stimuli. Additionally, Tas2Rs are responsible for detecting bitter compounds. They are expressed along with the *Trpm5* in BC (Lee *et al.*, 2012; Freund *et al.*, 2018; Gees *et al.*, 2014; Hollenhorst *et al.*, 2019, 2020b). In our experiments, the upstream activation of Tas2Rs with the bitter substance denatonium led to a change in the cytosolic $[Ca^{2+}]$i concentration, leading to the downstream activation of the TRPM5 channel. Many toxins and bacterial substances such as QSM possess a bitter taste, the activation of the Tas2Rs signaling cascade plays an important role in protection against harmful objects.

In this study, we clarified that some of Tas2Rs such as *Tas2r105* and *Tas2r108* are expressed in the tracheal epithelial tissue via PCR (Hollenhorst *et al.*, 2022). Moreover, our $[Ca^{2+}]$i imaging experiments with the bitter substance denatonium after transfecting WT HEK 293 cells with the plasmids of *Tas2r105* and *Tas2r108*, resulted in a significant change in the $[Ca^{2+}]$i compared to the non-transfected cells. Additionally, $[Ca^{2+}]$i imaging experiments on isolated tracheal cells from *Trpm5*-tauGFP mice (mice that express the green fluorescent protein specifically in BC) resulted in a significant change in $[Ca^{2+}]$i in BC after denatonium application. Taken together, these results strongly indicate that denatonium is being detected by *Tas2r105* and *Tas2r108* in BC. Moreover, we were able to inhibit the effect of denatonium by using the G-protein inhibitor gallein. Gallein binds specifically to the beta-gamma subunit of G-proteins and fluorescens when excited by certain wavelengths of light, making it a useful tool for studying G-protein signaling pathways in cells responsible for taste transduction (Sanz et al., 2017). This result demonstrates the importance of the G-Protein in BC taste receptor-dependent activation and its involvement in the activation and function of BC. Furthermore, this result utilizes the use of denatonium as a BC agonist that triggers the Tas2Rs signaling cascade and leads to the release of signaling molecules (Hollenhorst *et al.*, 2019, 2020b). Due to their roles in the physiology of taste transduction, inhibiting signaling molecules has limitations, but theoretically there may be situations where it would be beneficial to do so. Such situations can only be established using a mouse deficient in the different types of G-protein such as α-gustducin.

Neurogenic inflammation refers to the release of inflammatory mediators. In our investigations, in order to understand the role of BC in the generation of neurogenic inflammation in the respiratory tract, we created a model where different murine genotypes inhaled different concentrations of denatonium. WT mice exhibited a significant induction of plasma extravasation (leakage of proteins and fluids from blood vessels

into the surrounding tissues) after denatonium inhalation, accompanied with a significant increase in neutrophil extravasation. We think of this result as a protective response to inhaled irritants. The fact that the results from the same experimental model using *Trpm5*-KO mice had contradictive effects (Hollenhorst *et al*., 2022), presses on the importance role of BC in innate immunity, initiating immune cells recruitment and protecting the airways against inhaled irritants and toxins.

BC are cholinergic and are indeed capable of releasing ACh (Hollenhorst *et al*., 2020b). Additionally, ACh can be released from parasympathetic nerve fibers. AChRs are present in the epithelial cells, smooth muscle cells and nerve endings in trachea. To understand the role of AChRs in regulating inflammation and immune responses in the trachea, we designed an experiment where vehicle WT mice were compared to WT mice that were exposed to the cholinergic inhibitors' atropine and MEC, general inhibitors for mAChRs and nAChRs respectively. In this experiment, mice received *i.p.* injections of cholinergic inhibitors. The systemic cholinergic inhibition resulted in a significant decrease in plasma and neutrophile extravasations. Our findings suggest that AChRs play a role in promoting neurogenic inflammation and immune responses. Furthermore, the significant decrease in extravasation suggests the importance of BC-derived ACh in neurogenic inflammation induction and the release of neuropeptides such as CGRP and SP.

To be more specific, we have developed another method to inhibit AChRs. In this model mice inhaled similar concentrations of the cholinergic inhibitors' atropine and MEC, as well as different concentrations of denatonium. Strikingly, this method resulted in a significant increase in plasma extravasation as well as a significant increase in neutrophil recruitment in the inhibitor-treated mice compared to the vehicle-treated mice. Our result indicates the important role the AChRs play in neurogenic inflammation. In the two previously mentioned models, we used different routes of administration for atropine and MEC: one is *i.p.* and the other is IT. The *i.p.* route involves the delivery of atropine and MEC into the peritoneal cavity. In this way, it allows the substance to be absorbed through the peritoneal membrane to the blood stream. IT administration, on the other hand, involves the direct delivery of the inhibitors specifically into the trachea and lung. The difference in distribution, absorption, particle size, solubility, and metabolism between both methods can lead to different results. Additionally, the airway surface liquid volume (ASL) and concentration is normally 1 µL per cm^2 of mucosal surface (Wu *et al*., 1998). This concentration can impact the distribution and absorption of the inhibitors applied to the respiratory system. In the IT application, the inhibitors can mix with the ASL, affecting the concentration causing irritation and damage. On the other hand, the IT application of these substances may not have enough time to mix before being cleared out of the body, resulting in a reduced efficacy. Further, in the absence of tracheal epithelial damage, IT application of cholinergic inhibitors, can't inhibit the AChRs in the nerves. These mentioned situations may have altered our results of cholinergic inhibition in the different modes of application. The IT application may have

caused a more localized immune response in the trachea that led to a different pattern of neutrophil recruitment and plasma extravasation compared to the *i.p.* route. Further, when AChRs are inhibited via the local administration of atropine and MEC, the normal function of ACh signaling is disturbed rabidly. As a result, the downstream effects of ACh signaling are also affected, including the activation of *Trpv1* and the inhibition of *Trpa1*.

Next, we were able to deplete most of the *Trpa1*+ neurons along with 80% of the *Trpv1*+ neurons using DT and the *Trpa1*-DTR mice. Additionally, in the DRG neurons, we observed a significant decrease of neurons positive to CGRP+ and SP+ neuropeptides. Moreover, whole-mount preparations of the trachea showed a significant decrease in the volume of CGRP+ and SP+ neuronal fibers. This was confirmed using immunohistochemistry and RT-PCR. These experiments proved that most of the *Trpa1*+ and *Trpv1*+ neurons are overlapping. Additionally, the use of the *Trpa1*-DTR mice led to generating mice that are deficient in most of the sensory innervation (Hollenhorst *et al*., 2022). Nonetheless, the abolishing of the neurogenic inflammation was obvious after inhaling 1 and 10 mM denatonium, whereas plasma extravasation and neutrophil recruitment after the inhalation of 20 mM denatonium were different to the vehicle. However, the remaining un-depleted *Trpv1*+ neurons could be responsible for the slightly significant plasma and neutrophile extravasation. The inhibition of the TRPA1-mediated $[Ca^{2+}]i$ increase in the sensory ganglia, by depleting them, led to a scarce production of the neuropeptides, decreasing inflammation and constant mechanical hyperalgesia. *Trpa1*+ neurons in the airway detect irritants and respond by releasing neuropeptides such as SP and CGRP, promoting and modulating inflammatory responses. (Story *et al.*, 2003). Here, we proved that neurogenic inflammation is mediated by *Trpa1*+ or *Trpa1*+*/Trpv1*+ sensory neurons. Therefore, the balance between AChRs activation and sensory innervation is important for protection against uncontrolled neurogenic inflammation.

In our recent study, we have shown that *Trpm5*-deficiency attenuated neurogenic inflammation (Hollenhorst *et al*. 2022a). We found that *Trpm5*-KO mice had a significant reduction in airway inflammation (it decreased plasma and neutrophil extravasation) after denatonium stimulation using the previously mentioned technique. However, CGRP and SP are both involved in sensory signaling. Using CGRP and SP blockers inhibited the release of these peptides from sensory nerves, leading to significant decrease in neurogenic inflammation. These findings combined with the results obtained from using the cholinergic inhibitors and the *Trpa1*-DTR model are important for advancing our understanding of the underlying mechanisms of inflammation and sensory signaling. Additionally, I designed an experiment to study the effect of denatonium on the vessels in the trachea. After 1 mM denatonium *in vivo* inhalation, WT, *Trpm5*-deficient and the *Trpa1*-DTR mice tracheas were used for CD31 whole-mount preparations. Interestingly, there was a significant vasodilation effect only in the venules, arterioles and capillaries of the WT compared

to the vehicle. This result stresses the importance of BC and sensory innervation communications for the induction of vasodilation-related neurogenic inflammation in the airways.

In addition, we investigated the sensory ganglia including the JNC and the DRG for any incidence of the TRPM5 channel in the neuronal cell bodies. Remarkably, Western blotting and immunohistochemistry showed no positive trace for the channel. This result is important because it suggests that the TRPM5 is not essential for sensory neuronal function, at least not in the same way: it is for other physiological processes. Moreover, no significant difference was found when RT-PCR was employed to investigate whether the *Trpm5*-deficiency affected the *Trpv1* and *Trpa1* composition in the JNC and the DRG compared to the WT. This result suggests that the *Trpm5* deficiency does not significantly affect the expression of the *Trpv1* and *Trpa1* in these ganglia. In addition, this made a basic foundation for the coming experiments in figuring out the effect of BC on the innervating *Trpv1* and *Trpa1*-rich sensory neurons. This result raises many questions about the effect of TRPM5 in modulating sensory transmission.

Our utilized experiments in the rest of this study allowed us to identify the effect of BC-derived ACh on the sensory neuronal channels. For the first time, BC can be considered a potent negative regulator of the TRPA1 channel, and an activator of the TRPA1 channel. Previous research addressed the TRPM5 channel as a negative regulator of $[Ca^{2+}]i$ changes after stimulating the B lymphocytes with bacterial lipopolysaccharides (Startek *et al.*, 2018). However, the difference in this case is that the B lymphocytes themselves express the *Trpm5*, while here in this study the effect is external, meaning a neurotransmitter or a chemical is released from BC upon Tas2R activation, causing an effect.

Here, we suggest that BC play a role in pain sensation or that they are involved in the detection of noxious or irritant stimuli by modulating the activity of other pain-sensing channels such as *Trpv1* and *Trpa1*. To support this hypothesis, we performed $[Ca^{2+}]i$ experiments to evaluate the sensitivity of DRG and JNC dissociated neurons, by measuring EC_{50} from WT and *Trpm5*-KO mice. We used capsaicin, a known agonist for TRPV1, while CA is an agonist for TRPA1. As mentioned previously, we classified neurons that responded to the agonist as positive for its corresponding channel expression.

Trpm5-deficiency increased the sensitivity in both *Trpa1+* and *Trpv1+* neurons in the JNC and the DRG, as the EC_{50} for the TRPA1 and TRPV1 agonists decreased by more than 50%, for CA and capsaicin, respectively. These results suggest that the *Trpm5* may play a modulatory role in the activity of these channels and by lacking the *Trpm5,* the modulation effect was gone leading to an increase in sensitivity of the other channels.

Furthermore, another mouse model was used, the *Trpm5*-DTR. In this mouse, the *Trpm5*-expressing cells in the trachea (BC) can be specifically depleted by the administration of DT. Nevertheless, the depletion of the TRPM5 channel had a significant decrease in sensitivity than the WT. However, it was more potent in the *Trpm5*-deficient mice than in the *Trpm5*-DTR, with EC_{50} (for CA and capsaicin, respectively) = 144.2 μM and 14.84 nM, compared to 96.6 μM and 18.36 in the *Trpm5*-KO. This suggested that a total knockout of the gene had a stronger effect on the change of sensitivity for both channels than local depletion.

Despite these exciting results of the TRPV1, with increased sensitivity after knocking out or depleting the *Trpm5* gene, it should be argued that the loss of the channel in both *Trpm5*-DTR and *Trpm5*-deficient mice models may have resulted from the inflammatory status that came along with the deficiency. Although the DT is considered a powerful tool to analyze the different physiological functions *in vivo,* many studies suggested an inflammatory role for the DT after being injected into the animals (Gillet and Barbier, 2015; Horiguchi and Mekada, 2006; Kobayashi and Duffield, 2011). Studies on WT mice which were treated with DT found that some animals had proteinuria, unexpected death, elevated immune cell counts and weight loss. Additionally, in mice with the DTR, DT could trigger an inflammatory response in the cells surrounding targeted dead cells, causing swelling and pain (Gillet & Barbier, 2015; Oram & Holmes, 2006). Anyhow, the surviving animals healed properly 5-9 days after injection. In our experiments, we needed to sacrifice the mice 48 h later, which is a very short time to develop chronic symptoms and side effects. On the other hand, *i.p.* application of DT using WT mice and our previously mentioned neurogenic inflammation model after the inhalation of 1 mM den was similar to the vehicle treated mice. Indicating a healthy mouse model after DT injections. These findings highlight the complexity of the interactions between these three channels and their signaling pathways. Further research is needed to implicate the deletion of *Trpm5* on sensory perception.

Additionally, in the *Trpm5*-DREADD mice, BC can be selectively activated using CNO. Here, we aimed to study the effect of BC activation on neurons expressing *Trpa1* and *Trpv1*. Expectingly, the obtained results were opposite to the previous experiments. The EC_{50} of the dissociated DRG neurons for the TRPA1 agonist CA showed a much higher value than the WT after activating the DREADD receptor via CNO, with EC_{50} = 203.7 and 749.5, respectively. Here, activating BC only led to a potent inhibitory effect on the *Trpa1*+ neurons. This experiment provides insight into our understanding to the BC's complex effect on the *Trpa1*+ neurons. Similar to the *Trpm5*-DTR results, strikingly, the activation of the BC with CNO led to an increased sensitivity in the *Trpv1*+ neurons. The EC_{50} of the dissociated DRG sensory neurons for the TRPV1 agonist capsaicin showed a lower value than the WT after activating the BC via CNO, with EC_{50} = 50 nM and 1.22 nM, respectively, indicating a sensitizing *Trpv1*+ effect after CNO application. However, since the *Trpv1*+ neurons in the *Trpm5*-KO and *Trpm5*-DTR had an increased sensitivity, an opposite result could be

suggested here after activation. We could suggest a different process or pathway in the three different models, which all lead to activation but in a different context. In such cases, activating and inhibiting may produce the same result because the biological system is designed to respond in this particular way to this particular biological stimulation. Nevertheless, our study is suggesting complex interactions, between different kinds of cell types and receptors.

In line with the *Trpm5*-DREADD mice results, our $[Ca^{2+}]$i experiments to evaluate the sensitivity of JNC dissociated neurons after activating the tracheal BC with 1 mM denatonium for thirty minutes led to a decrease in the percent of the reacting *Trpa1*+ neurons in the WT. However, this result recovered slightly after one day and fully after one week of activation. On the other hand, *Trpm5*-deficient mice had a slight decrease in the activity of *Trpa1*+ neurons after activation with 1 mM denatonium, but the effect was different to the WT. The surgery with NaCl instead of denatonium is similar to the vehicle. However, the results of the BC activation on the *Trpv1*+ neurons via 1 mM denatonium is in harmony with the results of the *Trpm5*-DREADD model. A higher number of neurons were reacting to capsaicin after 30 minutes of denatonium stimulation as expected. The activity decreased gradually after one day and was similar to the vehicle after one week. In addition, the activity of *Trpv1*+ neurons after denatonium activation in the *Trpm5*-deficient mice was similar to the non-treated vehicle at all the different time points. Overall, with our findings up till now, specific BC activation suggested an inhibitory effect to the *Trpa1*+ neurons and an activation effect to the *Trpv1*+ neurons. Further experiments are needed to understand the implications of these results.

Tracheal epithelial cells are very important for the defense against infections. Studies have shown that BC act as a sensor for bacterial toxins, which triggers BC activation, leading to ACh release followed by mucociliary clearance (Hollenhorst *et al.*, 2019; Perniss *et al.*, 2021). Furthermore, our designed infection experiment that we utilized in this study helped us observe the results of bacterial pathogenesis on BC. After healthy WT and *Trpm5*-KO mice were infected with the gram-negative bacterium *Pseudomonas aeruginosa*, mice showed symptoms of weight loss, lethargy, and respiratory distress. Here, our findings are in line with our previously obtained results. In the infected mice models, *Trpa1*+ neurons were not responding to CA while *Trpv1*+ were very sensitive to capsaicin. However, in both the *Trpa1*+ and *Trpv1*+ neurons, the pattern of $[Ca^{2+}]$ change was remarkably similar in the *Trpm5*-deficient infected mice, with higher significance in each case than the WT. It should be taken into consideration that in the WT mice, $[Ca^{2+}]$ changes recovered faster to baseline after one week of infection. This result stresses the regulatory effect of BC on the sensory neurons. Indeed, bacterial infections involve a complex interplay of various bio-systems (immune cells, epithelial cells, and sensory neurons). The immune system is the body's primary defense against bacterial infections. Communication between white blood cells and epithelial cells through

cytokines and chemokines is important to induce inflammation and clear the infection (Conrad *et al.*, 1992; Hedges *et al.*, 1995). Additionally, mucus, neurotransmitters and antimicrobial peptides are produced by epithelial cells (Hammad and Lambrecht, 2015; Gerbe *et al.*, 2016; Hollenhorst *et al.*, 2022a). All these agents may cause an effect on the sensory neurons, causing the resulting change in sensitivity, directly or indirectly. Overall, the immune system and the sensory neurons work together to identify and neutralize pathogens from the system.

Chronic infections in the respiratory system can cause asthma. There is great scientific evidence associating bacterial infection with asthma induction (Kistemaker and Prakash, 2019). Chronic bacterial infections are characterized by persistent infection that lasts for a long time. This type of infection is caused by bacteria that produces biofilms, which can evade the immune system and create variations in cytokine production to facilitate the pathogen's persistence (Bade *et al*., 2021; Monack *et al*., 2004; Okada and Shirakawa, 2005; Rana *et al*., 2021). Inflammation and airway hyper-responsiveness are linked to activation of the sensory neurons. In our chronic bacterial infection model with *Rodentobacter heylii* we addressed a possible neuronal hypersensitivity due to the prolonged airway infection. However, the infection caused no significance in the increase in $[Ca^{2+}]i$ in the *Trpv1+* neurons after capsaicin stimulation in both genotypes, the WT and the *Trpm5*-deficient mice. On the contrary, *Trpa1+* neurons responded less to CA stimulation in both, WT and the *Trpm5*-deficient mice. Yet the change in WT mice was more prominent than in the *Trpm5*-deficient mice indicating an important function for BC in fighting bacterial infections. Additionally, because multiple mechanism and pathways are altered during an infection, leading to cytokines or other chemicals release. Our results indicates that the triggered pathways during an infection are not dependent solely on BC activation. Hence the change in the *Trpm5*-KO's *Trpa1+* neurons sensitivity.

The role of TRPA1in chronic infections should not be neglected. Interestingly, the TRPA1 channel is rising as a major asthma target for therapeutic purposes. For example, some TRPA1 antagonists were found to suppress neurogenic inflammation and airway tightness (Bautista *et al*., 2006, 2013; Bessac *et al.*, 2008). Nonetheless, this result clarifies that the effect of the continuous exposure to cellular-derived inflammatory chemokines and cytokines after activation via bacterial substances is not reversible when it comes to the *Trpa1+* neurons. On the other hand, the *Trpv1* was not affected from a chronic activation in our study. The direct detection of irritants in the airway from sensory neurons results in the activation of *Trpv1+* fibers, leading to the release of neurogenic peptides such as the CGRP, tachykinins, and neurokinins (Rogers, 1997). Thus, once the pain stimulation is transmitted, there is no further requirement of TRPV1 activation.

In the last set of experiments in this thesis, we suggest ACh to be the modulator of the communication between the BC and the sensory neurons. Previous research proved that BC are cholinergic and release ACh upon stimulation (Hollenhorst *et al*., 2019; Perniss *et al.*, 2021). ACh is known to play an important role in

the function of CNS and PNS. Here, we investigated the effect of ACh derived from BC on the activity of the *Trpv1* and *Trpa1* channels. incubating the dissociated JNC sensory neurons with ACh and then 200 μM CA and 50 nM capsaicin clarified the ACh inhibitory effect on the *Trpa1+* neurons and the excitatory effect on the *Trpv1+* neurons. This result was supported by making an EC_{50} diagram for both agonists.

Damage in the epithelial layer in the trachea due to infection or irritation via chemical substances such as denatonium lead to ACh release (Hollenhorst *et al.*, 2020; Hollenhorst *et al.*, 2022). It's well known that ACh is involved in the modulation of the release of neuropeptides such as SP and CGRP, causing neurogenic inflammation (Van der Kleij *et al*., 2009) In line with this, studies on the cholinergic pathway resulted in finding an anti-inflammatory role for ACh mediated by nAChRs on macrophages and monocytes. ACh interaction leads to cell deactivation and cytokine release inhibition, leading to the regulation of inflammation (Van der Kleij *et al*., 2009) in our study, the effect of ACh release from BC on the *Trpa1+* neurons and the *Trpv1+* neurons led to neurogenic inflammation due to peptide release

The activation of *Trpa1* might lead to the release of neuropeptides and neurotransmitters, which contribute to pain sensation. Thus, the *Trpa1* inhibition by ACh may have anti-inflammatory and analgesic effects and could be a therapeutical target used for therapeutic strategies. *Trpv1*, on the other hand, is activated by heat and noxious stimuli (Cao *et al*. 2007; Benítez-Angeles *et al.*, n.d.; Gavva *et al*. 2007; Kym, Kort, and Hutchins 2009). Similar to the *Trpa1*, *Trpv1* activation leads to the release of neuropeptides and neurotransmitters, contributing to pain and inflammation (Yoshida *et al.*, 2011). However, sensitizing this channel by ACh may have a negative impact on the induction of protective neurogenic inflammation and lead to an overshooting inflammation. Yet, there is a relationship between the activation of TRPA1 and cytokine storm, a study found that interleukin-1 beta (IL-1β), activates TRPA1 vagus nerve signaling leading to the inhibition of cytokine release, inducing hypothermia and reducing infection mortality (Silverman *et al*. 2023). These results show the importance of the TRPA1 channel in regulating chronic inflammation and pain responses.

The mechanism in which ACh affects *Trpa1* and *Trpv1* is not fully understood. We hypothesize that ACh affects the intracellular pathways that modulate the activity of these neurons. Additionally, our $[Ca^{2+}]i$ imaging experiment where dissociated JNC neurons were pre-incubated with the AChRs antagonists MEC and atropine resulted in a reversal of ACh's effect. This strongly suggests the involvement of AChRs in the inhibition of *Trpa1* and the activation of *Trpv1.* A possible explanation is that when ACh activates mAChRs, the production of cAMP is stimulated, which activates protein kinase A (PKA), then phosphorylates TRPA1, causing a reduction in its activity (Sullivan *et al.*, 1996; Kandel *et al.*, 2018; Wang *et al.*, 2019). On the other hand, the activation of TRPV1 by ACh can be mediated by the activation of nAChRs which can depolarize the sensory neurons, leading to the increase of $[Ca^{2+}]i$, which then binds and activates

TRPV1, leading to its opening, and the generation of an action potential (Fucile, 2004). However, the ACh effect on the *Trpa1* and *Trpv1* is very complex, and more research is needed to understand the mechanism of these interactions, especially in the context of sensory processing.

To further investigate the role of nAChRs in the ACh effect on the *Trpa1* and *Trpv1*, we pre-incubated dissociated JNC neurons with the nicotinic agonist DMPP. DMPP is an α3β4 subunit selective agonist (Brus and Jacobowitz, 1970). As a result, DMPP mimicked the ACh effect and led to the inhibition of *Trpa1* and the activation of *Trpv1*. Interestingly, this effect could be reversed through a pre-incubation of neurons with hexamethonium, a nicotinic α3β4 subunit antagonist (Asghar and Roth, 1971; Hone *et al*., 2015). The fact that hexamethonium inhibited the DMPP effect in *Trpa1*+ and *Trpv1*+ neurons suggests that ACh released from BC impacts *Trpa1* and *Trpv1* functions through the nAChR α3β4 subunit in sensory neurons.

ACh can have analgesic and hyperalgesic effects. In sensory neurons, the direct activation of the AChR via ACh or cholinergic agonists such as nicotine resulted in the reduction of pain. This was a result supported by using AChE which blocked the enzymatic reaction to break down ACh molecules (Balestrini *et al.*, 2021b, 2021c; Bautista *et al*., 2013). On the contrary, in the CNS, ACh can enhance pain transmission and promote hyperalgesia. Therefore, the effect of ACh on pain is different, depending on the type and location of AChRs. Despite the *Trpa1* inhibition via ACh can have pain-inhibiting effects, most probably it won't be a reliable analgesic since it's accompanied by the activation of *Trpv1*.

IN SUMMARY, this study reveals the functional role of ACh-induced $[Ca^{2+}]i$ signaling in regulating the TRPA1 and TRPV1 channels. This study also identifies the requirement of the nicotinic α3β4 subunit to achieve this effect. This result is in line with the known chemo-sensing role of both TRPA1 and TRPV1 channels in sensory neurons. Our observation that BC regulates the excitation and inhibition of the somatic nociceptor neurons via a mechanism depending on ACh production can be interpreted as a defense strategy to avoid acute pain resulting from the induction of neurogenic inflammation. This study supports the idea of considering the communications between the TRPM5, TRPA1, and TRPV1 channels a novel therapeutic target worth investigating against pain and inflammation.

References

1. Achanta, Satyanarayana, and Sven Eric Jordt. 2020. "Transient Receptor Potential Channels in Pulmonary Chemical Injuries and as Countermeasure Targets." *Annals of the New York Academy of Sciences* 1480 (1): 73–103. https://doi.org/10.1111/nyas.14472.
2. Ahmad, Raise, and Julie E Dalziel. 2020. "G Protein-Coupled Receptors in Taste Physiology and Pharmacology." *Frontiers in Pharmacology* 11 (November): 587664. https://doi.org/10.3389/fphar.2020.587664.
3. Andrè, Eunice, Barbara Campi, Serena Materazzi, Marcello Trevisani, Silvia Amadesi, Daniela Massi, Christophe Creminon, et al. 2008. "Cigarette Smoke–Induced Neurogenic Inflammation Is Mediated by α,β-Unsaturated Aldehydes and the TRPA1 Receptor in Rodents." *Journal of Clinical Investigation*, June. https://doi.org/10.1172/JCI34886.
4. Asgar, J., Y. Zhang, J. L. Saloman, S. Wang, M. K. Chung, and J. Y. Ro. *2015*. "The Role of TRPA1 in Muscle Pain and Mechanical Hypersensitivity under Inflammatory Conditions in Rats." *Neuroscience* 310: 206–15. https://doi.org/10.1016/j.neuroscience.2015.09.042.
5. Asghar, Khursheed, and Lloyd J. Roth. 1971. "Entry and Distribution of Hexamethonium in the Central Nervous System." *Biochemical Pharmacology* 20 (10). https://doi.org/10.1016/0006-2952(71)90189-4.
6. Avau, Bert, Sandra Steensels, Laurien Vancleef, Jorien Laermans, Jens Lesuisse, Johan Buyse, H Roger Lijnen, Jan Tack, and Inge Depoortere. 2015. "The Gustatory Signaling Pathway and Bitter Taste Receptors Affect the Development of Obesity and Adipocyte Metabolism in Mice." https://doi.org/10.1371/journal.pone.0145538.
7. Bade, Pauline, Fabrizio Simonetti, Stephanie Sans, Patricia Laboudie, Khadija Kissane, Nicolas Chappat, Sophie Lagrange, Florence Apparailly, Christine Roubert, and Isabelle Duroux-Richard. 2021. "Integrative Analysis of Human Macrophage Inflammatory Response Related to Mycobacterium Tuberculosis Virulence." *Frontiers in Immunology* 12 (June). https://doi.org/10.3389/fimmu.2021.668060.
8. Bader, Regine, Bertram Opitz, Wolfgang Reith, and Axel Mecklinger. 2014. "Is a Novel Conceptual Unit More than the Sum of Its Parts?: FMRI Evidence from an Associative Recognition Memory Study." https://doi.org/10.1016/j.neuropsychologia.2014.06.006.
9. Bader, Sandra, and Martin Diener. 2015. "Novel Aspects of Cholinergic Regulation of Colonic Ion Transport." *Pharmacology Research and Perspectives* 3 (3): 1–14. https://doi.org/10.1002/prp2.139.
10. Balestrini, Alessia, Victory Joseph, Michelle Dourado, Rebecca M. Reese, Shannon D. Shields, Lionel Rougé, Daniel D. Bravo, et al. 2021a. "A TRPA1 Inhibitor Suppresses Neurogenic Inflammation and Airway Contraction for Asthma Treatment." *The Journal of Experimental Medicine* 218 (4). https://doi.org/10.1084/jem.20201637.
11. Ballaz, Santiago, and James L. Mulshine. 2003. "The Potential Contributions of Chronic Inflammation to Lung Carcinogenesis." *Clinical Lung Cancer* 5 (1): 46–62. https://doi.org/10.3816/CLC.2003.N.021.
12. Bals, Robert, Daniel J. Weiner, and James M. Wilson. 1999. "The Innate Immune System in Cystic Fibrosis Lung Disease." *Journal of Clinical Investigation* 103 (3): 303–7. https://doi.org/10.1172/JCI6277.
13. Baluk, Peter, and Donald M. McDonald. 2018. "Imaging Lymphatics in Mouse Lungs." *Methods in Molecular Biology* 1846: 161–80. https://doi.org/10.1007/978-1-4939-8712-2_11.
14. Baluk P, McDonald DM. 2022. "Imaging Blood Vessels and Lymphatics in Mouse Trachea Wholemounts." In *Methods in Molecular Biology*, 2441:115–34. Humana Press Inc. https://doi.org/10.1007/978-1-0716-2059-5_10.
15. Baluk, Peter, Gavin Thurston, Thomas J. Murphy, Nigel W. Bunnett, and Donald M. Mcdonald. 1999. "Neurogenic Plasma Leakage in Mouse Airways." *British Journal of Pharmacology* 126 (2): 522–28. https://doi.org/10.1038/sj.bjp.0702323.
16. Bankova, Lora G., Daniel F. Dwyer, Eri Yoshimoto, Saltanat Ualiyeva, John W. McGinty, Hannah Raff, Jakob von Moltke, Yoshihide Kanaoka, K. Frank Austen, and Nora A. Barrett. 2018a. "The Cysteinyl Leukotriene 3

Receptor Regulates Expansion of IL-25–Producing Airway Brush Cells Leading to Type 2 Inflammation." *Science Immunology* 3 (28): 1–13. https://doi.org/10.1126/sciimmunol.aat9453.

17. Bankova LG, Dwyer DF, Yoshimoto E, Ualiyeva S, McGinty JW, Raff H, von Moltke J, Kanaoka Y, Frank Austen K, Barrett NA. 2018b. "The Cysteinyl Leukotriene 3 Receptor Regulates Expansion of IL-25–Producing Airway Brush Cells Leading to Type 2 Inflammation." *Science Immunology* 3 (28). https://doi.org/10.1126/SCIIMMUNOL.AAT9453.
18. Bautista, Diana M., Sven Eric Jordt, Tetsuro Nikai, Pamela R. Tsuruda, Andrew J. Read, Jeannie Poblete, Ebenezer N. Yamoah, Allan I. Basbaum, and David Julius. 2006. "TRPA1 Mediates the Inflammatory Actions of Environmental Irritants and Proalgesic Agents." *Cell* 124 (6): 1269–82. https://doi.org/10.1016/J.CELL.2006.02.023.
19. Bautista, Diana M., Maurizio Pellegrino, and Makoto Tsunozaki. 2013. "TRPA1: A Gatekeeper for Inflammation." *Annual Review of Physiology* 75 (February): 181–200. https://doi.org/10.1146/ANNUREV-PHYSIOL-030212-183811.
20. Benítez-Angeles, Miguel, Sara Luz Morales-Lázaro, Emmanuel Juárez-González, and Tamara Rosenbaum. 2020. "Molecular Sciences TRPV1: Structure, Endogenous Agonists, and Mechanisms." https://doi.org/10.3390/ijms21103421.
21. Bernal, Laura, Pamela Sotelo-Hitschfeld, Christine König, Viktor Sinica, Amanda Wyatt, Zoltan Winter, Alexander Hein, et al. 2021. "Odontoblast TRPC5 Channels Signal Cold Pain in Teeth." *Science Advances* 7 (13). https://doi.org/10.1126/SCIADV.ABF5567.
22. Bertrand, Claude, and Pierangelo Geppetti. 1996. "Tachykinin and Kinin Receptor Antagonists: Therapeutic Perspectives in Allergic Airway Disease." *Trends in Pharmacological Sciences* 17 (7): 255–59. https://doi.org/10.1016/0165-6147(96)10027-4.
23. Bessac, Bret F., Michael Sivula, Christian A. Von Hehn, Jasmine Escalera, Lauren Cohn, and Sven Eric Jordt. 2008. "TRPA1 Is a Major Oxidant Sensor in Murine Airway Sensory Neurons." *Journal of Clinical Investigation* 118 (5): 1899–1910. https://doi.org/10.1172/JCI34192.
24. Bezençon, C., A. Fürholz, F. Raymond, R. Mansourian, S. Métairon, J. Le Coutre, and Sami Damak. 2008. "Murine Intestinal Cells Expressing Trpm5 Are Mostly Brush Cells and Express Markers of Neuronal and Inflammatory Cells." *Journal of Comparative Neurology* 509 (5): 514–25. https://doi.org/10.1002/CNE.21768.
25. Brus, Ryszard, and David Jacobowitz. 1970. "The Effects of DMPP on Adrenergic Nerves in Perfused Hearts." *European Journal of Pharmacology* 11 (1): 1–12. https://doi.org/10.1016/0014-2999(70)90247-5.
26. BYCK, R. 1961. "THE EFFECT OF HEXAMETHONIUM ON THE CAROTID CHEMORECEPTOR RESPONSE TO NICOTINE AND CYANIDE." *British Journal of Pharmacology and Chemotherapy* 16 (1): 15–22. https://doi.org/10.1111/J.1476-5381.1961.TB00293.X.
27. Cao, Xuehong, Xuesong Cao, Hong Xie, Rong Yang, Gang Lei, Fen Li, Ai Li, Changjin Liu, and Lieju Liu. 2007. "Effects of Capsaicin on VGSCs in TRPV1-/- Mice." *Brain Research* 1163 (1): 33–43. https://doi.org/10.1016/J.BRAINRES.2007.04.085.
28. Care, DM Mcdonald. 1988. - American Journal of Respiratory and Critical. "Respiratory Tract Infections Increase Susceptibility to Neurogenic Inflammation in the Rat Trachea." *Atsjournals.Org*. Accessed April 4, 2022. https://www.atsjournals.org/doi/pdf/10.1164/ajrccm/137.6.1432.
29. Young, D., Hussell, T. & Dougan, G. (2002). Chronic bacterial infections: living with unwanted guests. *Nat Immunol* 3, 1026–1032
30. Coburn, R. F., and T. Tomita. 1973. "Evidence for Nonadrenergic Inhibitory Nerves in the Guinea Pig Trachealis Muscle. "*Https://Doi.Org/10.1152/Ajplegacy.1973.224.5.1072*224(5):1072–80.
31. Colquhoun, Lorna M, and James W Patrick. 1997. "Alpha3 , Beta2 , and Beta4 Form Heterotrimeric Neuronal Nicotinic Acetyicholine Receptors in Xenopus Oocytes." *Journal of Neurochemistry* 69: 2355–62.
32. Conrad, Douglas J., Hartmut Kuhn, Mary Mulkins, Ella Highland, and Elliott Sigal. 1992. "Specific Inflammatory Cytokines Regulate the Expression of Human Monocyte 15-Lipoxygenase." *Proceedings of the National Academy of Sciences of the United States of America* 89 (1): 217–21. https://doi.org/10.1073/PNAS.89.1.217.
33. Costa, Robson, Emerson M. Motta, Marianne N. Manjavachi, Maíra Cola, and João B. Calixto. 2012. "Activation of the Alpha-7 Nicotinic Acetylcholine Receptor (A7 NAchR) Reverses Referred Mechanical

Hyperalgesia Induced by Colonic Inflammation in Mice." *Neuropharmacology* 63 (5): 798–805. https://doi.org/10.1016/J.NEUROPHARM.2012.06.004.

34. Damak, Sami, Minqing Rong, Keiko Yasumatsu, Zaza Kokrashvili, Cristian A. Pérez, Noriatsu Shigemura, Ryusuke Yoshida, et al. 2006. "Trpm5 Null Mice Respond to Bitter, Sweet, and Umami Compounds." *Chemical Senses* 31 (3): 253–64. https://doi.org/10.1093/CHEMSE/BJJ027.
35. Daniel, E. E., M. Kannan, C. Davis, and V. Posey-Daniel. 1986. "Ultrastructural Studies on the Neuromuscular Control of Human Tracheal and Bronchial Muscle." *Respiration Physiology* 63 (1): 109–28. https://doi.org/10.1016/0034-5687(86)90034-4.
36. David, Reinhard, Anna Ciuraszkiewicz, Xenia Simeone, Avi Orr-Urtreger, Roger L. Papke, J. M. McIntosh, Sigismund Huck, and Petra Scholze. 2010. "Biochemical and Functional Properties of Distinct Nicotinic Acetylcholine Receptors in the Superior Cervical Ganglion of Mice with Targeted Deletions of NAChR Subunit Genes." *European Journal of Neuroscience* 31 (6): 978–93. https://doi.org/10.1111/j.1460-9568.2010.07133.x.
37. Deckmann, Klaus, Gabriela Krasteva-Christ, Amir Rafiq, Christine Herden, Judy Wichmann, Sascha Knauf, Christina Nassenstein, et al. 2015. "Cholinergic Urethral Brush Cells Are Widespread throughout Placental Mammals." *International Immunopharmacology* 29 (1): 51–56. https://doi.org/10.1016/j.intimp.2015.05.038.
38. Dey, R. D., H. W. Mitchell, and R. F. Coburn. 1990. "Organization and Development of Peptide-Containing Neurons in the Airways." *American Journal of Respiratory Cell and Molecular Biology* 3 (3): 187–88. https://doi.org/10.1165/AJRCMB/3.3.187.
39. Dhaka, Ajay, Veena Viswanath, and Ardem Patapoutian. 2006. "TRP Ion Channels and Temperature Sensation." *Annual Review of Neuroscience* 29: 135–61. https://doi.org/10.1146/ANNUREV.NEURO.29.051605.112958.
40. "Diphtheria Toxin - an Overview | ScienceDirect Topics." n.d. Accessed July 27, 2022. https://www.sciencedirect.com/topics/biochemistry-genetics-and-molecular-biology/diphtheria-toxin.
41. Driscoll, James A., Steven L. Brody, and Marin H. Kollef. 2007. "The Epidemiology, Pathogenesis and Treatment of Pseudomonas Aeruginosa Infections." *Drugs* 67 (3): 351–68. https://doi.org/10.2165/00003495-200767030-00003.
42. Eftekhari, Sajedeh, Karin Warfvinge, Frank W. Blixt, and Lars Edvinsson. 2013. "Differentiation of Nerve Fibers Storing CGRP and CGRP Receptors in the Peripheral Trigeminovascular System." *J Pain Off J Am Pain Soc* 14 (11): 1289–1303. https://doi.org/10.1016/j.jpain.2013.03.010.
43. Ezekowitz, RAB, and JA Hoffmann. 2002. *Innate Immunity*. https://books.google.de/books?hl=en&lr=lang_en&id=PHz5BwAAQBAJ&oi=fnd&pg=PR9&dq=Innate+immunity+is+the+first+line+of+defense+&ots=yyMtUlbYCT&sig=ZibBWmFxJWFIXYHc2wUi56iAqnk.
44. Ferdowsi, Parisa Vahidi, Kiran D.K. Ahuja, Jeffrey M. Beckett, and Stephen Myers. 2021. "TRPV1 Activation by Capsaicin Mediates Glucose Oxidation and ATP Production Independent of Insulin Signalling in Mouse Skeletal Muscle Cells." *Cells* 10 (6). https://doi.org/10.3390/cells10061560.
45. Ferry, Xavier, Stephan Brehin, Rehab Kamel, and Yves Landry. 2002. "G Protein-Dependent Activation of Mast Cell by Peptides and Basic Secretagogues." *Peptides* 23 (8): 1507–15. https://doi.org/10.1016/S0196-9781(02)00090-6.
46. Figini, Michela, Costanza Emanueli, Eileen F. Grady, Kimberly Kirkwood, Donald G. Payan, John Ansel, Craig Gerard, Pierangelo Geppetti, and Nigel Bunnett. 1997. "Substance P and Bradykinin Stimulate Plasma Extravasation in the Mouse Gastrointestinal Tract and Pancreas." *The American Journal of Physiology* 272 (4 Pt 1). https://doi.org/10.1152/AJPGI.1997.272.4.G785.
47. Figini, Michela, Panthea Javdan, Fabio Cioncolini, and Pierangelo Geppetti. 1995. "Involvement of Tachykinins in Plasma Extravasation Induced by Bradykinin and Low PH Medium in the Guinea-pig Conjunctiva." *British Journal of Pharmacology* 115 (1): 128–32. https://doi.org/10.1111/j.1476-5381.1995.tb16329.x.
48. Fucile, S. 2004. "Ca2+ Permeability of Nicotinic Acetylcholine Receptors." *Cell Calcium* 35: 1–8.
49. Gavva, Narender R., Anthony W. Bannon, David N. Hovland, Sonya G. Lehto, Lana Klionsky, Sekhar Surapaneni, David C. Immke, et al. 2007. "Repeated Administration of Vanilloid Receptor TRPV1 Antagonists Attenuates

Hyperthermia Elicited by TRPV1 Blockade." *Journal of Pharmacology and Experimental Therapeutics* 323 (1): 128–37. https://doi.org/10.1124/JPET.107.125674.

50. Gees, Maarten, Yeranddy A. Alpizar, Tomas Luyten, Jan B. Parys, Bernd Nilius, Geert Bultynck, Thomas Voets, and Karel Talavera. 2014. "Differential Effects of Bitter Compounds on the Taste Transduction Channels Trpm5 and IP3 Receptor Type 3." *Chemical Senses* 39 (4): 295–311. https://doi.org/10.1093/CHEMSE/BJT115.
51. Gerbe, François, Emmanuelle Sidot, Danielle J. Smyth, Makoto Ohmoto, Ichiro Matsumoto, Valérie Dardalhon, Pierre Cesses, et al. 2016. "Intestinal Epithelial Tuft Cells Initiate Type 2 Mucosal Immunity to Helminth Parasites." *Nature* 529 (7585): 226–30. https://doi.org/10.1038/NATURE16527.
52. Gillet, Daniel, and Julien Barbier. 2015. "Diphtheria Toxin." *The Comprehensive Sourcebook of Bacterial Protein Toxins*, June, 111–32. https://doi.org/10.1016/B978-0-12-800188-2.00004-5.
53. Grace, M. S., M. Baxter, E. Dubuis, M. A. Birrell, and M. G. Belvisi. 2014. "Transient Receptor Potential (TRP) Channels in the Airway: Role in Airway Disease." *British Journal of Pharmacology* 171 (10): 2593–2607. https://doi.org/10.1111/bph.12538.
54. Grando, Sergei A., Koichiro Kawashima, Charles J. Kirkpatrick, Wolfgang Kummer, and Ignaz Wessler. 2015. "Recent Progress in Revealing the Biological and Medical Significance of the Non-Neuronal Cholinergic System." *International Immunopharmacology* 29 (1): 1–7. https://doi.org/10.1016/J.INTIMP.2015.08.023.
55. Greco, R., C. Tassorelli, G. Sandrini, P. Di Bella, S. Buscone, and G. Nappi. 2008. "Role of Calcitonin Gene-Related Peptide and Substance P in Different Models of Pain." *Cephalalgia: An International Journal of Headache* 28 (2): 114–26. https://doi.org/10.1111/J.1468-2982.2007.01468.X.
56. Greka, Anna, and Peter Mundel. 2012. "Cell Biology and Pathology of Podocytes." *Annual Review of Physiology* 74: 299–323. https://doi.org/10.1146/ANNUREV-PHYSIOL-020911-153238.
57. Hammad, Hamida, and Bart N. Lambrecht. 2015. "Barrier Epithelial Cells and the Control of Type 2 Immunity." *Immunity* 43 (1): 29–40. https://doi.org/10.1016/J.IMMUNI.2015.07.007.
58. Hedges, S., M. Svensson, W. Agace, and C. Svanborg. 1995. "Cytokines Induce an Epithelial Cell Cytokine Response." *Advances in Experimental Medicine and Biology* 371 (A): 189–93. https://doi.org/10.1007/978-1-4615-1941-6_38.
59. Hellenthal, Katharina E.M., Laura Brabenec, Eric R. Gross, and Nana Maria Wagner. 2021. "Trp Channels as Sensors of Aldehyde and Oxidative Stress." *Biomolecules*. MDPI. https://doi.org/10.3390/biom11101401.
60. Hernandez, Adrian F., Jennifer B. Green, Salim Janmohamed, Ralph B. D'Agostino, Christopher B. Granger, Nigel P. Jones, Lawrence A. Leiter, et al. 2018. "Albiglutide and Cardiovascular Outcomes in Patients with Type 2 Diabetes and Cardiovascular Disease (Harmony Outcomes): A Double-Blind, Randomised Placebo-Controlled Trial." *The Lancet* 392 (10157): 1519–29. https://doi.org/10.1016/S0140-6736(18)32261-X.
61. Hollenhorst, Monika I, Silke Appenzeller, | Lei Li, Jörg Vogel, Stephanie Wiederhold, Mike Althaus, Brendan J Canning, Antoine-Emmanuel Saliba, and Gabriela Krasteva-Christ. 2019. "Tracheal Brush Cells Release Acetylcholine in Response to Bitter Tastants for Paracrine and Autocrine Signaling | Innokentij Jurastow 2,3 | Rajender Nandigama 4 |." https://doi.org/10.1096/fj.201901314RR.
62. Hollenhorst, Monika I., Innokentij Jurastow, Rajender Nandigama, Silke Appenzeller, Lei Li, Jörg Vogel, Stephanie Wiederhold, et al. 2020. "Tracheal Brush Cells Release Acetylcholine in Response to Bitter Tastants for Paracrine and Autocrine Signaling." *FASEB Journal* 34 (1): 316–32. https://doi.org/10.1096/FJ.201901314RR.
63. Hollenhorst, Monika and Gabriela Krasteva-Christ. 2023. "Chemosensory Cells in the Respiratory Tract as Crucial Regulators of Innate Immune Responses." *The Journal of Physiology*, April. https://doi.org/10.1113/JP282307.
64. Hollenhorst, Monika I., Praveen Kumar, Maxim Zimmer, Alaa Salah, Stephan Maxeiner, Mohamed Ibrahem Elhawy, Saskia B. Evers, et al. 2022. "Taste Receptor Activation in Tracheal Brush Cells by Denatonium Modulates ENaC Channels via Ca2+, CAMP and ACh." *Cells* 11 (15). https://doi.org/10.3390/cells11152411.
65. Hollenhorst, Monika I., Rajender Nandigama, Saskia B. Evers, Igor Gamayun, Noran Abdel Wadood, Alaa Salah, Mario Pieper, et al. 2022a. "Bitter Taste Signaling in Tracheal Epithelial Brush Cells Elicits Innate Immune Responses to Bacterial Infection." *Journal of Clinical Investigation*. https://doi.org/10.1172/jci150951.

66. Hone, Arik J., J. Michael McIntosh, Layla Azam, Jon Lindstrom, Linda Lucero, Paul Whiteaker, Juan Passas, Jesús Blázquez, and Almudena Albillos. 2015. "α-Conotoxins Identify the A3β4∗ Subtype as the Predominant Nicotinic Acetylcholine Receptor Expressed in Human Adrenal Chromaffin Cells." *Molecular Pharmacology* 88 (5): 881–93. https://doi.org/10.1124/mol.115.100982.
67. Horiguchi, Yasuhiko, and Eisuke Mekada. 2006. "Toxin Receptors." *The Comprehensive Sourcebook of Bacterial Protein Toxins*, 106–19. https://doi.org/10.1016/B978-012088445-2/50011-1.
68. Hsu, Chun Chun, and Lu Yuan Lee. 2015. "Role of Calcium Ions in the Positive Interaction between TRPA1 and TRPV1 Channels in Bronchopulmonary Sensory Neurons." *Journal of Applied Physiology* 118 (12): 1533–43. https://doi.org/10.1152/japplphysiol.00043.2015.
69. Hulme, E. C., N. J.M. Birdsall, and N. J. Buckley. 1990a. "Muscarinic Receptor Subtypes." *Annual Review of Pharmacology and Toxicology* 30: 633–73. https://doi.org/10.1146/ANNUREV.PA.30.040190.003221.
70. Juárez-Contreras, Rebeca, Karina Angélica Méndez-Reséndiz, Tamara Rosenbaum, Ricardo González-Ramírez, and Sara Luz Morales-Lázaro. 2020. "TRPV1 Channel: A Noxious Signal Transducer That Affects Mitochondrial Function." *International Journal of Molecular Sciences* 21 (23): 1–17. https://doi.org/10.3390/IJMS21238882.
71. Kabbani, Nadine, Jacob C. Nordman, Brian A. Corgiat, Daniel P. Veltri, Amarda Shehu, Victoria A. Seymour, and David J. Adams. 2013. "Are Nicotinic Acetylcholine Receptors Coupled to G Proteins?" *BioEssays* 35 (12): 1025–34. https://doi.org/10.1002/bies.201300082.
72. Kamato, Danielle, Lyna Thach, Rebekah Bernard, Vincent Chan, Wenhua Zheng, Harveen Kaur, Margaret Brimble, Narin Osman, Peter J Little, and Suowen Xu. 2015. "Structure, Function, Pharmacology, and Therapeutic Potential of the G Protein, Gα /q,11," 24. https://doi.org/10.3389/fcvm.2015.00014.
73. Kamei, Jun, Naoki Aizawa, Takayuki Nakagawa, Shuji Kaneko, Haruki Kume, Yukio Homma, and Yasuhiko Igawa. 2018. "Attenuated Lipopolysaccharide-Induced Inflammatory Bladder Hypersensitivity in Mice Deficient of Transient Receptor Potential Ankilin1." *Scientific Reports* 8 (1): 1–10. https://doi.org/10.1038/s41598-018-33967-x.
74. Kandel, Chrissy, Patricia Schmidt, Alexander Perniss, Maryam Keshavarz, Paul Scholz, Sabrina Osterloh, Mike Althaus, Wolfgang Kummer, and Klaus Deckmann. 2018. "ENaC in Cholinergic Brush Cells." *Frontiers in Cell and Developmental Biology* 6 (AUG). https://doi.org/10.3389/FCELL.2018.00089.
75. Kaske, Silke, Gabriele Krasteva, Peter König, Wolfgang Kummer, Thomas Hofmann, Thomas Gudermann, and Vladimir Chubanov. 2007a. "TRPM5, a Taste-Signaling Transient Receptor Potential Ion-Channel, Is a Ubiquitous Signaling Component in Chemosensory Cells." https://doi.org/10.1186/1471-2202-8-49.
76. Kistemaker, L. E.M., and Y. S. Prakash. 2019. "Airway Innervation and Plasticity in Asthma." *Physiology* 34 (4): 283–98. https://doi.org/10.1152/PHYSIOL.00050.2018.
77. Kleij, H. P.M. Van der, P. Forsythe, and J. Bienenstock. 2009. "Autonomic Neuroimmunology." *Encyclopedia of Neuroscience*, 1003–8. https://doi.org/10.1016/B978-008045046-9.00642-2.
78. Knowles, Michael R., and Richard C. Boucher. 2002. "Mucus Clearance as a Primary Innate Defense Mechanism for Mammalian Airways." *The Journal of Clinical Investigation* 109 (5): 571–77. https://doi.org/10.1172/JCI15217.
79. Kobayashi, Akio, and Jeremy S. Duffield. 2011. "Use of Genetic Mouse Models to Study Kidney Regeneration." *Regenerative Nephrology*, 37–66. https://doi.org/10.1016/B978-0-12-380928-5.10003-X.
80. Konishi, Mitsuru, Yoku Hayakawa, and Kazuhiko Koike. 2019. "Role of Muscarinic Acetylcholine Signaling in Gastrointestinal Cancers." *Biomedicines* 7 (3). https://doi.org/10.3390/BIOMEDICINES7030058.
81. Krasteva, G., P. Hartmann, T. Papadakis, M. Bodenbenner, L. Wessels, E. Weihe, B. Schütz, et al. 2012. "Cholinergic Chemosensory Cells in the Auditory Tube." *Histochemistry and Cell Biology* 137 (4): 483–97. https://doi.org/10.1007/s00418-012-0911-x.
82. Kumar, Praveen, Petra Scholze, Martin Fronius, Gabriela Krasteva-Christ, and Monika I. Hollenhorst. 2020. "Nicotine Stimulates Ion Transport via Metabotropic B4 Subunit Containing Nicotinic ACh Receptors." *British Journal of Pharmacology* 177 (24): 5595–5608. https://doi.org/10.1111/BPH.15270.
83. Kummer, W., K. S. Lips, and U. Pfeil. 2008. "The Epithelial Cholinergic System of the Airways." *Histochemistry and Cell Biology* 130 (2): 219–34. https://doi.org/10.1007/s00418-008-0455-2.

84. Kummer, Wolfgang, and Klaus Deckmann. 2017. "Brush Cells, the Newly Identified Gatekeepers of the Urinary Tract." *Current Opinion in Urology* 27 (2): 85–92. https://doi.org/10.1097/MOU.0000000000000361.
85. Kummer, Wolfgang, and Gabriela Krasteva-Christ. 2014a. "Non-Neuronal Cholinergic Airway Epithelium Biology." *Current Opinion in Pharmacology* 16 (1): 43–49. https://doi.org/10.1016/j.coph.2014.03.001.
86. Kusumakshi, Soumya, Anja Voigt, Sandra Hübner, Irm Hermans-Borgmeyer, Ana Ortalli, Martina Pyrski, Janka Dörr, et al. 2015. "A Binary Genetic Approach to Characterize TRPM5 Cells in Mice." *Chemical Senses* 40 (6): 413–25. https://doi.org/10.1093/CHEMSE/BJV023.
87. Kym, Philip R., Michael E. Kort, and Charles W. Hutchins. 2009. "Analgesic Potential of TRPV1 Antagonists." *Biochemical Pharmacology* 78 (3): 211–16. https://doi.org/10.1016/J.BCP.2009.02.014.
88. Lee, Eunjung, Dae Young Jung, Jong Hun Kim, Payal R. Patel, Xiaodi Hu, Yongjin Lee, Yoshihiro Azuma, et al. 2015. "Transient Receptor Potential Vanilloid Type-1 Channel Regulates Diet-Induced Obesity, Insulin Resistance, and Leptin Resistance." *FASEB Journal* 29 (8): 3182–92. https://doi.org/10.1096/fj.14-268300.
89. Lee, Lu Yuan, and Jerry Yu. 2014. "Sensory Nerves in Lung and Airways." *Comprehensive Physiology* 4 (1): 287–324. https://doi.org/10.1002/CPHY.C130020.
90. Leroux, Alice, Bruno Paiva dos Santos, Jacques Leng, Hugo Oliveira, and Joëlle Amédée. 2020. "Sensory Neurons from Dorsal Root Ganglia Regulate Endothelial Cell Function in Extracellular Matrix Remodelling." *Cell Communication and Signaling* 18 (1). https://doi.org/10.1186/s12964-020-00656-0.
91. Levy, Dan, Rami Burstein, and Andrew M. Strassman. 2005. "Calcitonin Gene-Related Peptide Does Not Excite or Sensitize Meningeal Nociceptors: Implications for the Pathophysiology of Migraine." *Ann Neurol* 58 (5): 698–705. https://doi.org/10.1002/ana.20619.
92. Li, Jing, Carrie V. Vause, and Paul L. Durham. 2008. "Calcitonin Gene-Related Peptide Stimulation of Nitric Oxide Synthesis and Release from Trigeminal Ganglion Glial Cells." *Brain Res* 1196 (February): 22–32. https://doi.org/10.1016/j.brainres.2007.12.028.
93. Lin, Weihong, Ejiofor A.D. Ezekwe, Zhen Zhao, Emily R. Liman, and Diego Restrepo. 2008. "TRPM5-Expressing Microvillous Cells in the Main Olfactory Epithelium." *BMC Neuroscience* 9 (November). https://doi.org/10.1186/1471-2202-9-114.
94. Liu, Boyi, Yan Tai, Ana I. Caceres, Satyanarayana Achanta, Shrilatha Balakrishna, Xiaomei Shao, Junfan Fang, and Sven Eric Jordt. 2016. "Oxidized Phospholipid OxPAPC Activates TRPA1 and Contributes to Chronic Inflammatory Pain in Mice." *PLoS ONE* 11 (11): 1–15. https://doi.org/10.1371/journal.pone.0165200.
95. Liu, L., W. Zhu, Z. S. Zhang, T. Yang, A. Grant, G. Oxford, and S. A. Simon. 2004. "Nicotine Inhibits Voltage-Dependent Sodium Channels and Sensitizes Vanilloid Receptors." *Journal of Neurophysiology* 91 (4): 1482–91. https://doi.org/10.1152/jn.00922.2003.
96. Liu, Lieju, Lei Chen, Wolfgang Liedtke, and S. A. Simon. 2007. "Changes in Osmolality Sensitize the Response to Capsaicin in Trigeminal Sensory Neurons." *Journal of Neurophysiology* 97 (3): 2001–15. https://doi.org/10.1152/JN.00887.2006.
97. Lottig, Lena, Sandra Bader, Marcel Jimenez, and Martin Diener. 2019. "Evidence for Metabotropic Function of Epithelial Nicotinic Cholinergic Receptors in Rat Colon." *British Journal of Pharmacology* 176 (9): 1328–40. https://doi.org/10.1111/bph.14638.
98. Malin, David H., J. Ronald Lake, Christina K. Schopen, John W. Kirk, Elizabeth E. Sailer, Brent A. Lawless, Timothy P. Upchurch, Merle Shenoi, and Nancy Rajan. 1997. "Nicotine Abstinence Syndrome Precipitated by Central but Not Peripheral Hexamethonium." *Pharmacology Biochemistry and Behavior* 58 (3): 695–99. https://doi.org/10.1016/S0091-3057(97)90006-X.
99. Manna, Pulak R., Zackery C. Gray, and P. Hemachandra Reddy. 2022. "Healthy Immunity on Preventive Medicine for Combating COVID-19." *Nutrients* 14 (5): 1–21. https://doi.org/10.3390/nu14051004.
100. Mathison, Ronald, and Joseph S Davison. 1993. "Attenuated Plasma Extravasation to Sensory Neuropeptides in Diabetic Rats." *Agents Actions*. Vol. 38.
101. Matsuda, Megumi, Yul Huh, and Ru Rong Ji. 2019a. "Roles of Inflammation, Neurogenic Inflammation, and Neuroinflammation in Pain." *Journal of Anesthesia* 33 (1): 131. https://doi.org/10.1007/S00540-018-2579-4.
102. Matsukawa, A, CM Hogaboam, … NW Lukacs - Reviews in, and undefined 2000. n.d. "Chemokines and Innate Immunity." *Europepmc.Org*. Accessed April 4, 2022. https://europepmc.org/article/med/11256744.

103. McDonald, Donald M., Jeffrey J. Bowden, Peter Baluk, and Nigel W. Bunnett. 1996. "Neurogenic Inflammation: A Model for Studying Efferent Actions of Sensory Nerves." *Advances in Experimental Medicine and Biology* 410: 453–62. https://doi.org/10.1007/978-1-4615-5891-0_70.
104. Meseguer, Victor, Yeranddy A. Alpizar, Enoch Luis, Sendoa Tajada, Bristol Denlinger, Otto Fajardo, Jan Albert Manenschijn, et al. 2014. "TRPA1 Channels Mediate Acute Neurogenic Inflammation and Pain Produced by Bacterial Endotoxins." *Nature Communications* 5. https://doi.org/10.1038/ncomms4125.
105. Messlinger, Karl. 2018. "The Big CGRP Flood - Sources, Sinks and Signalling Sites in the Trigeminovascular System." *Journal of Headache and Pain* 19 (1): 1–7. https://doi.org/10.1186/S10194-018-0848-0/FIGURES/2.
106. Meurs, Herman, Bart G.J. Dekkers, Harm Maarsingh, Andrew J. Halayko, Johan Zaagsma, and Reinoud Gosens. 2013. "Muscarinic Receptors on Airway Mesenchymal Cells: Novel Findings for an Ancient Target." *Pulmonary Pharmacology and Therapeutics* 26 (1): 145–55. https://doi.org/10.1016/J.PUPT.2012.07.003.
107. Millar, N. S. 2003. "Assembly and Subunit Diversity of Nicotinic Acetylcholine Receptors." *Biochemical Society Transactions* 31 (Pt 4): 869–74. https://doi.org/10.1042/BST0310869.
108. Misu, Yoshimi, and Takao Kubo. 1972. "Effects of Hexamethonium and Other Agents on Noradrenaline Output Released by the Sympathetic Nerve Stimulation in the Isolated Perfused Rabbit's Heart." *Japanese Journal of Pharmacology* 22 (3): 359–70. https://doi.org/10.1254/JJP.22.359.
109. Moffatt, C. J., and P. J. Franks. 2004. "Implementation of a Leg Ulcer Strategy." *British Journal of Dermatology* 151 (4): 857–67. https://doi.org/10.1111/J.1365-2133.2004.06200.X.
110. Monack, Denise M., Anne Mueller, and Stanley Falkow. 2004. "Persistent Bacterial Infections: The Interface of the Pathogen and the Host Immune System." *Nature Reviews Microbiology* 2 (9): 747–65. https://doi.org/10.1038/nrmicro955.
111. Montell, Craig, and Gerald M. Rubin. 1989. "Molecular Characterization of the Drosophila Trp Locus: A Putative Integral Membrane Protein Required for Phototransduction." *Neuron* 2 (4): 1313–23. https://doi.org/10.1016/0896-6273(89)90069-X.
112. Montoro, Daniel T., Adam L. Haber, Moshe Biton, Vladimir Vinarsky, Brian Lin, Susan E. Birket, Feng Yuan, et al. 2018. "A Revised Airway Epithelial Hierarchy Includes CFTR-Expressing Ionocytes." *Nature* 560 (7718): 319–24. https://doi.org/10.1038/S41586-018-0393-7.
113. Moran, Magdalene M. 2018. "TRP Channels as Potential Drug Targets." *Annual Review of Pharmacology and Toxicology* 58 (January): 309–30. https://doi.org/10.1146/ANNUREV-PHARMTOX-010617-052832.
114. Moroni, Mirko, Ruud Zwart, Emanuele Sher, Bruce K. Cassels, and Isabel Bermudez. 2006. "A4β2 Nicotinic Receptors with High and Low Acetylcholine Sensitivity: Pharmacology, Stoichiometry, and Sensitivity to Long-Term Exposure to Nicotine." *Molecular Pharmacology* 70 (2): 755–68. https://doi.org/10.1124/mol.106.023044.
115. Nassenstein, Christina, Gabriela Krasteva-Christ, and Harald Renz. 2018. "New Aspects of Neuroinflammation and Neuroimmune Crosstalk in the Airways." *Journal of Allergy and Clinical Immunology* 142 (5): 1415–22. https://doi.org/10.1016/j.jaci.2018.09.011.
116. Nazir, Samantha-Su Taylor, Noor Ivan, Urits Antonella, Paladini Monica Sri, Sadhu Clay, Gibb Tyler, Carlson Dariusz, et al. 2021. "Complex Regional Pain Syndrome: A Comprehensive Review." https://doi.org/10.1007/s40122-021-00279-4.
117. Nelson, S, WR Summer - 1998. "Innate Immunity, Cytokines, and Pulmonary Host Defense." *Elsevier*. Accessed April 4, 2022. https://www.sciencedirect.com/science/article/pii/S0891552005701987.
118. Ni, Amy, Erin Lashnits, Li Chin Yao, Peter Baluk, and Donald M. McDonald. 2010. "Rapid Remodeling of Airway Vascular Architecture at Birth." *Developmental Dynamics: An Official Publication of the American Association of Anatomists* 239 (9): 2354. https://doi.org/10.1002/DVDY.22379.
119. O'Connor, Terence M., Joseph O'Connell, Darren I. O'Brien, Triona Goode, Charles P. Bredin, and Fergus Shanahan. 2004. "The Role of Substance P in Inflammatory Disease." *Journal of Cellular Physiology* 201 (2): 167–80. https://doi.org/10.1002/JCP.20061.
120. Okada, Masaji, and Taro Shirakawa. 2005. "Frontier of Mycobacterium Research - Host vs. Mycobacterium." *Kekkaku* 80 (9): 613–29.

121. Oram, Diana Marra, and Randall K. Holmes. 2006. "Diphtheria Toxin." *The Comprehensive Sourcebook of Bacterial Protein Toxins*, 245–56. https://doi.org/10.1016/B978-012088445-2/50018-4.
122. Owsianik, Grzegorz, Karel Talavera, Thomas Voets, and Bernd Nilius. 2006. "Permeation and Selectivity of TRP Channels." *Annual Review of Physiology* 68: 685–717. https://doi.org/10.1146/ANNUREV.PHYSIOL.68.040204.101406.
123. Pan, Jun, Leyi Zhang, Xuan Shao, and Jian Huang. 2020. "Acetylcholine From Tuft Cells: The Updated Insights Beyond Its Immune and Chemosensory Functions." *Frontiers in Cell and Developmental Biology* 8 (July). https://doi.org/10.3389/FCELL.2020.00606.
124. Papke, Roger L., Linda P. Dwoskin, Peter A. Crooks, Guangrong Zheng, Zhenfa Zhang, J. Michael McIntosh, and Clare Stokes. 2008. "Extending the Analysis of Nicotinic Receptor Antagonists with the Study of A6 Nicotinic Receptor Subunit Chimeras." *Neuropharmacology* 54 (8): 1189–1200. https://doi.org/10.1016/j.neuropharm.2008.03.010.
125. Papke, Roger L., Clare Stokes, M. Imad Damaj, Ganesh A. Thakur, Khan Manther, Millet Treinin, Deniz Bagdas, Abhijit R. Kulkarni, and Nicole A. Horenstein. 2018. "Persistent Activation of A7 Nicotinic ACh Receptors Associated with Stable Induction of Different Desensitized States." *British Journal of Pharmacology* 175 (11): 1838–54. https://doi.org/10.1111/bph.13851.
126. Perniss, Alexander, Shuya Liu, Brett Boonen, Maryam Keshavarz, Anna Lena Ruppert, Thomas Timm, Uwe Pfeil, et al. 2020. "Chemosensory Cell-Derived Acetylcholine Drives Tracheal Mucociliary Clearance in Response to Virulence-Associated Formyl Peptides." *Immunity* 52 (4): 683-699.e11. https://doi.org/10.1016/j.immuni.2020.03.005.
127. Perniss, Alexander, Patricia Schmidt, Aichurek Soultanova, Tamara Papadakis, Katja Dahlke, Anja Voigt, Burkhard Schütz, Wolfgang Kummer, and Klaus Deckmann. 2021. "Development of Epithelial Cholinergic Chemosensory Cells of the Urethra and Trachea of Mice." *Cell and Tissue Research* 385 (1): 21–35. https://doi.org/10.1007/S00441-021-03424-9.
128. Puskar, Nyssa L., Xinan Xiu, Henry A. Lester, and Dennis A. Dougherty. 2011. "Two Neuronal Nicotinic Acetylcholine Receptors, A4β4 and A7, Show Differential Agonist Binding Modes." *Journal of Biological Chemistry* 286 (16): 14618–27. https://doi.org/10.1074/jbc.M110.206565.
129. Quie, Paul G. 1986. "Lung Defense against Infection." *The Journal of Pediatrics* 108 (5 PART 2): 813–16. https://doi.org/10.1016/S0022-3476(86)80750-8.
130. Ramsey, I. Scott, Markus Delling, and David E. Clapham. 2006. "An Introduction to TRP Channels." *Annual Review of Physiology* 68: 619–47. https://doi.org/10.1146/ANNUREV.PHYSIOL.68.040204.100431.
131. Rana, Khokan, Soumya Ranjan Nayak, Alice Bihary, Ajay Ku Sahoo, Kanhu Charan Mohanty, Subrata ku Palo, Debadutta Sahoo, Sanghamitra Pati, and Pujarini Dash. 2021. "Association of Quorum Sensing and Biofilm Formation with Salmonella Virulence: Story beyond Gathering and Cross-Talk." *Archives of Microbiology* 203 (10): 5887–97. https://doi.org/10.1007/s00203-021-02594-y.
132. Reardon, Colin, Gordon S. Duncan, Anne Brüstle, Dirk Brenner, Michael W. Tusche, Peder S. Olofsson, Mauricio Rosas-Ballina, Kevin J. Tracey, and Tak W. Mak. 2013. "Erratum: Lymphocyte-Derived ACh Regulates Local Innate but Not Adaptive Immunity (Proceedings of the National Academy of Sciences of the United States of America (2013) 110 (1410-1415) DOI: 10.1073/Pnas.1221655110)." *Proceedings of the National Academy of Sciences of the United States of America* 110 (13): 5269. https://doi.org/10.1073/PNAS.1302921110.
133. Reid, Lynne, Barbara Meyrick, Veena B Antony, Ling-Yi Chang, James D Crapo, and Herbert Y Reynolds. 2005. "The Mysterious Pulmonary Brush Cell A Cell in Search of a Function." https://doi.org/10.1164/rccm.200502-203WS.
134. Rinner, I., and K. Schauenstein. 1993. "Detection of Choline-acetyltransferase Activity in Lymphocytes." *Journal of Neuroscience Research* 35 (2): 188–91. https://doi.org/10.1002/jnr.490350209.
135. Rogers, D F. 1997. "REVIEW NEUROGENIC INFLAMMATION IN LUNG DISEASE: BURNT OUT?" *Inflammopharmacology*. Vol. 5.

136. Rosas-Ballina, Mauricio, Peder S. Olofsson, Mahendar Ochani, Sergio I. Valdés-Ferrer, Yaakov A. Levine, Colin Reardon, Michael W. Tusche, et al. 2011. "Acetylcholine-Synthesizing T Cells Relay Neural Signals in a Vagus Nerve Circuit." *Science (New York, N.Y.)* 334 (6052): 98–101. https://doi.org/10.1126/SCIENCE.1209985.
137. Russell, F. A., R. King, S. J. Smillie, X. Kodji, and S. D. Brain. 2014. "Calcitonin Gene-Related Peptide: Physiology and Pathophysiology." *Physiol Rev* 94 (4): 1099–1142. https://doi.org/10.1152/physrev.00034.2013.
138. Saimi, Yoshiro, and Ching Kung. 2002. "Calmodulin as an Ion Channel Subunit." *Annual Review of Physiology* 64: 289–311. https://doi.org/10.1146/ANNUREV.PHYSIOL.64.100301.111649.
139. Sanz, Guenhaël, Isabelle Leray, Adeline Muscat, Adrien Acquistapace, Tao Cui, Julie Rivière, Silvia Vincent-Naulleau, Valeria Giandomenico, and Lluis M Mir. 2017. "Gallein, a Gβγ Subunit Signalling Inhibitor, Inhibits Metastatic Spread of Tumour Cells Expressing OR51E2 and Exposed to Its Odorant Ligand." *BMC Res Notes* 10: 541. https://doi.org/10.1186/s13104-017-2879-z.
140. Seybold, V. S. 2009. "The Role of Peptides in Central Sensitization." *Handbook of Experimental Pharmacology* 194: 451–91. https://doi.org/10.1007/978-3-540-79090-7_13.
141. Shapiro, Darien, Cassandra E. Deering-Rice, Erin G. Romero, Ronald W. Hughen, Alan R. Light, John M. Veranth, and Christopher A. Reilly. 2013. "Activation of Transient Receptor Potential Ankyrin-1 (TRPA1) in Lung Cells by Wood Smoke Particulate Material." *Chemical Research in Toxicology* 26 (5): 750–58. https://doi.org/10.1021/tx400024h.
142. Shukla, Arun K. 2016. "G Protein-Coupled Receptors (GPCRs)." *International Journal of Biochemistry and Cell Biology* 77 (August): 183. https://doi.org/10.1016/j.biocel.2016.05.008.
143. Silva, Talita de Melo e, Catherine Miriam Czeisler, and José Javier Otero. 2021. "Development of Lung Innervation." *Oxford Research Encyclopedia of Neuroscience*, October. https://doi.org/10.1093/ACREFORE/9780190264086.013.308.
144. Silverman, Harold A., Aisling Tynan, Tyler D. Hepler, Eric H. Chang, Manojkumar Gunasekaran, Jian Hua Li, Tomás S. Huerta, et al. 2023. "Transient Receptor Potential Ankyrin-1-Expressing Vagus Nerve Fibers Mediate IL-1β Induced Hypothermia and Reflex Anti-Inflammatory Responses." *Molecular Medicine* 29 (1). https://doi.org/10.1186/s10020-022-00590-6.
145. Soderberg, Kelly A., Geoffrey W. Payne, Ayuko Sato, Ruslan Medzhitov, Steven S. Segal, and Akiko Iwasaki. 2005. "Innate Control of Adaptive Immunity via Remodeling of Lymnh Node Feed Arteriole." *Proceedings of the National Academy of Sciences of the United States of America* 102 (45): 16315–20. https://doi.org/10.1073/PNAS.0506190102.
146. Souza Monteiro de Araujo, Daniel, Romina Nassini, Pierangelo Geppetti, and Francesco De Logu. 2020. "TRPA1 as a Therapeutic Target for Nociceptive Pain." *Expert Opinion on Therapeutic Targets* 24 (10): 997–1008. https://doi.org/10.1080/14728222.2020.1815191.
147. Staerz, Anna, Udo Weimar, and Nicolae Barsan. 2016. "Understanding the Potential of WO3 Based Sensors for Breath Analysis." *Sensors (Switzerland)* 16 (11). https://doi.org/10.3390/s16111815.
148. Startek, Justyna B., Karel Talavera, Thomas Voets, and Yeranddy A. Alpizar. 2018. "Differential Interactions of Bacterial Lipopolysaccharides with Lipid Membranes: Implications for TRPA1-Mediated Chemosensation." *Scientific Reports* 8 (1). https://doi.org/10.1038/S41598-018-30534-2.
149. Stauderman, Kenneth A., L. Scott Mahaffy, Michael Akong, Gönül Veliçelebi, Laura E. Chavez-Noriega, James H. Crona, Edwin C. Johnson, et al. 1998. "Characterization of Human Recombinant Neuronal Nicotinic Acetylcholine Receptor Subunit Combinations A2β4, A3β4 and A4β4 Stably Expressed in HEK293 Cells." *Journal of Pharmacology and Experimental Therapeutics* 284 (2): 777–89.
150. Story, Gina M., Andrea M. Peier, Alison J. Reeve, Samer R. Eid, Johannes Mosbacher, Todd R. Hricik, Taryn J. Earley, et al. 2003. "ANKTM1, a TRP-like Channel Expressed in Nociceptive Neurons, Is Activated by Cold Temperatures." *Cell* 112 (6): 819–29. https://doi.org/10.1016/S0092-8674(03)00158-2.
151. Sullivan, James P., Diana Donnelly-Roberts, Clark A. Briggs, David J. Anderson, Murali Gopalakrishnan, Marietta Piattoni-Kaplan, Jeffrey E. Campbell, et al. 1996. "A-85380 [3-(2(S)-Azetidinylmethoxy) Pyridine]: In Vitro Pharmacological Properties of a Novel, High Affinity A4β2 Nicotinic Acetylcholine Receptor Ligand." *Neuropharmacology* 35 (6): 725–34. https://doi.org/10.1016/0028-3908(96)84644-2.

152. Talavera, Karel, Maarten Gees, Yuji Karashima, Víctor M. Meseguer, Jeroen A.J. Vanoirbeek, Nils Damann, Wouter Everaerts, et al. 2009. "Nicotine Activates the Chemosensory Cation Channel TRPA1." *Nature Neuroscience 2009 12:10* 12 (10): 1293–99. https://doi.org/10.1038/nn.2379.
153. Talbot, Sébastien, Simmie L. Foster, and Clifford J. Woolf. 2016. "Neuroimmunity: Physiology and Pathology." *Annual Review of Immunology* 34 (May): 421–47. https://doi.org/10.1146/ANNUREV-IMMUNOL-041015-055340.
154. Tallini, Yvonne N., Bo Shui, Kai Su Greene, Ke Yu Deng, Robert Doran, Patricia J. Fisher, Warren Zipfel, and Michael I. Kotlikoff. 2006. "BAC Transgenic Mice Express Enhanced Green Fluorescent Protein in Central and Peripheral Cholinergic Neurons." *Https://Doi.Org/10.1152/Physiolgenomics.00092.2006* 27 (3): 391–97. https://doi.org/10.1152/PHYSIOLGENOMICS.00092.2006.
155. Trä nkner, Dimitri, Nadeau Hahne, Ken Sugino, Mark A. Hoon, and Charles Zuker. 2014. "Population of Sensory Neurons Essential for Asthmatic Hyperreactivity of Inflamed Airways." *Proceedings of the National Academy of Sciences of the United States of America* 111 (31): 11515–20. https://doi.org/10.1073/pnas.1411032111.
156. Tsai, Sheng Ta, Tzu Hsuan Wei, Yu Wan Yang, Ming Kuei Lu, Shao San, Chon Haw Tsai, and Yi Wen Lin. 2021. "Transient Receptor Potential V1 Modulates Neuroinflammation in Parkinson's Disease Dementia: Molecular Implications for Electroacupuncture and Rivastigmine." *Iranian Journal of Basic Medical Sciences* 24 (10): 1336–45. https://doi.org/10.22038/IJBMS.2021.56156.12531.
157. Turner, Heather N., and Emily R. Liman. 2022. "The Cellular and Molecular Basis of Sour Taste." *Annual Review of Physiology* 84: 41–58. https://doi.org/10.1146/ANNUREV-PHYSIOL-060121-041637.
158. Ualiyeva, Saltanat, Nils Hallen, Yoshihide Kanaoka, Carola Ledderose, Ichiro Matsumoto, Wolfgang G. Junger, Nora A. Barrett, and Lora G. Bankova. 2020. "Airway Brush Cells Generate Cysteinyl Leukotrienes through the ATP Sensor P2Y2." *Science Immunology* 5 (43). https://doi.org/10.1126/SCIIMMUNOL.AAX7224.
159. Vane, John R., Jane A. Mitchell, Ian Appleton, Annette Tomlinson, David Bishop-Bailey, Jamie Croxtall, and Derek A. Willoughby. 1994. "Inducible Isoforms of Cyclooxygenase and Nitric-Oxide Synthase in Inflammation." *Proceedings of the National Academy of Sciences of the United States of America* 91 (6): 2046–50. https://doi.org/10.1073/PNAS.91.6.2046.
160. Venkatachalam, Kartik, and Craig Montell. 2007a. "TRP Channels TRP: Transient Receptor Potential." https://doi.org/10.1146/annurev.biochem.75.103004.142819.
161. Wang, Changming, Leying Gu, Yonglan Ruan, Xiao Geng, Miao Xu, Niuniu Yang, Lei Yu, et al. 2019. "Facilitation of MrgprD by TRP-A1 Promotes Neuropathic Pain." *FASEB Journal* 33 (1): 1360–73. https://doi.org/10.1096/fj.201800615RR.
162. Wonnacott, Susan. 2014. "Nicotinic ACh Receptors." *Tocris Scientific Review Series*, 1–31.
163. Wood, J. D. 1984. "Enteric Neurophysiology." *The American Journal of Physiology* 247 (6 Pt 1). https://doi.org/10.1152/AJPGI.1984.247.6.G585.
164. Wu, D. X.Y., C. Y.C. Lee, S. N. Uyekubo, H. K. Choi, S. J. Bastacky, and J. H. Widdicombe. 1998. "Regulation of the Depth of Surface Liquid in Bovine Trachea." *American Journal of Physiology - Lung Cellular and Molecular Physiology* 274 (3 18-3). https://doi.org/10.1152/AJPLUNG.1998.274.3.L388.
165. Wyatt, Amanda, Philipp Wartenberg, Michael Candlish, Gabriela Krasteva-Christ, Veit Flockerzi, and Ulrich Boehm. 2017. "Genetic Strategies to Analyze Primary TRP Channel-Expressing Cells in Mice." *Cell Calcium* 67 (November): 91–104. https://doi.org/10.1016/j.ceca.2017.05.009.
166. Yoshida, Naoki, Kimiko Kobayashi, Lina Yu, Shenglan Wang, Rengaowa Na, Satoshi Yamamoto, Koichi Noguchi, and Yi Dai. 2011. "Inhibition of TRPA1 Channel Activity in Sensory Neurons by the Glial Cell Line-Derived Neurotrophic Factor Family Member, Artemin." *Molecular Pain* 7 (1): 41. https://doi.org/10.1186/1744-8069-7-41.
167. Zhang, Zhong wei, Sukumar Vijayaraghavan, and Darwin K. Berg. 1994. "Neuronal Acetylcholine Receptors That Bind α-Bungarotoxin with High Affinity Function as Ligand-Gated Ion Channels." *Neuron* 12 (1): 167–77. https://doi.org/10.1016/0896-6273(94)90161-9.

Résumé

Alaa Salah
Gender: Female
Nationality: Palestinian
Date of birth: 04.10.1988

EDUCATION

2018.08 - current **Ph.D. candidate,** Department of Anatomy and Cell Biology, College of Medicine, University of Saarland, Homburg, Germany. Thesis: Brush Cell-Derived Acetylcholine Activation of Cholinergic Neurons Negatively Regulates Calcium-Dependent Responses in the Innervating Sensory Neurons. Supervisor: Prof. Dr. Gabriella Krasteva-Christ.

2010.09 - 2012.06 **Master of Science,** Department of Genetics and Biotechnology, Mediterranean Agronomic Institute of Chania, Chania, Greece. Thesis: Silencing of seven propyl 4-hydroxylases reduces AGPS content, and induces alternations in growth and fruit-ripening programs in two of them. Supervisor: Dr. Panagiotis Kalaitzis.

2006.09 - 2010.06 Bachelor of Science, Department of Biological Science**s,** College of Science, Birzeit University, Birzeit, Palestine. Thesis: A Report Study about Telomeres in Cancer. Supervisor: Prof. Dr. Ahed Abdulkhaliq.

WORK EXPERIENCE

2012.10 - 2015.05 **Research Scientist**, Microbiology Research Lab, Department of Microbiology, College of Medicine, Al-Quds University, Abu-Dis, Palestine.

SCHOLARSHIPS

2013.06 - 2013.07 Research funding from the German Research Foundation to work as a researcher at Dr. Manfred Höfle's Lab, Helmholtz Centre for Infection Research, Braunschweig, Germany.

2011.06 - 2011.08 Research funding from The German Academic Exchange Service**;** DAAD, to work as a researcher at Prof. Dr. Ralf Reski's lab at the Faculty of Biology, University of Freiburg.

Publications

Publication 1: Zayed, Butmeh, Pecellin, **Salah**, Alalam, Steinert, Höfle, Bitar, and Brettar (**2020**). Environmental Drivers of *Legionella pneumophila*: Abundance and Genotype Composition across the West Bank: Relevance of a Genotype-Based Ecology for Understanding Legionella Occurrence.

Publication 2: Zayed, Pecellin, **Salah**, Alalam, Butmeh, Steinert, Lesnik, Brettar, Höfle MG, and Bitar (**2020**). Characterization of *Legionella pneumophila* Populations by Multilocus Variable Number of Tandem Repeats (MLVA): Genotyping from Drinking Water and Biofilm in Hospitals from Different Regions of the West Bank.

Publication 3: Hollenhorst, Nandigama, Evers, **Salah,** Gamayun, Wadood, Pieper, Kusumakshi, Stukalov, Gebhardt, Nadolni, Herr, Beisswenger, Burow, Hübner, Kichko, Peter Reeh, Munder, Wienhold, Witzenrath,Bals, Flockerzi, Gudermann, Bischoff, Lipp, Zierler, Chubanov, Pichlmair, König, Boehm, and Krasteva-Christ (**2022**). Bitter taste signaling in tracheal epithelial brush cells elicits innate immune responses to bacterial infection.

Publication 4: Hollenhorst, Kumar, **Salah**, Maxeiner, Flockerzi, Gudermann, Chubanov, Boehm, and Krasteva-Christ (**2022**). Taste receptor activation in tracheal brush cells by denatonium modulates ENaC channels via Ca 2+, cAMP, and ACh.